UNIVERSITÀ DEGLI STUDI DI PALERMO

Dottorato in Chemical, Environmental, Biomedical, Hydraulic and materials Engineering

Dipartimento di Ingegneria

Membrane based electrochemical technologies for sustainable energy production and minerals recovery.

IL DOTTORE

Ing. Syed Abdullah Shah

IL TUTOR

Prof. Ing. Giorgio Domenico Maria Micale

IL COORDINATORE:

Prof. Ing. Giorgio Domenico Maria Micale

I CO-TUTORS

Prof. Ing. Andrea Cipollina

Prof. Ing. Alessandro Tamburini

Dr. Alberto Figoli

Dr. Enrica Fontananova

CICLO XXXVI

ANNO CONSEGUIMENTO TITOLO 2024

ACKNOWLEDGEMENTS

I am profoundly grateful to all those who have played a pivotal role in making this Ph.D. journey a reality. Their steadfast support and encouragement have been the cornerstone of my achievement.

Foremost, I offer my most profound appreciation to my dedicated advisor, Prof. Giorgio Micale, whose unwavering guidance, mentorship, and unwavering belief in my abilities have driven my doctoral research. His expertise and patience have left an indelible mark on my academic growth and professional development.

I am equally indebted to my co-supervisors, Prof. Andrea Cipollina, Prof. Alessandro Tamburini, Dr. Alberto Figoli, Dr. Enrica Fontananova, and Dr. Francesso Galiano, for their invaluable insights, constant support, and contributions that have significantly enriched this research. Their expertise and willingness to engage in discussions and offer guidance have been pivotal to the success of this dissertation.

My sincere thanks go out to the "**SEArcularMINE"** EU Project, UniPa, and Istituto la Tecnologia della Membrane (CNR-ITM) for providing the essential resources and research facilities that have been indispensable to the successful completion of this work.

I want to convey my most profound appreciation to my family, who have supported me throughout this academic journey. Their boundless love, encouragement, and understanding have been a constant source of motivation.

I must express my heartfelt gratitude to my beloved wife, Clara Valli, for her unwavering patience, understanding, and encouragement. Her unwavering support and sacrifices have been instrumental in my pursuit of this academic milestone. Thank you for being my pillar of strength and sharing this journey with me.

My warmest thanks go to my friends and colleagues for their camaraderie, discussions, and shared experiences, which have enriched this academic journey.

I extend my sincere thanks to all who have directly or indirectly contributed to this research endeavor, no matter how small or large your role. Your contributions have been a crucial part of this work.

This research would not have been possible without the support and contributions of every one of you. Thank you for being an integral part of this significant chapter in my academic and personal growth.

Table of Contents

List of figures

List of tables

Nomenclature

A	Active membrane area (m^2)
C	Molar concentration (moL/L)
C_o	Initial concentration (moL/L)
CE	Current Efficiency (%)
C_t	Concentration at specific time (moL/L)
C_{Co-ion}^{m}	Co-ion in membrane (moL/kg)
$C_{Counter-ion}^{m}$	Counter ion in membrane (moL/kg)
C_{fix}^{m}	Membrane fixed charge (mol/kg)
F	Faraday constant (C moL/L)
FC	F-Value calculated
F_{cr}	F-Value Critic
I	Electric current (I)
Mg-CGCR	Magnesium Hydroxide Crystallization Reactor
M_{sol}	Volume of desorption solution
MW_i	Molar weight of the ion
N	Number of cell pairs (-)
SPC	Specific Energy consumption (kWh/kg)
SP	Specific productivity (kg/m^2year)
t	Operation time (hours)
$t_{1\ year}$	One-year time production, hours
U	External voltage (V)
V_0	Initial Volume (L)
V_t	Volume at specific time (L)
OCV	Open circuit voltage (V)
P	Power (W)
P_d	Power density (W/m^2 cell pair)
$P_d$corr	Corrected power density (W/m^2 cell pair)
R_{blank}	Blank resistance (Ω)
R_{cell}	Resistance of cell pair (Ω)
R_{stack}	Stack internal resistance (Ω)
R_{load}	Load resistance

V_{stack}	Stack potential (V)
W_u	Water uptake
W_{wet}	Wet mass of membrane (g)
W_{dry}	Dry mass of membrane (g)
T	Temperature (K)
v	Fluid flow velocity (cm/s)
α	perm selectivity
z_i	Ion valance number

AEM	Anion exchange membrane
BPM	Bipolar Membrane
CEM	Cation exchange membrane
CRM	Critical Raw Material
ERS	Electrode rinse solution
EDBM	Electrodialysis with Bipolar Membrane
EU	European Union
MLD	Minimum Liquid Discharge
IEMs	Ion exchange membrane
HC	High compartment
LC	Low compartment
RED	Reverse Electrodialysis
SGP	Salinity Gradient power
SWRO	Sea water Reverse osmosis
ZLD	Zero Liquid Discharge

Summary

With the advancement of high-salinity wastewater, salt resource regeneration has been recognized as a critical necessity for process sustainability and economic advantages. In recent years, bipolar membrane electrodialysis (BMED) and reverse electrodialysis (RED) have emerged as possible alternatives for treating saline wastewater. Unlike other methods of directly obtaining salts or condensed wastewater, BMED and RED can simultaneously utilize and convert the dissolved waste salt into renewable energy, higher-value acid, and alkali, which has numerous advantages, including outstanding environmental and economic benefits. The applications of BMED and RED in blue energy production and high-value acid/alkali generation from saline wastewater were thoroughly examined in this study. Furthermore, the influence of the operational parameters on the performance of both electro-membrane technologies is discussed. This study guides the application of bipolar membrane electrodialysis and reverse electrodialysis technologies in saline wastewater treatment and the high-value conversion of salt resources into energy, acids, and alkalis.

Chapter 2 aimed to extract critical raw materials from saltworks brines using two ion exchange membranes. Concentrated brines were also recycled through electrodialysis with bipolar membranes. New non-woven cloth ion-exchange membranes were tested, including ultra-thin polyester and thin polypropylene cloth. An inter-laboratory experiment was conducted to assess the effect of current density on membrane performance using 2 M NaCl. Both membrane combinations generated NaOH/HCl solutions up to 0.8 M at 300 A m^{-2}. Thin polypropylene membranes had better energy efficiency and productivity than ultra-thin ones.

Chapter 3 explored Electrodialysis with Bipolar Membranes (EDBM) for treating synthetic mixed salt solutions resembling waste brine from saltworks. Lab-scale EDBM operated at 100 and 300 A/m^2 using SUEZ ion exchange membranes. Investigated was the impact of initial monovalent (NaCl) and mixed salt (NaCl and Na_2SO_4) feed solutions on performance. Higher NaCl concentration favored faster NaOH production. The mixed solution had a modest influence. Current efficiency ranged from 60-70% under 100 A/m^2; energy use was 1.80 kWh/kg_{NaOH} for 0.8 M brine.

Chapter 4 of the research demonstrated that brine valorization can be used for renewable energy production through electro-membrane process technology. This technology can capture and convert the salinity gradient power (SGP) conveyed by concentrated bitterns discharged from saltworks. Doing so reduces the disposal of concentrated salty water, which helps protect the environment. A laboratory-scale RED unit was used to study the SGP potential of these brines, and ion exchange membranes from different suppliers were tested. The results showed that membranes supplied by Fujifilm, Fumatech, and Suez was effective. The maximum power density achieved was around 10.5 W/m^2 cell pair, using Fujifilm Type 10 membranes, a temperature of 40°C, and a fluid velocity of 3 cm s^{-1}. This study paves the way for further research and development of this technology for renewable energy production.

Chapter 5 In response to the climate emergency and the world's increasing population, this research explores cost-effective and sustainable energy production through bitterns and power harvesting using a reverse electrodialysis (RED) system. The study investigates two distinct homogeneous Ion Exchange Membranes (IEMs) developed by Fujifilm Manufacturing Europe BV and Suez under various conditions.

The membranes' characteristics, including ion sorption, fixed charged water uptake, and perm selectivity, were examined using real and pre-treated Margi brine saltwork solutions and synthetic 5 M NaCl brine at 30°C. Fujifilm IEMs exhibited superior properties, with reinforced (polyolefin) Fujifilm IEMs demonstrating high electrical resistance, particularly in the presence of treated and untreated total dissolved solids (TDS), alongside exceptional perm selectivity.

Notably, Fujifilm IEMs displayed higher monovalent ion sorption and counter-ion concentrations compared to Suez membranes, while co-ion concentrations were similar. In RED applications with hypersaline Margi-A and Nubia-A brine, Fujifilm IEMs achieved remarkable power densities of 3.57 W/m^2 and 4.32 W/m^2, whereas Suez IEMs displayed significantly lower power densities of 0.77 W/m^2 and 0.69 W/m^2 at 1 cm/s flow velocity. Power densities for spiked brine were comparable to the membranes at a flow velocity of 3 cm/s.

Chapter 1

Fundamental Principles and design for Sustainable Brine Discharge and management.

Abstract

In recent years, there has been a significant increase in the use of desalination plants to provide potable water in communities worldwide. One of the challenges faced by these plants is the production of brine, a concentrated solution with high salinity, which poses significant environmental challenges. It is essential to find a cost-effective and environmentally friendly brine management system for proper disposal. Several disposal options have been tested, but they all have limitations and high costs. Conventional treatments such as physicochemical, oxidation, and biological processes have been explored with varying degrees of success. However, membrane-based technologies, such as electrodialysis and reverse electrodialysis, are emerging as a cost-effective solution for managing brine concentration. These technologies can help minimize brine volume, recover valuable resources, and improve renewable energy recovery. This thesis explores these membrane processes and their potential to recover valuable resources while minimizing brine volume and improving renewable energy recovery.

1.1. Introduction

It is worth noting that the 2018 United Nations (UN) World Water Development Report, as documented in UnesDoc [1], revealed that almost half of the global population, approximately 3.6 billion individuals, reside in regions that undergo water scarcity for at least a month annually. This is a critical matter that demands attention and must take appropriate measures to combat it. As the world's population continues to increase, effective planning and management of water resources become increasingly crucial. In countries that face water scarcity, the use of unconventional resources plays a pivotal role in achieving sustainable development and adapting to changes in the climate [2] put forward a groundbreaking proposal for water resource planning, emphasizing ecosystem management and sustainable development. Future water sector planning should aim to decrease the utilization of water from natural reservoirs and encourage the adoption of alternative methods to ensure the long-term viability of water resources [3]. Numerous water supply approaches utilizing non-conventional sources are currently being implemented in region with limited water availability, demonstrating of both seawater and brackish water, collection of rainwater, extraction of atmospheric water, and recycling of wastewater [4]. Among the technologies capitalizing on non-conventional water sources, the desalination of seawater and brackish water has garnered significant attention due to its viability in fulfilling essential domestic and municipal requirements [2]. The global desalination capacity growth over a three-decade span indicates a potential expansion to over 200 million m3/day by the year 2030 [5].

In the context of scaling up desalination operations and facilities, a significant obstacle arises in the form of brine generation. In the broader context, Brine is a liquid solution with increased salinity and temperature that is the product of many industrialized and mining processes. Such as by-products of saltworks miming, mining processes and distillation operations, may have a major adverse effect on marine life and the environment [6]. Various coastally located plants and seawater desalination units typically pump brine back into the sea, potentially causing ecosystem and environmental issues, whereas land-based plants for groundwater desalination or industrial activities either deep-inject or surface dispose of brine without treatment in many cases. Unsafe disposal and processing of this concentration, as well as the stringent regulations in place in many countries, make sustainable brine management a major area of concern for areas all over the globe. As demonstrated in **Figure 1,** the number of scholarly papers on brine management has increased during the last two decades.

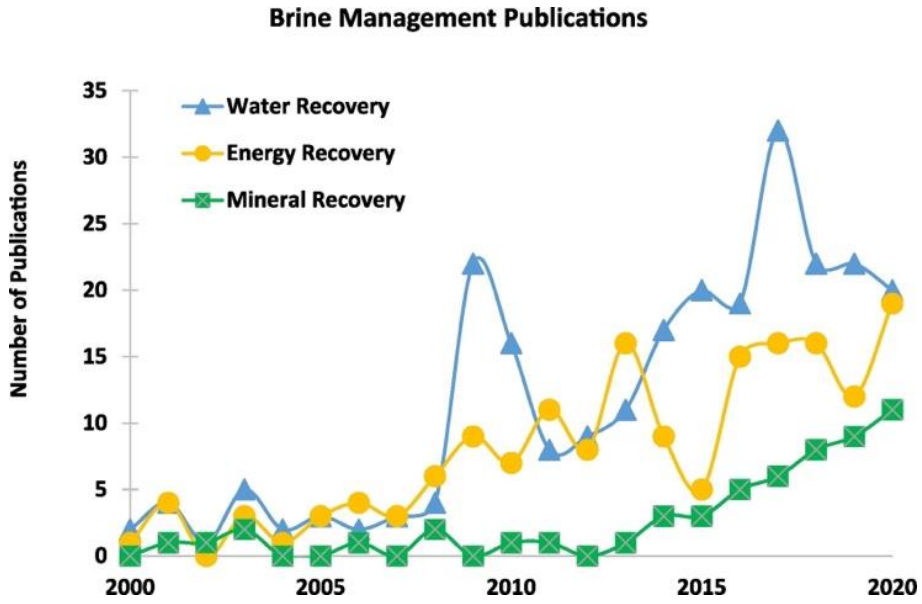

Figure 1. Brine Management research articles during the last two decades [7].

Brine reduction is a challenge for most desalination plants. Reverse osmosis (RO) desalination recovers about half of the water, while thermal (MSF) desalination recovers even less, around a quarter to a third. [2] [8]. Desalination leaves a lot of fresh water (45–70%) as brine discharge. Water recovery from brine can enhance water production, save on brine treatment and disposal costs, and reduce environmental impact. Maximizing water recovery and generating energy are two benefits of brine. Mora and de Rijck suggested that 60% of global electricity can come from brine's salinity gradient potential (SGP) [9]. Other studies indicated that 2.6 TW could come from estuaries and more from brine [10], [11]. This highlights the advantages of using brine from desalination plants for osmotic power generation, as brine is more saline. Brine also contains valuable minerals that can be recovered for economic and environmental gains [12], [13].

1.2. Constituents of brine

A clean feed source is essential for desalination plants, so coastal water quality is crucial. The Gulf region has the most significant number of desalination plants in the world, with Saudi Arabia generating 22% of the global brine. The coast can experience many environmental troubles at discharge points, and these are amplified by the excessive use of the Gulf as a water source and an effluent receiver from different industrial and commercial activities [14].

Concentrated brine can ascend due to high-temperature levels. Brine has different properties from other types of wastewaters, depending on the concentration of the salinity levels. The saltier the brine, the more it differs from other wastewater sources. When the effluent is denser than the seawater, it can detach the plumes and make them sink to the sea bottom, causing damage and harm to marine life. Some studies have reported that desalination plant outfall can reduce seagrass density and disturb marine ecosystems [15]. However, other studies have also reported that desalination plants have little effect on the coastal environment [16]. The domain can suffer from high salt and pollutant levels in intense brine discharges. These impacts can affect the physical and chemical properties and the living organisms of the water that receives them. The improper brine disposal from inland desalination contaminated the soil and groundwater [17].

Brine is not only a by-product of seawater desalination plants but also generated by other industrial processes. Some examples are drilling for oil and gas, making food and drinks, producing textiles, tanning leather, and treating water with demineralization and reverse osmosis. The brine from different sources has different properties because of the different types of water they use and the different methods they apply to treat them.

Extremely high quality and a large volume of water are utilized in the textile industry application and processes. It makes the water very soft by using a unique process. This process uses ion-exchange resins that need to be refreshed and produce wastewater with much salt in it [18]. The dyeing process for textile fibres also requires much salt to ensure the color sticks to the fabric. Even after being treated, these dyeing waters still have much salt [19].

Hypersaline brine is produced by oil and gas companies' actions near wells of oil and gas located around mountain areas. To dissolve the salt, fresh water is injected into wells to extract the oil, and the brine is returned to the surface as a by-product. The oil is recovered on the surface, and excess brine goes through further treatment before discharging within the environment [20].

Pharmaceutical firms often employ high-quality water sources for their manufacturing procedures, which are typically membrane-based and generate varied volumes of brine with different compositions and strengths. The process uses much water, resulting in high waste effluent flows with many dissolved salts [21].

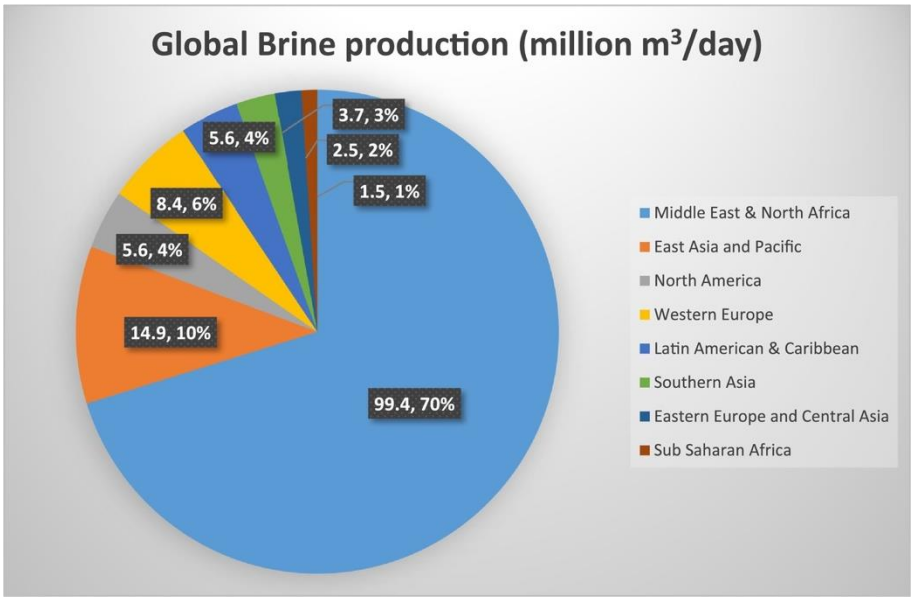

Figure 2. Global desalination plant brine output as of 2018 by region (in million m^3/d) [7].

Brine produced from saltworks contains a high concentration of total dissolved solids (TSDs) in the range of 300 g/L. The brine stream of sweater mining is a primary source of minerals and energy via electro-membrane processing technologies [13], [22].

1.3. Brine management strategies

Currently, 100% of water recovery from desalination technologies is not achieved, resulting in a vast volume of brine wastes and causing long terms several long-term critical issues to ecosystems, groundwater, and aquatic nature [23]. Several methods have been proposed and implanted to brine management. Nevertheless, more research is required to provide ecologically beneficial and financially effective management alternatives for the brine. A valuable brine minimization strategy could be direct disposal by reducing the volume of produced brine from the activities. Zero liquid discharge (ZLD) is the lasted approach introduced to rejected brine treatment. This strategy aims to mitigate brine discharge while reclaiming water and salts, lowering possible environmental impact and resulting in a more sustainable solution. However, the ZLD process is costly because of its high energy requirements. Different appreciated practices need to be followed to overcome these problems associated with brine disposal, considering all essential parameters, such as geographical region, brine rejected volume and disposal cost. Lower energy consumption, improve process efficiency, obta zero liquid discharged, and adopt renewable energy sources. Each technology that is currently available is essential to understand. The minimization approaches can be achieved via sustainable electro-membrane process technologies.

1.4. Brine Treatment & Minimization Approaches

Effective management of the brine is crucial to ensure the safety of both human well-being and the environment. However, seawater desalination technologies produce freshwater for consumption and use of human, brine managements could be divided into two main primary strategies: (I) direct disposal into environment and (II) brine treatment and recovery technologies [24].

1.4.1. Direct discharge of brine into the natural environment

The most commonly method used for brine discharge are deep well injection, sewer discharges, surface water discharges, land application and evaporation ponds [25]. In general, brine disposal method is influenced by many factors [2]. The factors include quantity, quality and composition of the brine stream, the option permissibility, receiving site availability, availability of the discharge site's location, capital and operational costs [24]. Surface water disposal and sewer disposal entail the immediate release of the brine into natural water bodies (such as rivers, lakes, sea, etc.) or into wastewater collection system. Furthermore, injection brine into deep wells is less commonly utilized compared to surface water and sewer discharges due to concerns about potential long-term groundwater contamination. Conversely, the evaporation of brine is widely implemented in the countries where high solar energy is available. Lastly, smaller quantities of the brine solution could be used for irrigation salt tolerant grasses and plants, serving as a land application method [26].

Surface water direct discharges or sewer discharges are typically the most cost-effective and practical methods for directly disposing of brine. This holds especially true when the brine stream aligns well with the characteristics of the receiving water body and when the discharge point is near the desalination plant [24]. Hence, the assessments of brine characteristics, transportation logistics, outfall construction systems, and environmental monitoring are associated to surface water and sewer disposal method. This method is a feasible option for offshore or near sea desalination plants. This is because the expenses related to construction of pipelines or outfall system would be significantly minimized. Moreover, sewer disposal would be feasible if the brine concentration is similar to that of the receiving wastewater and if current wastewater treatment is sufficient [25]. On the other hand, deep well injection of the discharge brine streams is more expensive than surface water and sewer disposal but most suitable for inland desalination plants. The high cost of the deep well injection is due to the long pipeline systems, conditioning of brine, controlling, and site geological assessments. Additionally, for

inland desalination facilities situated in arid, semi-arid, dry, and hot regions, a viable brine disposal solution could involve the use of evaporation ponds [2]. The practicality of evaporation ponds is influenced by factors like pond dimensions, depth, choice of lining material, and the extent of monitoring, all of which have cost implications. The irrigation of specific salt tolerant plants know as halophytes with brine solution is presently quite limited. This limitation arises from the fact that halophyte species typically grown in highly arid and semi-arid environments characterized by exceedingly high temperature, making them relatively rare to find [27]. Therefore, land application of brine stream depends on local weather, as well as salt tolerant plants availability and land.

1.5. Brine treatment and recovery technologies

As mentioned above, seawater and specifically desalination brine contain various minerals that could be useful in industrial applications. These minerals could be costly and scarce when sought in their non-aqueous states. Recovering the minerals found in desalination brine has the potential to address three significant challenges: alleviating mineral scarcity, mitigating the environmental consequences associated with brine discharge, and reducing desalination costs. The cost of seawater desalination could decline as valuable products are generated through mineral recovery [28].

Loganathan et al. [28] have elaborated on the advantages of mineral recovery from seawater and brine. These benefits encompass reductions in desalination costs, the substitution of costly commercial fertilizers with those rich in seawater nutrients, decreased reliance on land mining for ores, and the comparatively lower energy requirements for mineral recovery from seawater and brine as opposed to land-based sources. The historical precedent for recognizing valuable resources in seawater and brine dates back to 2200 BC when the Chinese first extracted sodium chloride (salt) from seawater. Since then, ongoing research has explored the extraction of valuable metals and minerals such as gold, bromine, magnesium, uranium, cesium, lithium, rubidium, and more from seawater and brine (Mavukkandy et al. [5].

Given the well-know environmental impacts of traditional brine disposal and discharge methods, continuous research and the adoption of various alternative brine management, recovery, and treatment technologies have gained prominence. Among these, conventional technologies include zero-liquid discharge (ZLD) treatment systems. ZLD brine treatment

systems are designed to maximize water recovery while minimizing brine volume, all without harm to the environment (Panagopoulos et al., 2019). It's important to note that ZLD systems are complex combinations of various desalination technologies aimed at eliminating brine waste while yielding pure water from the desalination plant [29]].

Furthermore, studies have demonstrated that ZLD systems produce highly concentrated brine waste, which can undergo further processing for use as a valuable industrial material or disposed of through environmentally friendly methods [29]. Additionally, brine treatment can serve a multitude of industrial and commercial purposes, including the recovery of pure water, salt concentration, energy regeneration, and valuable metal extraction for various industrial processes.

Based on the literature, conventional brine treatment systems can be categorized as either thermal-based or membrane-based technologies. These systems represent a promising step towards addressing the challenges posed by brine disposal while tapping into the hidden potential of seawater and brine resources.

1.5.1. Brine treatment via membrane-based technologies

Based on the above previous contribution, the most widely used membrane technologies for rejected brine treatment and minimization are membrane distillation (MD) [30], Membrane crystallization, pressure retarded osmosis (PRO) [31], electrodialysis (ED) [32], reverse electrodialysis (RED) [22], multi-effect distillation (MED) [33] and, multi-stage flash (MSF) [33]. The brine minimization approaches will not allow for lowering the rejected brine final volume disposal but also contribute to reducing the effect of the environmental issues and costs associated with brine disposal. Some of the membrane-based brine management technologies are below.

1.5.1.1.Membrane Distillation (MD)

Membrane distillation (MD) is an innovative non-isothermal membrane process technology with low cost and energy. The driving force for the passage of water molecules from the feed to the permeate side is a partial pressure difference on both sides of the membrane. Due to the hydrophobic nature of the membrane, only vapor can go through it, and not distilled water containing a liquid solution [34]. MD has some benefits over other standard desalination methods, such as: (i) it completely blocks ions and other substances that do not evaporate, (ii)

it works at lower temperatures and pressures than other membrane separation technologies that use pressure, (iii) it has minimal chemical reactions between the membranes and the solutions, (iv) it does not require membranes with high mechanical strength, and (v) it has smaller vapour gaps than traditional distillation methods. However, on the other hand, MD has significant constraints because the streams must be aqueous and dilute enough to avoid wetting the hydrophobic microporous membranes [34].

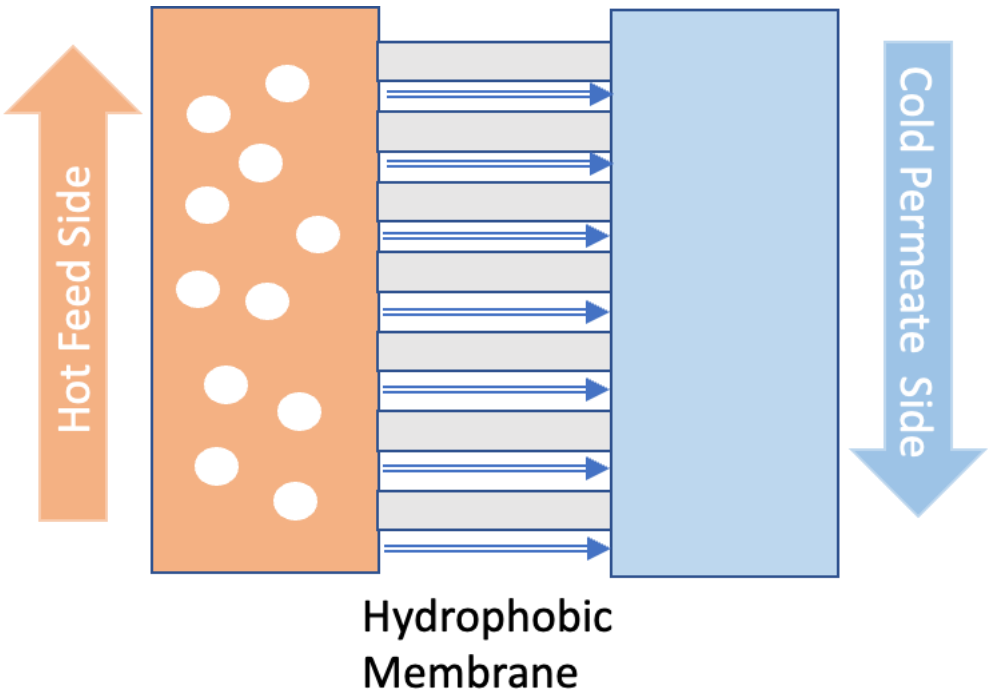

Figure 3. Schematic illustration of Membrane process

Interestingly, there exist four predominant configurations of membrane distillation (MD), each with its distinct characteristics. These configurations are referred to as Air Gap MD (AGMD), Direct Contact MD (DCMD), Sweeping Gas MD (SGMD), and Vacuum MD (VMD). According to the existing body of literature, the direct contact MD configuration stands out as the most widely employed method for brine membrane distillation processes.

In the Direct Contact Membrane Distillation (DCMD) process, the treatment of brine solution operates on the principle of preheating the incoming feed brine solution before it reaches the membrane. Once this feed brine solution is heated on one side, the generated vapor then permeates through the membrane's pores. Subsequently, the vapor undergoes a condensation process, ultimately yielding a cold freshwater distillate [35]. Conversely, the brine solution does not pass through the membrane due to its hydrophobic nature [36].

1.5.1.2.Membrane crystallization (MCr)

This is a novel proposal related to implementing membrane technology for the separation and purification of many streams and waste in several fields of crystallization operations. The Membrane Crystallization (MCr) process offers a promising approach for treating brine solutions with the aim of recovering valuable metals and minerals. As elucidated the MCr process achieves this by concentrating feed solutions, such as brine, beyond their saturation limits. [37]. Typically, the driving force is a temperature differential between the two sides of the membrane. The membrane's hydrophobic nature prevents liquid from entering the pores. As a result, only volatile components pass through the membrane and condense at the permeating sites. The growth of crystal nucleation occurs in a supersaturated environment [38].

The advantages of utilizing MD and MCr include treating highly concentrated streams, extremely low operating temperatures and pressures, high permeate quality irrespective of water feed parameters (theoretical 100% rejection of nonvolatile substances), easy setup, and high permeate quality. The impact of total dissolved solids concentration on MD and MCr is not very high compared to other pressure-driven membrane technologies. These procedures are, therefore, appropriate for treating RO reject brines. In addition, MCr provides significant benefits over conventional crystallization methods, including well-controlled growth kinetics and nucleation, quick crystallization rates, short induction times, and control over the saturation level and rate [38]

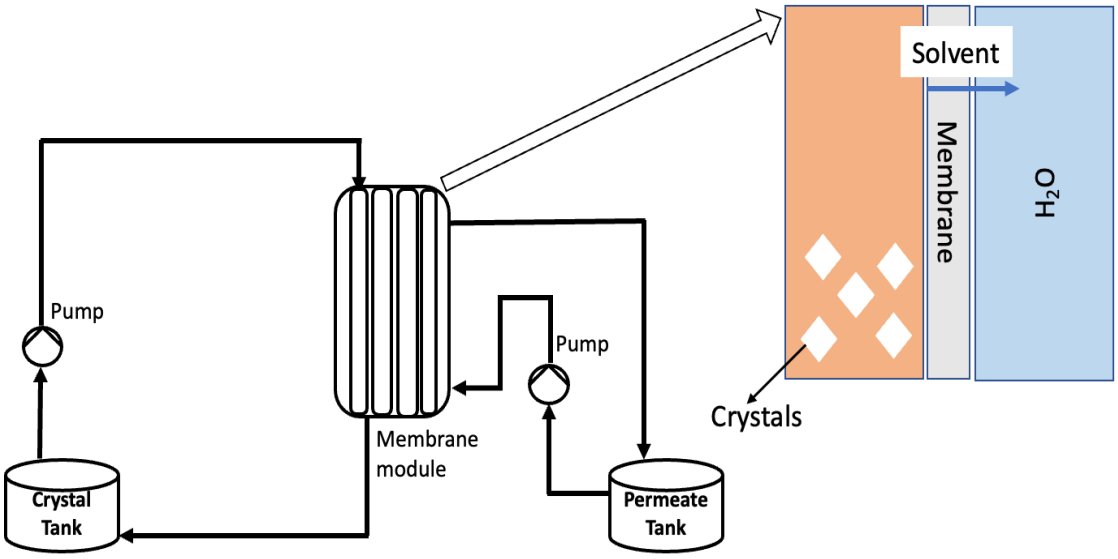

Figure 4. Schematic illustration of MCr process plant.

1.5.1.3 Electrodialysis (ED), and electrodialysis reversal (EDR)

Maigrot and Sabates introduced the concept of electrodialysis (ED) application in 1890 [39], and it has been utilized for the water treatment and production food grade salt from seawater for more than three decades [40]. ED has also been used to produce acid-base under the influence of an electric potential. The ED stack comprises alternative cation and anion exchange membranes (IEMs) sandwiched between the cathode and anode. The electrolyte solution passes through the cell pairs. The cations move toward the cathode through the cation exchange membrane while being repelled by the anion exchange membranes [41]

Similarly, anions move to the anode side through the anion exchange membrane, which the cation exchange membranes reject. In the end, one side of the electrolyte solution concentration is depleted while being enriched on the other side. The industrial ED system comprises 100 to 400 cells pair and is widely used for municipal wastewater treatment and brackish water desalination. The primary benefits of adopting ED over RO are its ease of use, much higher water recovery rate, longer membrane lifespan, and lack of pre- or post-treatment.

Electrodialysis with Bipolar membrane (EDBM) is an emerging brine valorization technology that attracts many researchers due to its significant applications in wastewater treatment. The EDBM unit, as shown in ***Figure 5***, is composed of a stack of repeating triplets made of three channels (i.e., acid, alkaline, and salt), a monopolar cation, anion, exchange membranes, and bipolar membrane (BPM) made of three-layer (I) positive charge on the side, (II) negative charge on the other side of BPM, and (III) interface layer as a catalyst. During operation, when a direct electric current is applied, the water molecules in the junction of the anion and cation-exchange layers of the BPM are dissociated into protons (H^+) and hydroxide (OH^-) ions. The cations and anions in the feed saline solution migrate through the (CEM) and (AEM) toward the cathode and anode, respectively, ultimately producing acidic and alkaline solutions [13]

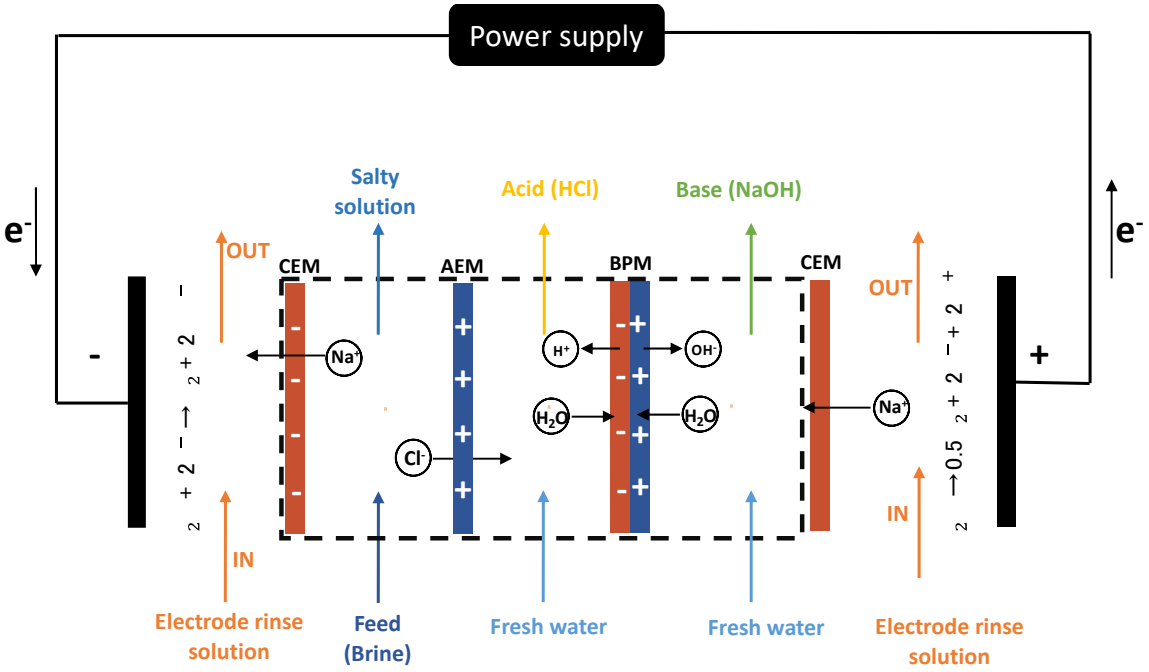

Figure 5. Schematic diagram of Electrodialysis with Bipolar membrane (EDBM).

Reverse electrodialysis (RED) is another promising near-to-commercialization salinity gradient power (SGP) technology. The RED system generates power by direct conversion of salinity different potential using ion exchange membrane while in contrast, pressure retarded osmosis process has required a turbine for power generation. **Figure *6*,** shows the basic concept of RED process technology, where a series of cation exchange membranes (CEMs) and anion exchange membranes (AEMs) arranged in an alternate sequence. A spacer has been placed between the cation and anion exchange membranes to separate them from one another and to make a channel where a high and low-concentrated solution can flow; electrochemical potential can be generated as cation and anion moved in opposite directions toward the electrodes. The positive ions diffuse through cation exchange membranes, while negative ions diffuse through anion exchange membranes. Finally, these chemical ions convert to electrical current via a redox reaction at the electrodes of the stack, as shown in **Figure *6*.**

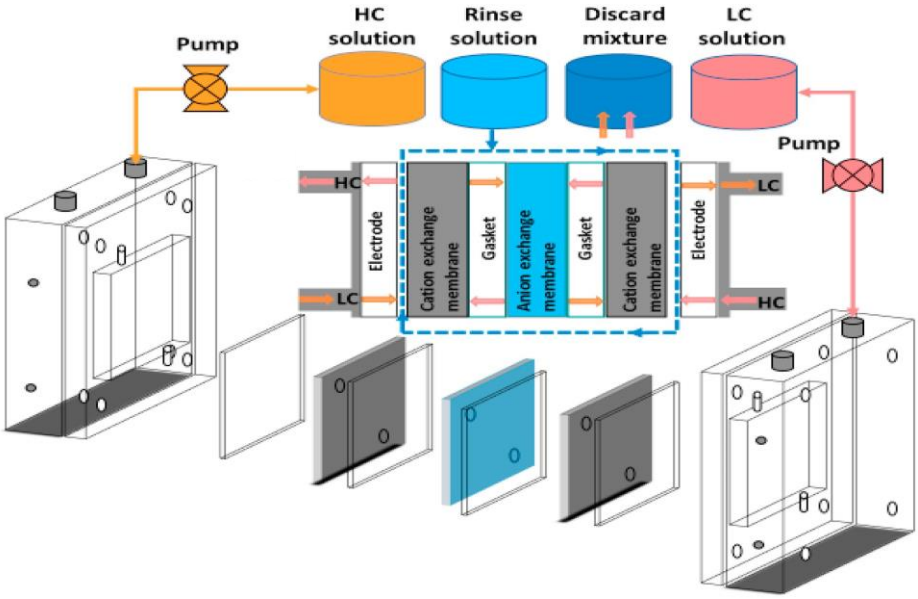

Figure 6. Schematic diagram of the RED unit [42].

Furthermore, the Fouling of ED and RED membranes is a common issue that has to be solved by pretreatment. For instance, some compounds in the feed solution, like sulfates or organic matter, are common precursors of membrane fouling problems.

Thesis aims and outline.

This thesis aims to investigate the potential of bipolar membrane electrodialysis (BMED) and reverse electrodialysis (RED) as innovative and sustainable technologies for treating saline wastewater. The primary focus is on concurrently generating renewable energy, high-value acids, and alkalis from dissolved waste salt, contributing to the critical necessity of salt resource regeneration. The research endeavors to address the environmental and economic challenges associated with saline wastewater treatment and harness the inherent energy and resource value in the process.

The study begins by exploring the extraction of critical raw materials from saltworks brines, employing ion exchange membranes to recycle concentrated brines through electrodialysis with bipolar membranes. Evaluation of non-woven cloth ion-exchange membranes and the impact of current density on membrane efficiency using a synthetic solution of sodium chloride form key aspects of the investigation.

Subsequently, Electrodialysis with Bipolar Membranes (EDBM) is examined for its effectiveness in treating synthetic mixed salt solutions resembling waste brine from saltworks. The study investigates the influence of initial monovalent and mixed salt feed solutions on the

performance of lab-scale EDBM, with a particular emphasis on NaOH production and energy efficiency.

The research then showcases the potential of brine valorization for renewable energy production through electro-membrane process technology. A laboratory-scale reverse electrodialysis (RED) unit captures and converts salinity gradient power (SGP) conveyed by concentrated bitterns discharged from saltworks. Different ion exchange membranes from various suppliers are tested, emphasizing the technology's efficacy for renewable energy production.

Expanding the exploration, the thesis delves into cost-effective and sustainable energy production through bitterns and power harvesting using a reverse electrodialysis (RED) system. It compares homogeneous Ion Exchange Membranes (IEMs) from different suppliers under various conditions, evaluating their characteristics and performance in real and pre-treated brine solutions. The findings underscore the superior properties of specific IEMs and their remarkable power densities in RED applications.

This thesis aims to contribute to the broader understanding of bipolar membrane electrodialysis and reverse electrodialysis technologies in saline wastewater treatment. It seeks to highlight their potential for transforming saline waste into valuable resources, fostering sustainability, and creating economically viable pathways for addressing environmental challenges associated with saline wastewater.

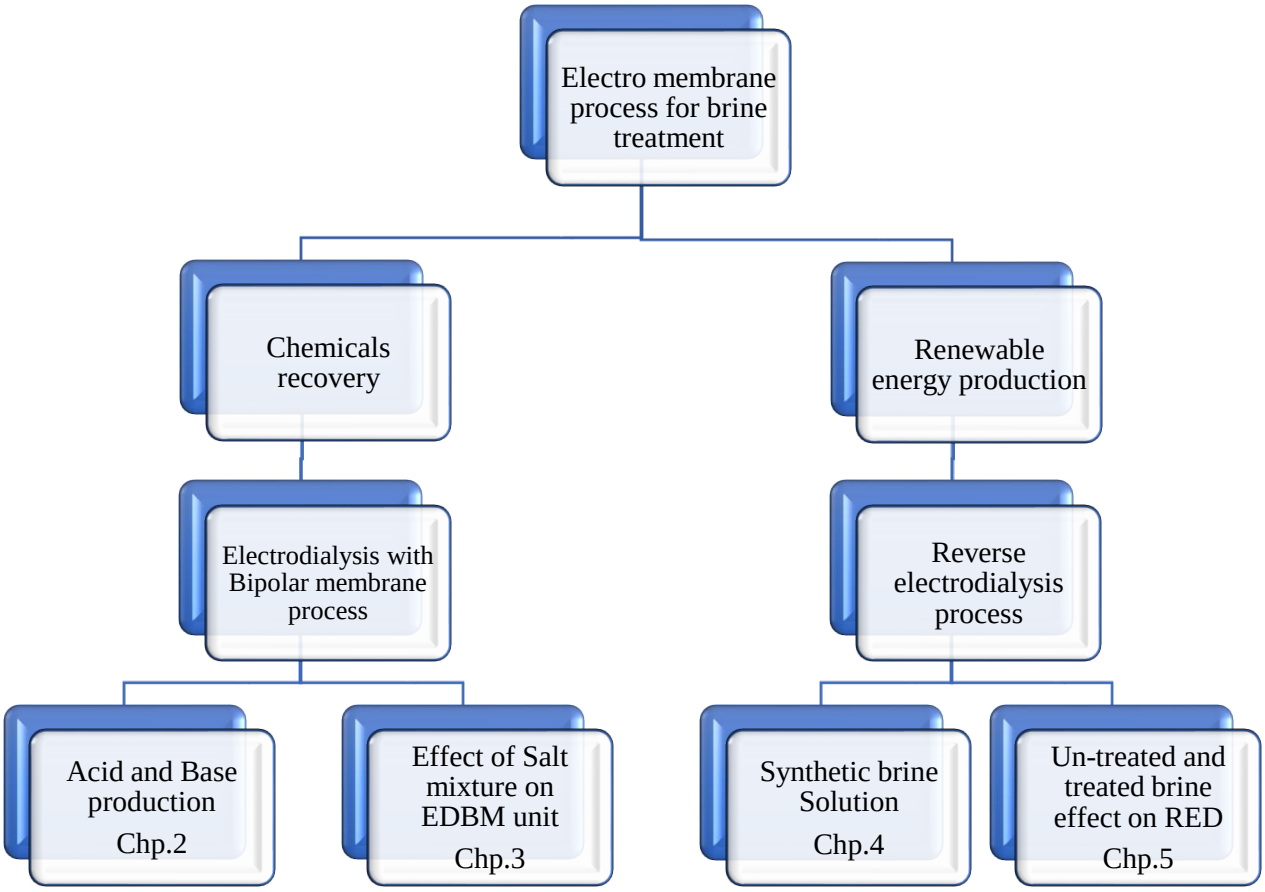

Figure 7. Visual illustration of the thesis outline, connecting the different chapters.

Chapter 2

Electrodialysis with Bipolar Membranes for generating NaOH and HCl solutions from brines: an inter-laboratory evaluation of thin and ultrathin non-woven cloth-based ion exchange membranes.

Graphical abstract:

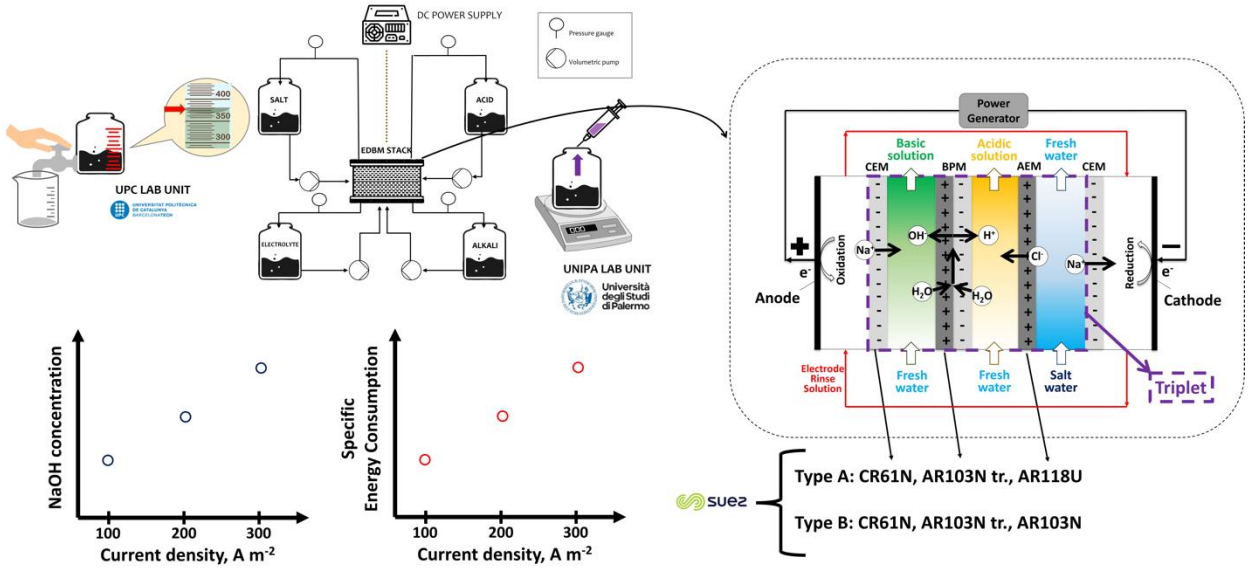

Abstract

The SEArcularMINE project addresses the critical raw materials (CRMs) shortage in Europe by recovering these materials from brines from salt works. To ensure a fully circular scheme, the project uses Electrodialysis with Bipolar Membranes (EDBM) to valorize concentrated brines and generate the necessary reactants (acids and alkalis). The study evaluated the performance of new non-woven cloth ion exchange membranes (Suez) - an ultra-thin non-woven polyester cloth and a thin polypropylene cloth as their support structure. The anion layer was also treated with a catalyst to promote the water dissociation reaction. An inter-laboratory exercise using 2 M NaCl evaluated the effect of current density (100, 200, and 300 $A \cdot m^{-2}$) on the performance of two combinations of membranes. Statistical analysis ANOVA showed agreement with the results obtained in both laboratories. Both combinations of membranes were able to generate NaOH/HCl solutions up to 0.8 M while working at 300 $A \cdot m^{-2}$. Thin polypropylene membranes performed better and showed lower Specific Energy Consumption (SEC) and higher Specific Productivity (SP) than thin polypropylene ones. Thin polypropylene membranes reported SEC between 2.18 and 1.69 and SP between 942.58 and 314.43 kWh kg m^{-2} y^{-1}. Overall, the project's approach towards EDBM, acid/base production, and brine management promises to address the issue of CRM shortage in Europe.

Keywords: EDBM; Acid/Base production; Brine management; Brine intensification, Ion-exchange membrane, AR118, CR61P

This chapter has been published as:

Tamara León[†], Syed Abdullah Shah[†], Julio López, Andrea Culcasi, Lluis Jofre, Andrea Cipollina, José Luis Cortina, Alessandro Tamburini, and Giorgio Micale. "Electrodialysis with Bipolar Membranes for the Generation of NaOH and HCl Solutions from Brines: An Inter-Laboratory Evaluation of Thin and Ultrathin Non-Woven Cloth-Based Ion-Exchange Membranes" *Membranes* 12, no. 12: 1204. https://doi.org/10.3390/membranes12121204

[†] These authors contributed equally to this work.

2.1 General Overview

The world population has grown continuously in recent years, posing new challenges for sustainable development. According to the European Union (EU) Circular Economy action plan, raw material consumption is expected to double by 2060, while waste production will increase by 70% by 2050 [43] Furthermore, the European Union has classified some raw materials as "critical" due to (i) their importance for producing goods across many industrial sectors and (ii) their high supply risk. The critical raw materials (CRMs) list [44] aims to recover these materials following a circular economy process, in agreement with the Green Deal action plan, which will allow to [44] reduce their reliance on non-European countries, as over 90% of raw materials are imported [45].

Seawater mining has been proposed as one of the most promising alternative ways to recover CRMs (e.g., magnesium, lithium) from seawater [46]. For example, brines from the desalination industry can be used effectively for materials recovery because of the high concentration of ions in the solution. In order to meet EU emissions targets, these saline wastewaters should be appropriately treated using methods such as Zero Liquid Discharge (ZLD) or Minimum Liquid Discharge (MLD). The ZLD and MLD approaches rely on pre-treatment and pre-concentration steps to achieve 95% water recovery; however, ZLDs also include post-concentration processes based on energy-intensive practices to achieve zero liquid waste emissions [47]. Nevertheless, ZLD and MLD processes barely put efforts centred on valorizing these concentrated streams to recover valuable compounds (e.g., single [48] or mixed salts [49]). However, the need to develop on-site chemicals production of commodities such as strong acids and bases has identified the use of Electrodialysis with Bipolar Membranes (EDBM) as a technology driver to achieve this objective through the valorization of waste brines.

Although EDBM is an electro-membrane technology postulated for decades to produce acids and bases from brines [50], two main technical limitations slow down its application at full-scale, such as: (i) the lack of high-performance ion exchange membranes (IEMs) (e.g., cationic (CEM), anionic (AEM) and bipolar (BPM)) and (ii) the economic feasibility of the produced chemicals. It should be mentioned that the market cost of strong acids, such as HCl and H_2SO_4, and strong alkalis, like, for example, NaOH, is affected by the transportation cost. The need to

mature this technology is supported by developing: (i) a deeper evaluation of the IEMs properties; (ii) new processing routes of brines as potential feed streams to be valorized; and (iii) new concepts of materials circularity and sustainability to overcome the economic feasibility barriers. As an example, the efforts devoted by the EU in promoting at the same time circular approaches and recovery of raw materials and/or production of chemicals in the case of the project creating a Sustainable Circular Approach to Mineral Extraction, SEArcularMINE (**Figure 8**) [51].

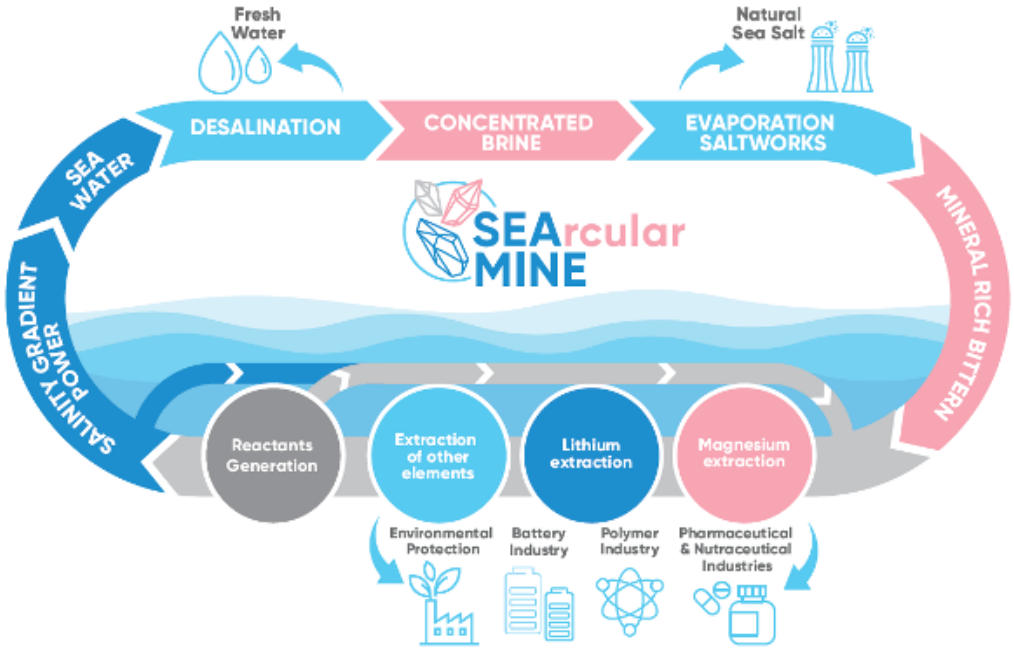

Figure 8. SEArcularMINE concept scheme (from [51])

Specifically, the SEArcularMINE project aims to use an innovative circular approach to valorize bitterns from saltworks to extract CRMs such as magnesium [52], lithium [53],[54], and other elements [55]. As the SEArcularMINE project is based on a fully circular concept, the reactants needed for its processes must be produced in situ. Therefore, to avoid the need for external chemical reagents, the concentrated and exhausted brines will be used in the EDBM process to generate the necessary alkaline and acidic reactants [56].

An EDBM unit is composed of a stack of repeating units. These, namely triplets, are made up of three channels (i.e., acid, alkaline, and salt), a monopolar CEM, a monopolar AEM, and a BPM, as illustrated in **Figure 9**. During operation, when a direct electric current is applied, the water molecules in the junction of the anion and cation exchange layers of the BPM are dissociated into protons (H^+) and hydroxide (OH^-) ions. The cations and anions in the feed

saline solution migrate through the CEM and AEM towards the cathode and anode, ultimately producing acidic and alkaline solutions [57].

EDBM has received significant attention from many researchers due to its wide range of applications [58]. The production of inorganic acids and bases from salts [59],[60] is one of the most common (semi-)industrial applications of EDBM [17]. EDBM has proven to be a promising and efficient method for chemical production due to its simplicity, as it requires just two inputs: electric energy and a saline feed [60]. As an example, several authors have evaluated the performance of EDBM for the valorization of brines [61], [62][63],[64]. Yang et al. [61] used seawater reverse osmosis (SWRO) brines to produce acid and base solutions at the laboratory scale, using CEMs and AEMs provided by Qianqiu® and BPMs provided by Fundtech®. In order to avoid scaling, the authors pre-treated the SWRO brine with $NaOH/CO_2(g)$ to remove Mg and Ca (<1.2 mg/L). Regarding EDBM tests, they achieved a concentration of acid and base solutions higher than 1 M with an average Specific Energy Consumption (SEC) of 7 kWh kg^{-1} HCl and Current Efficiencies (CEs) in the 50–60% range. In a similar work, Reig et al. [20] treated an SWRO brine in an electrodialysis unit, obtaining a NaCl-concentrated solution free of divalent ions that were fed to the EDBM. Tests were carried out in a lab-scale EDBM unit comprising PC Cell® membranes to produce 2 M of HCl and NaOH working at current densities of 300–400 A m^{-2} and with SEC values of 1.8–3.6 kWh kg^{-1} NaOH and CEs of 60-80%. Herrero et al. [63] utilized a lab-scale EDBM unit equipped with RALEX® monopolar membranes and Fumatech® BPMs. In this study, they reported the production of acid and base solutions from 3.3 mol L^{-1} to 3.6 mol L^{-1} from NaCl. These high concentrations were obtained by providing an electric current density of 1 kA/m^2 working at a salt-to-acid (and base) volume ratio of 20, thus resulting in high SECs (20–40 kWh kg^{-1} HCl). Finally, Davis et al. [64] investigated the use of Neosepta® membranes, achieving a maximum concentration of less than 0.4 M of acid and base with SECs in the range of 1–2 kWh kg^{-1} NaOH and 3.65 kWh kg^{-1} HCl.

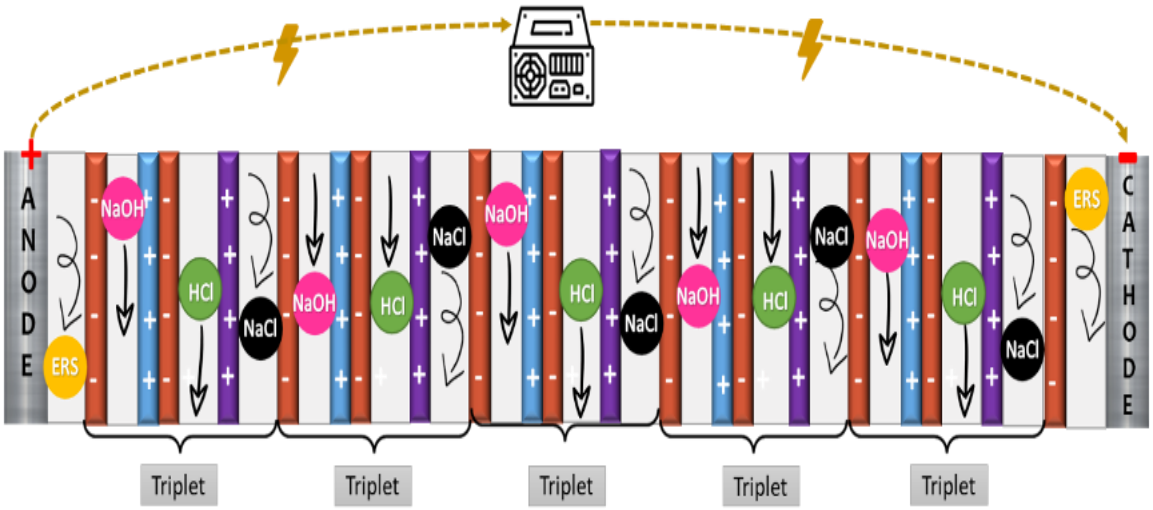

Figure 9. EDBM- unit scheme containing five triplets.

Numerous BPMs are available from different manufacturers for EDBM applications; several research studies have analyzed their performance and crucial properties[59], [65], [66]. As a result, the main challenges on EDBM are associated with the influence of the feed water composition on membrane performance, particularly the presence of dissolved organic matter or scaling forming agents in terms of operation problems (e.g., organic fouling, biofouling, and/or scaling). Other challenges were centred on modifying the membrane properties, mainly by increasing the separation factors of monovalent to divalent ions [67], [68], reducing the membrane electrical resistance [69], and decreasing the membrane cost by modifying the production processes. One option to improve the performance of IEMs manufacturers (e.g., SUEZ) might be using a non-woven polyester cloth in substitution of a woven acrylic cloth. The non-woven cloth membranes have a lower electrical resistance that reduces the required voltage to achieve a target salinity reduction and, consequently, a lower energy consumption. Since the membranes are made of non-woven cloth, they will not generate "strings" hanging on the exterior of the stack as the edge of the membranes become dry, as happens with the use of woven cloths. A second option was to convert membranes which use woven cloths, to a non-woven structure. AEM (AR103P) and CEM (CR61P) are cast on woven polypropylene cloth and are typically used in food and beverage applications. These membranes have been replaced by the AR103N and CR61N with a thin non-woven polypropylene cloth designed to provide a superior membrane product with lower power consumption and a smoother surface to reduce scaling and other deposits. Both membranes have been proposed as cation-selective and anion-selective layers of a BPM. The anion layer is treated with a catalyst to aid in the water-splitting

function of the membrane [70]. Additionally, this could improve the limitations described when using standard AEMs where H^+ is transported to the saline stream and limiting the concentration of acid that can be achieved. The performance of this new family of AEM (AR118U) as proton-blocking, allowing for higher concentrations in the acid and caustic streams (e.g., up to 1 M), has not been studied.

This work aims to present a comprehensive analysis of the performance of the EDBM process in the production of HCl and NaOH using a new family of IEMs incorporating thin non-woven polypropylene cloth (AR103N and CR61N) and ultra-thin non-woven polyester cloth (AR118U). To compare their performance, the Stack was assembled with different membrane types, namely Type A (AR118U, CR61N, AR103tr.) and Type B (AR103N, CR61N, AR103tr.). The BPM was built in both configurations by facing a CEM with an AEM (a treated AR103N (AR103.tr) in both cases). The treated AEM is a proprietary commercial product where a surface treatment of the active layer with a catalyst is performed to reduce the electrical consumption of the water-splitting reaction [71]. Feed solutions of NaCl simulating the bitterns generated in sea-water solar saltworks after the crystallization of salt and the removal of Mg were treated in the EDBM.

To accomplish this, experiments using two lab-scale EDBM units with the same membrane stack and located at different laboratories (UNIPA and UPC) were carried out in parallel to assess the complete reproducibility of the system performance. The inter-laboratory experimental plan examines the influence of several parameters, such as initial salt concentration and applied current density, on the leading performance indicators, such as SEC, CEs, and Specific Productivity (SP) of NaOH. Membrane performance results have been compared to literature findings relevant to widely used IEMs (e.g., monopolar and bipolar membranes) reported for producing NaOH and HCl.

2.2 Materials and Methods

2.1.1 Reagents and membranes

NaCl (99.7% chemSolute), HCl (37% Merck), NaOH (98-100% Honeywell Flute), and Na2SO4 (99-100% Honeywell Flute) were used to prepare the synthetic solutions. All the reactants were of analytical grade.

Suez kindly provided the monopolar CEMs and the AEMs. The BPMs were assembled by combining a CEM (containing quaternary ammonium groups) with a surface treated AEM (containing sulfonic acid groups). In the treated AEM, a catalyst enhances the water dissociation reaction (AEM-tr.). The needed voltage across the BPM for the water dissociation reaction is achieved by an immobilized metal (i.e., iron II) acting as a catalyst [72]. Woven polyester spacers with a thickness of 650 µm provided by SUEZ were adopted to give dimensional stability to the channels. The membranes selected for the experimental campaign of this work are the following a) AEMs: AR118U and AR103N, b) CEMs: CR61N, c) BPMs: a combination of AR103N-treated and CR61N. Two different combinations of these membranes during stack assembly were tested: (i) Type A (AR118U, CR61N, AR103tr.) and (ii) Type B (AR103N, CR61N, AR103tr.). Although all the membranes selected for this work are indeed non-woven cloth, there is a difference among them. The membranes ending in U (i.e., AR118U) have an ultra-thin non-woven polyester cloth as a support structure. In contrast, the others (ended in N) have a thin polypropylene non-woven cloth acting as their support structure. N-type reports a slightly higher perm selectivity; however, type U is thinner than type N. More details on the characteristics of each membrane are reported in **Table *1***, along with the features of some other commercially available membranes, for comparison.

Table 1. The main characteristics of some membranes used for EDBM.

Manufacture	Membrane	Identification	Functional groups	Ion Exchange Capacity	Wet Thickness (µm)	Composition	Permselectivity (%)	Refs.
[1]SUEZ	AEM	AR103P	quaternary ammonium	2.37 (meq/dry g resin)	570	Woven polypropylene	92	[73]
	CEM	CR61P	sulfonic acid	2.2 (meq/dry g resin)	580		94	
	AEM- treated	[4]AR103A tr.	quaternary ammonium	2.37 (meq/dry g resin)	300		92	
[1]SUEZ	AEM	[2]AR103N	quaternary ammonium	2.37 (meq/dry g resin)	300	Thin non-woven polypropylene	92	[73]
	AEM	[3]AR188U	quaternary ammonium	2.37 (meq/dry g resin)	130	Ultra-thin non-woven polyester cloth	90	

	CEM	[2,3] CR61N	sulfonic acid	2.2 (meq/dry g resin)	300	Ultra-thin non-woven polyester cloth	95	
	AEM-treated	[2,3,4] AR103N tr.	quaternary ammonium	2.37 (meq/dry g resin)	300		92	
LLC Innovative Enterprise Schekinozoat	AEM	MB-1	quaternary ammonium	4.0 (eq/L)	<900	Polyestrye ne divinylben zene with polyethyle ne binder	98	[74]
	CEM		sulfonic acid	1.4 (eq/L)	<900		98	
MEGA	AEM	BMI-9000	quaternary ammonium	1.3 (meq/dry g resin)	450	Gel polystyren e crosslinke d with divinylben zene	91	[72]
	CEM		sulfonic acid	1.6 (meq/dry g resin)	450		91	

[1]SUEZ BPMs are not cited in this table since they are the combination of treated AEMs with CEMs.

[2]Type A membranes used for the experimental campaigns in the present work.

[3]ype B membranes were used for the experimental campaigns in the present work.

[4]AEMs with catalyst (i.e. immobilized iron II) by immersing them in transition metal solution.

2.2.2. Laboratory-scale experiment setup

Experiments were performed in two EDBM laboratory-scale units supplied by SUEZ (Electromat MkI ED STACK). Each EDBM unit incorporates a membrane stack (HDWR MK-1) with an active membrane area of 0.028 m^2 (0.167 m x 0.167 m). The membrane assembly contained the following components: (i) 5 repeating units, (ii) anode electrode (stainless steel with platinum coating), (iii) cathode electrode (stainless steel with platinum coating), and (iv) spacers (polystyrene). Considering that the EDBM unit is indeed an electrochemical one, an electrode rinse solution (ERS) flowing between electrodes and membranes is required to spread the driving force (i.e., electricity).

The EDBM units are designed for a closed-loop (batch) configuration with four separate hydraulic circuits for the acid, base, salt, and electrode rinse solutions. Each hydraulic circuit was assembled with a volumetric pump and equipped with a pressure gauge for that purpose.

The electrolyte solutions are stored in four different containers with a volume capacity of 2 L. The EDBM process requires the application of an electric field as a driving force, so each EDBM unit was also equipped with a power supply working under galvanostatic mode. During the experiments, several operating parameters were monitored: (i) temperature, (ii) external voltage and current, (iii) electrical conductivity of the electrolyte solutions, (iv) volume evolution for all the containers, (v) pressure, and (vi) flow rate. The target of the experiments was to reach a final concentration of acid and alkali up to 0.8 M.

EDBM experiments were run in parallel at the same conditions at UNIPA and UPC premises with an almost identical setup. However, some minor differences in each setup are highlighted for completeness in

Table 2*, and displayed in*

Figure *10*. It is worth noting that these differences did not affect the results' quality or the experiments' reproducibility.

Table 2. Differences between UPC and UNIPA EDBM lab scale setups

	UPC	**UNIPA**
Pump system	4 centrifugal pumps (BED 1-4 from PCCell GmbH)	4 peristaltic pumps (BT601S from Lead Fluid Technology, CO LTD, China)
Sampling	Samples are taken directly from tanks coupled with ball valve taps	Samples are taken from the tanks using syringes.
Power Supply	Switching mode Power Supply (HCS-3202)	Switching mode Power Supply (BK PRECISION 1902B)
Volume evolution in the vessels	Vessels were volumetric cylin ders, allowing the monitoring of volumes variation	The volume is the result of relating mass and density. The mass evolution is controlled using analytical scales.

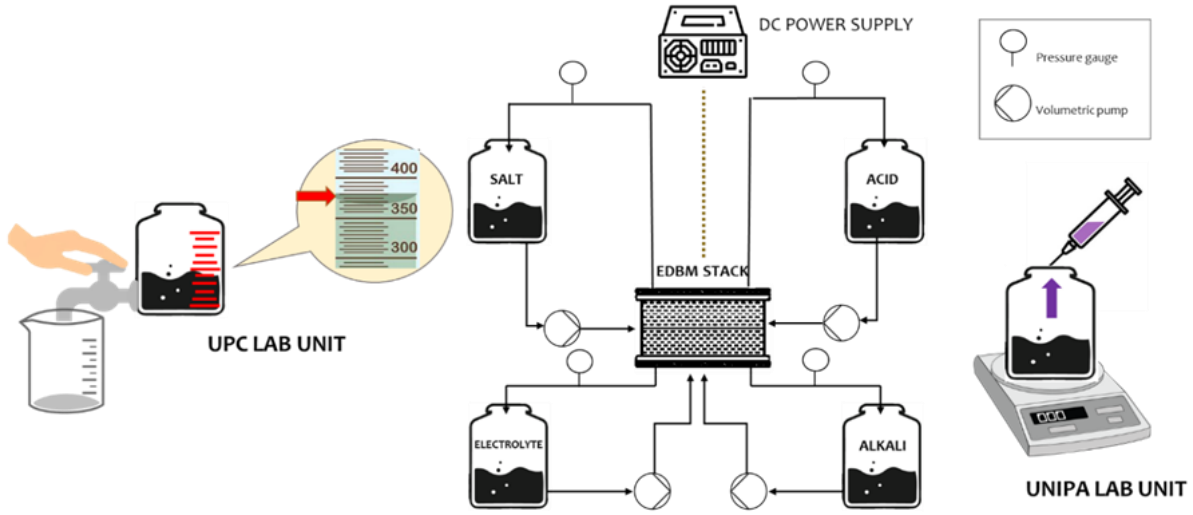

Figure 10. Scheme of EDBM units installed at UPC and UNIPA facilities along with a few procedural differences.

2.2.3 Analytical methodologies and chemical analysis

Sixteen samples on average (four per each compartment, 5 mL each) were taken during each EDBM experiment. HCl and NaOH samples were analyzed by acid/base titration. At UPC facilities, titration was performed using an automatic titrator (T70, Mettler Toledo) equipped with an automated titration stand (Rondolino, Mettler Toledo); HCl and NaOH solutions 100 µM (previously standardized) were used as titrants. At UNIPA, titration was executed using as titrants a standard HCl 0.10 M and Na_2CO_3 0.05 M solutions and methyl orange as pH indicator.

The pH and conductivity evolution were monitored using conductivity meters (3320, Xylem Analytic Germany FmbH D-82362 Weilheim) and pH meters (3320, Xylem Analytic Germany FmbH D-82362 Weilheim; Crison pH Basic 20) at both premises.

2.2.4 Experimental campaign

Initially, preliminary tests were performed to ensure the experimental results were reproducible. These tests were performed under identical process conditions in terms of applied current, mean channel flow velocity, and initial acid, base, salt, and electrode rinse solution composition (see Table 3). Synthetic brine solutions (a.k.a. salt solutions) prepared with NaCl, and distilled water were used in the execution of EDBM experiments. The experiments were carried out with an initial non-zero concentration of acid and base, as shown in Table 3, to reduce the electrolyte solutions' electrical resistance. Then, the effect of

varying (i) the combination of membranes (Type A and B) and (ii) the applied current density was investigated.

Table 3. sums up the operational conditions adopted in EDBM experiments.

Table 3. Operational conditions adopted in EDBM experiments include current density, initial concentrations of the different streams, flow rates and initial volume of the products containers.

Current Density	Channel	Initial concentration	Initial volume	Flowrate
100-300 A m^{-2}	Acid	0.05M HCl	1.0 L	50 L h^{-1}*
	Base	0.05M NaOH	1.0 L	50 L h^{-1}*
	Salt	2M NaCl	1.5 L	50 L h^{-1}*
	ERS	0.25M Na_2SO_4	1.5 L	50 L h^{-1}*

* Corresponding fluid velocity in the channel equal to 7 m/s.

2.2.5 Performance parameters of the performance of NaOH and HCl production by EDBM

All the performance parameters were referred to the amount of NaOH produced due to its economic and industrial interest.

Specific Energy Consumption (SEC, kWh kg$^{-1}_{NaOH}$) refers to the amount of energy necessary to produce one kilogram of NaOH [75]. It was calculated according to

$$SEC = \frac{I \cdot \int_0^t U \cdot dt}{3.6 \cdot 10^6 \cdot (C_{NaOH,t} \cdot V_{NaOH,t} - C_{NaOH,0} \cdot V_{NaOH,0}) \cdot M_{NaOH}} = \frac{F \cdot \int_0^t U \cdot dt}{3.6 \cdot 10^6 \cdot M_{NaOH} \cdot CE \cdot N \cdot t}, \quad (1)$$

Where U (V) and I (A) are the external voltage and applied current to the stack, respectively, $C_{NaOH,t}$ (mol·L^{-1}) is the concentration of NaOH at a specific time (t) during the experiment, $C_{NaOH,0}$ (mol·L^{-1}) is the initial concentration of NaOH, V_{NaOH} (L) is the volume of the base solution, M_{NaOH} (kg·mol^{-1}) is the molecular weight of NaOH, and t (h) is the operation time.

Current Efficiency (CE) refers to the percentage of current consumed for the water dissociation reaction to take place [76]. *CE* was calculated as

$$CE = \frac{(C_{NaOH,t} \cdot V_{NaOH,t} - C_{NaOH,0} \cdot V_{NaOH,0}) \cdot F}{I \cdot N \cdot t}, \quad (2)$$

Where F (96,485 C•mol^{-1}) is the Faraday constant, N is the number of triplets of the EDBM stack (i.e., 5 in this work).

Finally, it is essential to relate the installed membrane area with the amount of NaOH that can potentially be produced in a working year (assumed to be 8000 hours) [75]. This relationship is critical when the process is scaled up to the industrial production level. This parameter is called Specific Productivity (SP, kg NaOH m^{-2} y^{-1}) and was calculated according to

$$SP = \frac{M_{NaOH} \cdot (C_{NaOH,t} \cdot V_{NaOH,t} - C_{NaOH,t_0} \cdot V_{NaOH,t_0})}{N \cdot 3 \cdot S \cdot 8000}, \quad (3)$$

Where S (m^2) is the active area of a membrane, and the 8000-factor accounts for a one-year time production of NaOH.

2.2.6 Reproducibility analysis procedure to assess the inter-laboratory results

To affirm that reproducibility was achieved among the results from UNIPA and UPC, the ANalysis of VAriance (ANOVA) was conducted using Single Factor ANOVA in Excel®. ANOVA allows comparing more than two groups simultaneously to determine whether there is a relationship between them. Applying ANOVA's formula, the Factor statistic (F-value) is used to analyse multiple data groups to determine the variability between samples and within samples [77]. Through statistical analysis, the relevance of the factor of performing the EDBM experiments in different laboratories was analyzed. Considering a significance level (α) of 0.05, results are considered statistically different if the F-value calculated (Fc) is minor than the critical F-value (Fcr), which is called the null hypothesis [77].

2.2.7 Diffusion of OH^- and H^+ through the EDBM stack

We performed a diffusion experiment to study the diffusion of OH^- and H^+ through the EDBM stack assembled with Type A and Type B ion exchange membranes. During this experiment, we chose the average salt, acid, and base concentration value. The salt compartment of 1.5 L was fed with a concentration of 1.8 M NaCl. In addition, a solution of 1 L of acid and a base of 0,5 M was circulated in the EDBM unit. A 1 L of Na_2SO_4 (0,25M) was used as an electrode rinse solution. During the diffusion test, no electric current was applied. A sample of 5 mL of

60 minutes was collected from the acid and base compartment, and their concentration was measured by the acid-base titration method.

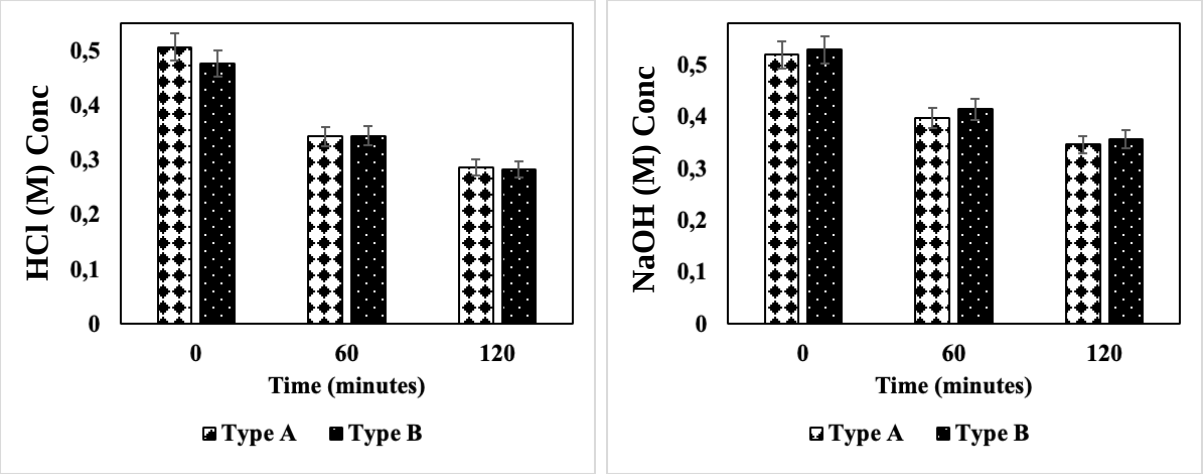

Figure 11. The NaOH and HCl concentration decreased during the diffusion test.

Figure 11, illustrates the OH^- and H^+ concentrations throughout the diffusion test for Type A and Type B membranes used during this study. The change in acid and base concentration for both types of ion exchange membranes is identical. The decrease in the acid compartment after 1 hour was 32%, and the change was 16% in the last part of the experiment. Similarly, the change during 1 hour in the base compartment was 21% and 12% after 120 minutes of the investigation. The conductivity of the salt compartment decreased from 126 mS/cm to 102 mS/cm during the investigation, while the pH value of the salt compartment reduced from 8,4 to 2 during the early stage of the test for both types of membranes.

2.3. Results and Discussion

The results of the reproducibility analysis and the study of the effect of current density and saline concentration in the salt tank are presented and thoroughly discussed in this section.

2.3.1 Reproducibility analysis

EDBM experiments were carried out in two different laboratories to demonstrate the results' reproducibility and the experimental method's reliability. Therefore, the information presented in this section results from the efforts of the two institutions. Additionally, the information

displayed has been corroborated at least four times, thus demonstrating the accuracy of the experimental results.

Figure 12, presents the HCl and NaOH concentrations measured at different time intervals in the acid and base channels, respectively, obtained with the two laboratory EDBM units at UPC and UNIPA with a starting concentration of 2 M NaCl in the feed compartment and at a current density of 100 A m^{-2}.

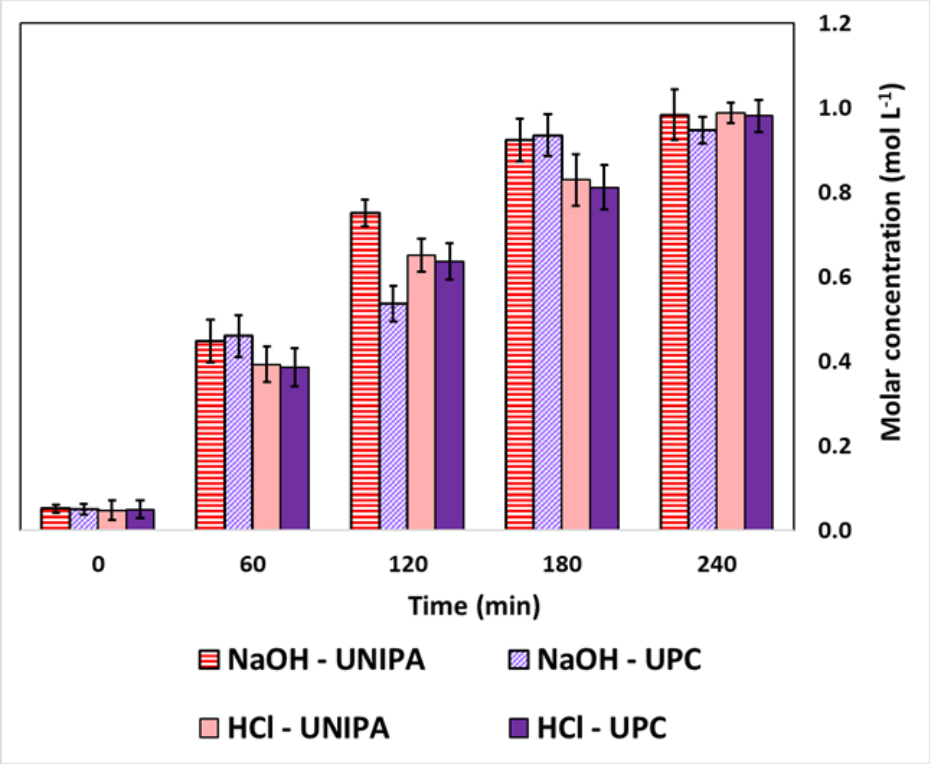

Figure 12. HCl and NaOH concentrations were measured at different time intervals for the experiments performed at UNIPA and UPC premises. Initial salt composition: 2 M NaCl. Applied current density: 100 A m^{-2}.

In both the UPC and UNIPA experiments, the duration of the experiments was 240 min. Since these tests were performed in a closed-loop configuration with constant applied current, the HCl and NaOH concentrations increased over time, as expected. The acidic solution reached a concentration of 0.99 M for UNIPA and 0.98 M for UPC at the end of the experiments. Similarly, the concentration of the alkaline solution was 0.98 M for UNIPA and 0.95 M for UPC at the end of the experiments. Notably, the concentration increase rate was not constant throughout the investigation but decreased over time. Indeed, as shown in the first hour of the experiments, the concentration of both the acid and alkaline solutions changed from 0.05 M to 0.45 M for NaOH and from 0.05 M to 0.39 M for HCl. In the last hour of the experiment, the

concentration increase rate fell from 0.40 M h^{-1} to 0.06 M h^{-1} during the experiment for NaOH, whereas it decreased from 0.34 M h^{-1} to 0.16 M h^{-1} during the experiment for HCl.
Indeed, the higher the concentration gradient of the species across the membranes, the more significant the effect of non-ideal phenomena such as diffusion and water transport.

Moreover, the latter is strongly affected by the osmotic pressure difference across the membranes, which depends on the solution composition. Furthermore, a significant reduction in the pH of the saline solution was observed in both UNIPA and UPC experiments, resulting in a pH less than 2. This can be attributed to the higher mobility of protons compared to hydroxide ions, thus leading to greater acid diffusion in the saline compartment compared to the base compartment. The concentration trends for both acid and base showed slight deviations between the results of both institutions. The ANOVA analysis was performed for both the acid and the alkaline solutions. The analysis of the acid solution determined values of Fc lower than Fcr (0.01 < 4.965). Likewise, for the base solution, the values of Fc were also lower than Fcr (0.033 < 4.965). Therefore, statistically, the effect of performing EDBM experiments at different laboratories on the profile concentrations was not significant.

Figure 13, shows the SEC and the CE as functions of time.

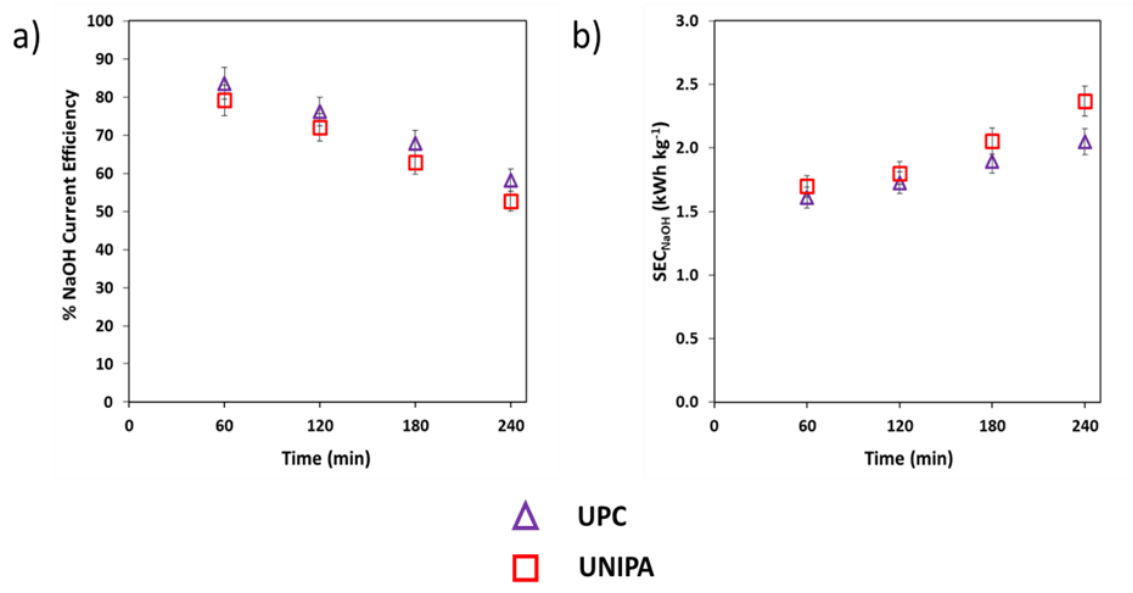

Figure 13. a) Current efficiency and b) Specific Energy Consumption (SEC) as function of time for the experiment carried out in UNIPA and UPC premises. Initial salt concentration: 2 M NaCl. Applied current density: 100 Am^{-2}.

The SEC_{NaOH} increased gradually in the experiments from 1.69 kWh kg-1 to 2.34 kWh kg-1 at UNIPA and from 1.61 kWh kg-1 to 2.05 kWh kg-1 at UPC during the experiments (Figure

13b). The ANOVA analysis was also performed with the SEC values to demonstrate reproducibility in the experiments at UNIPA and UPC. The analysis revealed that Fc was less than Fcr (i.e., 0.892 < 5.318), suggesting that the effect of performing EDBM experiments at different laboratories on SEC values was not statistically significant. Conversely, Figure 13a depicts the CE evolution as a function of time. Since CE refers to the fraction of electric current used to produce water dissociation, it was expected to decrease throughout the experiment. UNIPA reported a decrease in CE from 79.2% to 52.70%, while UPC reported a reduction in CE from 83.55% to 58.25%. The drop in CE can be attributed to unfavorable phenomena such as back diffusion and water transport across the membranes [78]. The ANOVA analysis also used the CE data to demonstrate the reproducibility of both laboratories. The results showed that Fc was lower than Fcr (i.e., 0.641<5.318). As a result, the effect of conducting EDBM experiments at different laboratories was not statistically significant in terms of CE values too. It can be concluded that considering the ANOVA analysis carried out among the monitored parameters (i.e., HCl and NaOH concentrations, SEC, and CE) from both laboratories, the experimental collected data was not statistically different. Therefore, the results coming from the two laboratories are reproducible. Once reproducibility was confirmed, the experimental campaign was divided between the two institutions to expand the range of the data collected. The analysis results at various applied current densities and combinations of membranes will be presented and discussed in the following sections.

2.3.2 Effect of Current Density in the Different Types of Membrane Configurations Used in the EDBM Set-Ups

The applied current is one of the most critical parameters of the EDBM operation [79]. Three different values of current density (i.e., 100, 200, and 300 A m^{-2}) were adopted and tested for the two combination of membranes during stack assembly (i.e. Type A and Type B). In the experiments, the initial operating conditions reported in **Table 3**, were employed. The results were demonstrated in terms of concentrations, SEC, CE, obtained when varying the current density.

The current efficiency is influenced by the applied current as well as by the investigated membranes. **Figure *14***, shows a growing trend in the concentration values of the products as the applied current was increased for both Type A and Type B.

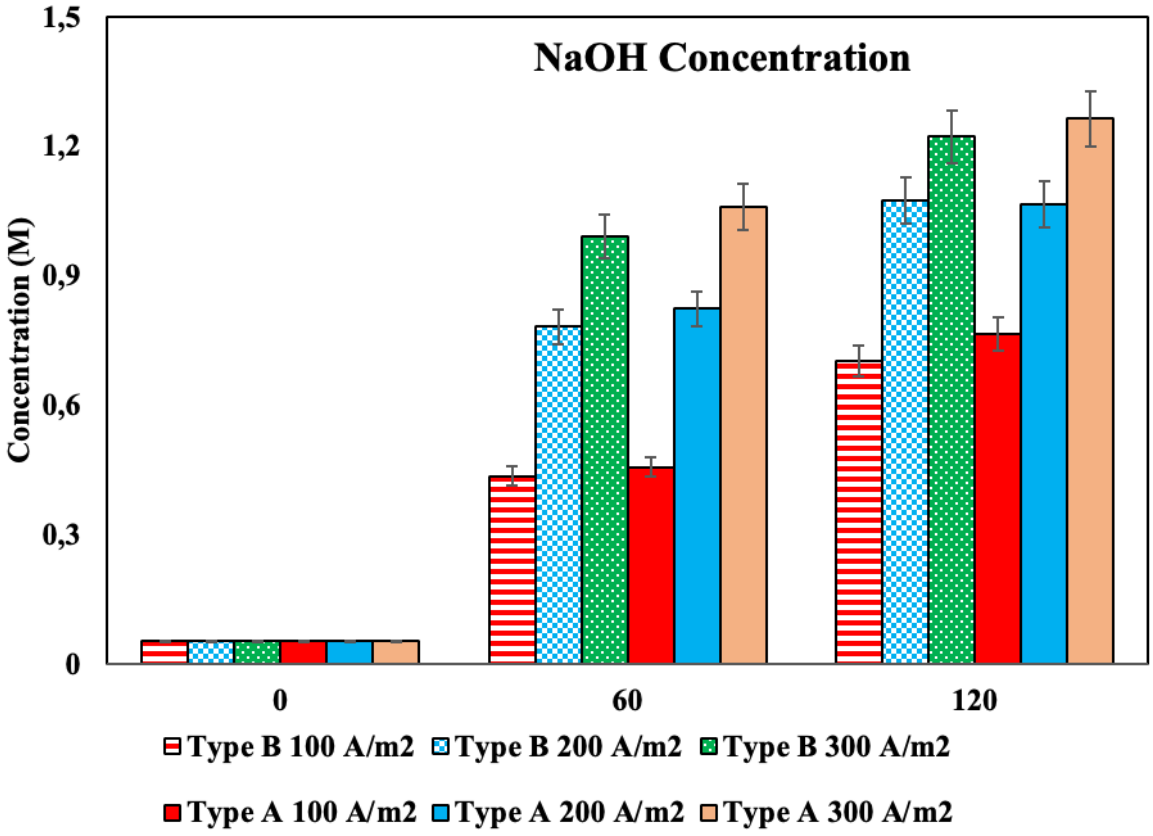
NaOH Concentration
Concentration (M)
1,5
1,2
0,9
0,6
0,3
0
0
60
120
Type B 100 A/m2
Type B 200 A/m2
Type B 300 A/m2
Type A 100 A/m2
Type A 200 A/m2
Type A 300 A/m2

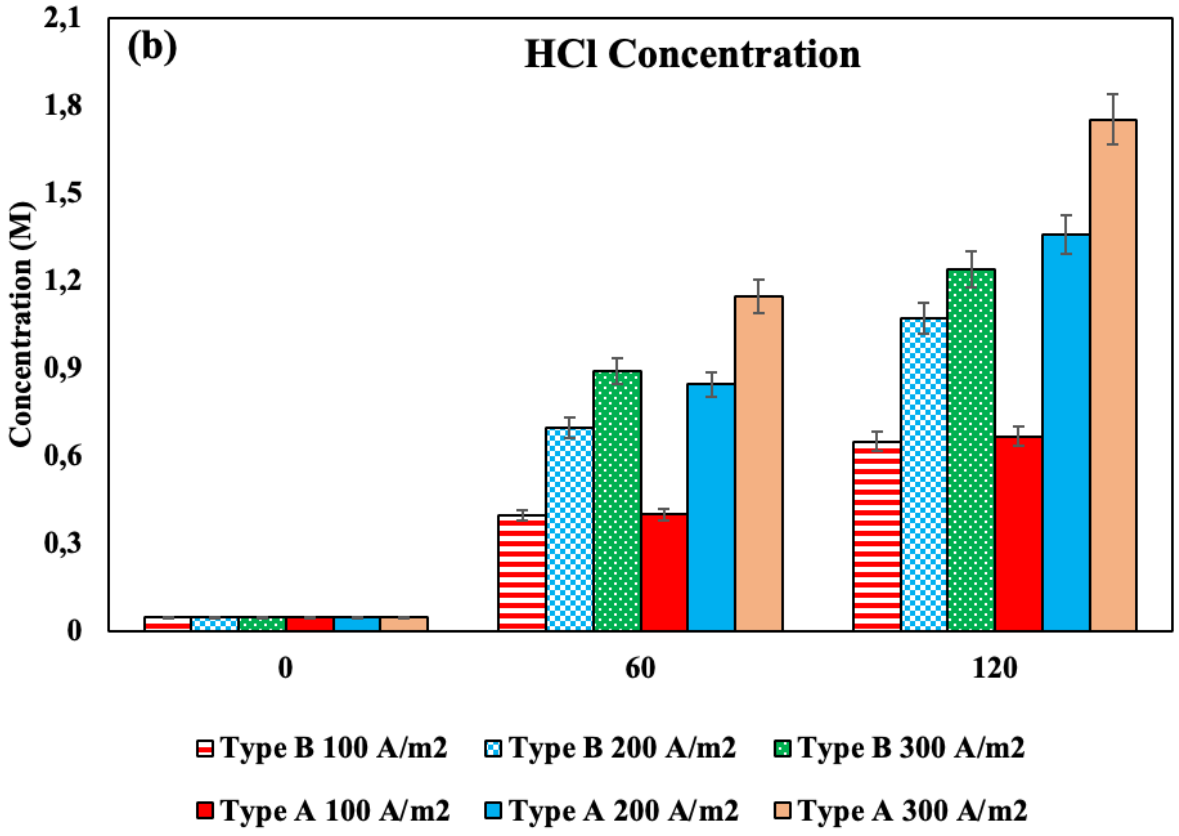
(b)
HCl Concentration
Concentration (M)
2,1
1,8
1,5
1,2
0,9
0,6
0,3
0
0
60
120
Type B 100 A/m2
Type B 200 A/m2
Type B 300 A/m2
Type A 100 A/m2
Type A 200 A/m2
Type A 300 A/m2

Figure 14. Concentration profile (M) of HCl and NaOH versus time at three different current densities for Type A and Type B membranes: densities: 300 A m-2, 200 A m-2 and 100 A m-2. Initial NaCl con-centration 2 M.

At the end of the experiments (i.e., after 120 minutes of operation), Type A exhibited more concentrated acid and alkali solutions than Type B. The most concentrated solutions were generated when applying 300 A m^{-2}. Hence, as the current density increases, the final concentration of products attained during the same process time also increases. This is due to the faster rate of water dissociation in the BPM junctions as the applied current increases.

Figure *15* shows the current efficiency profiles of both types of membranes over time when varying the applied current density. The current efficiency decreased over time regardless of the applied current or the type of membranes. Two significant phenomena cause the current efficiency to decrease. Firstly, there is a higher acid and base ion diffusion into the salt compartments as the process progresses. In fact, as the experiments were conducted in a closed loop, the acid concentration gradient across the anion exchange membrane and the base concentration gradient across the cation exchange membrane increased over time. Therefore, some of the produced acid and base species are neutralized in the saline compartment. The other phenomenon causing the decreased current efficiency over time is the non-ideal perm selectivity of the bipolar membranes. This reduces the membrane flux of protons and hydroxide ions, partially replaced by sodium and chloride ions transport through the bipolar membrane layers, resulting in lower current efficiency [80]. In our experiments, higher applied currents are associated with lower current efficiencies. At 100, 200, and 300 A m^{-2}, the current efficiencies for Type A at the end of the test were 72.0%, 55.2%, and 48.5%, respectively. On the other hand, the current efficiencies for Type B at the end of the test were 65.45%, 58.3%, and 48.91%, respectively.

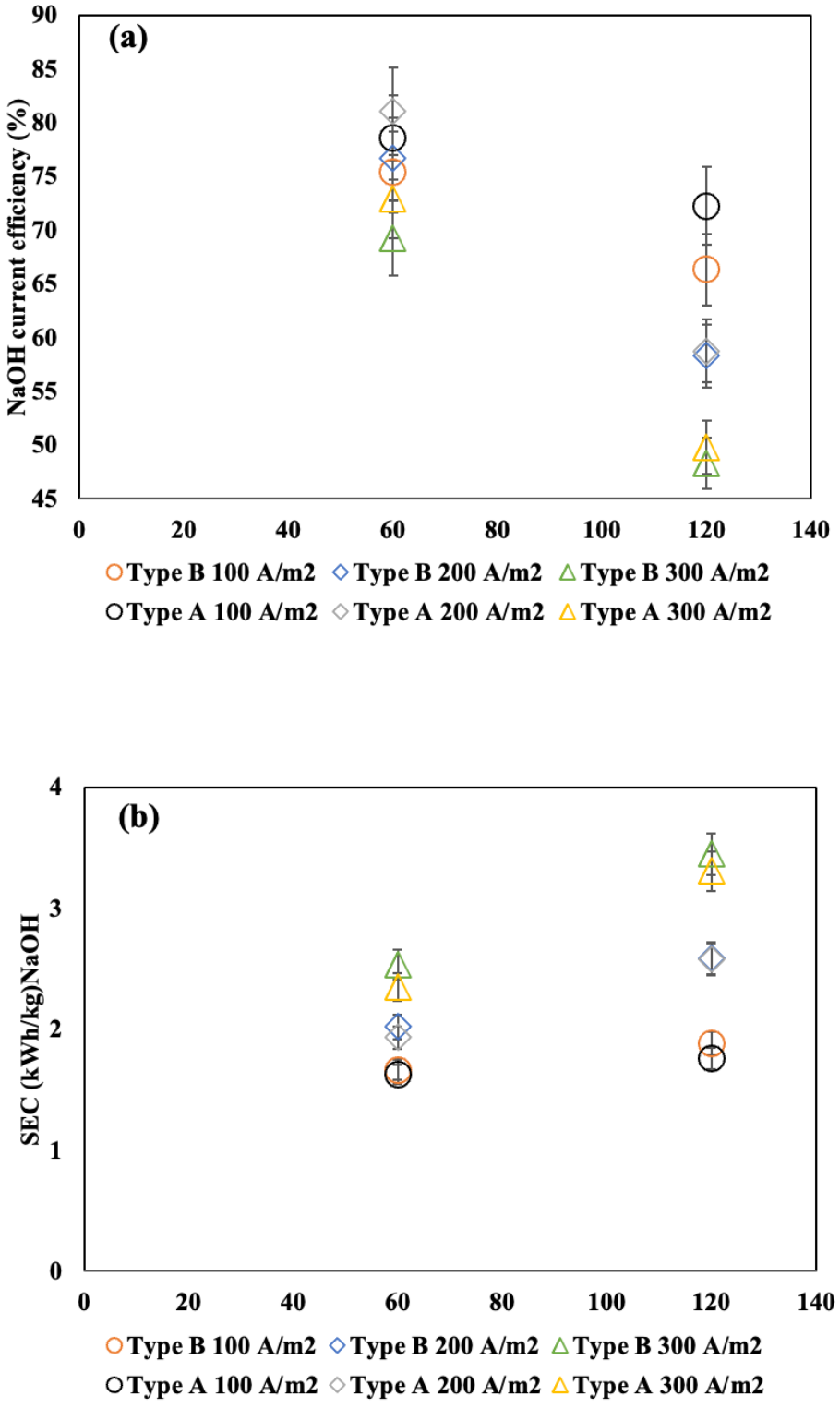

Figure 15. a) Current efficiency and b) Specific Energy Consumption (SEC) versus time at three different current densities: 300 A m-2, 200 A m-2 and 100 A m-2. Initial NaCl concentration 2 M for Type A and Type B membranes.

Figure *15* (b), depicts the Specific Energy Consumption at 100, 200, and 300 A m^{-2}. The SEC increased over time, regardless of the applied current. This was the result of two opposing effects. On the one hand, the applied voltage is reduced over time, thus reducing the SEC. On the other hand, as previously observed, there was also a decrease in current efficiency. The latter phenomenon prevailed, resulting in an overall increase in the SEC. When operating at 100, 200, and 300 A m^{-2}, the final SEC values for Type A were 1.80, 2.63, and 3.29 kWh/kg, respectively. Similarly, Type B reported SEC values of 1.87, 2.9, and 3.33 kWh/kg, respectively.

Results were compared with the ones previously published in the literature (see **Table 4***) [76], [81]–[83]. In the present paper, the CE (%) values were lower than the previous studies reaching a maximum of 72% with Type A with an average SEC of about 2. The average current efficiency values obtained, as shown in* **Table *4***, are consistent with those reported in the literature. Reig et al. [76] obtained the highest values, likely due to a lower effect of non-ideal phenomena (e.g., non-perfect stack sealing or misalignment of the membranes and spacers or even micro-holes in the membranes). In addition, the SEC values obtained in the present work are among the lowest recorded in the literature due to the operating conditions utilised. Indeed, in the present work, the applied maximum current density was 300 A·m^{-2}, whereas most previous works used a higher current density (see **Table *4***). This study highlighted that the SEC is strongly influenced by the reached acid and base concentrations, the average concentration of NaCl in the salt channel, and the current efficiency. For example, when high acid and base concentrations are obtained, the higher diffusive flows across the monopolar membranes to the saline compartment significantly reduce current efficiency. Additionally, the high pH gradient causes an increase in the Nernst potential. The two latter phenomena lead to a rise in SEC. The operating time reported in the literature varies greatly. However, the operating time is proportional to the volume of the solutions in the external tanks. At the same operating and design conditions, a longer time will be required as the volume of solutions increases.

Furthermore, when comparing the five different types of membranes shown in **Table 4,** the SUEZ membrane produced acid and alkaline solutions with similar concentrations to those obtained with PCCell membranes in the shortest time. SUEZ membranes had a relatively low SEC despite having one of the largest active membrane areas among those studied. Further research could focus on technical-economic analyses to investigate the profitability of EDBM technology using various types of membranes.

Table 4. Comparison between current data vs Other published literature.

Setup			Experimental conditions					Concentrations (mol/L)			Performance parameters		Ref.
Membranes		Membrane stack	Active area (cm^2)	Nº triplets	Current density ($A \cdot m^{-2}$)	Operation time (min)	Operation mode	Initial Salt solution	Final HCl	Final NaOH	SEC (kWh/kg)	CE (%)	
SUEZ	AEM: AR118U & AR103N	HDWR MK-1) Suez	280	5	100-300	120	Batch	2 M NaCl	1.77	1.25	3.29	48.5	This work
	CEM: CR61N												
	BM: AR103N-treated layered with CR61N												
PCCell	CEM: PC-SK	PCCell ED64-	64	3	520	405	Batch	3.2 M NaCl	2.01	1.87	2.71 (NaOH)	88 - 55	[76]
	AEM: PC Acid 60												
	BM: PC BP												
MEGA	CEM: M-PP RALEX	Elektrolyse Project	100	1	1000	2400	Semi-batch	1 M NaCl	3.17	3.63	41.0 (HCl)	n.d.	[82]
	AEM: M-PP RALEX												
Fumatec	BM: Fumasep FBM												
Qiang	CEM	Shandong Tianwei	88	3	570	140	Batch	Pre-treated RO concentrate	0.65	n.d.	9.0 (HCl)	n.d.	[81]
	AEM												
Fumatec	BM												
Neosepta	CEM: Neosepta CMX	PC-Cell EDQ380	385	8	121	-	Single-pass	0.19 M NaCl	0.15	0.14	3.65 (HCl)	80	[83]
	AEM: Neosepta ACM												
	BM: Neosepta BP-1												

2.3.3 Performance parameters of the two types of membranes

This paragraph compares the performance of the two types of membranes (i.e., A and B) investigated in this study. The comparison was carried out in four different scenarios. Each

corresponds to two different NaOH concentrations reached, either 0.4 M or 0.8 M, and two different applied current densities, either 100 or 300 A m^{-2}, corresponding to the lower and upper values of the current density range investigated in this work. These scenarios are reported in **Table *5***.

Table 5. List of the investigated scenarios.

	Current density (A m^{-2})	NaOH target concentration
Scenario 1	100	0.4 M
Scenario 2	100	0.8 M
Scenario 3	300	0.4 M
Scenario 4	300	0.8 M

Histograms were used to compare the performance parameters: Specific Energy Consumption (SEC), Current efficiency, Yield, Specific Productivity (SP), effective production, and Production time. The performance parameters were determined based on sodium hydroxide, which is the most valuable commercial product. The histograms of the performance parameters are reported in **Figure 16**.

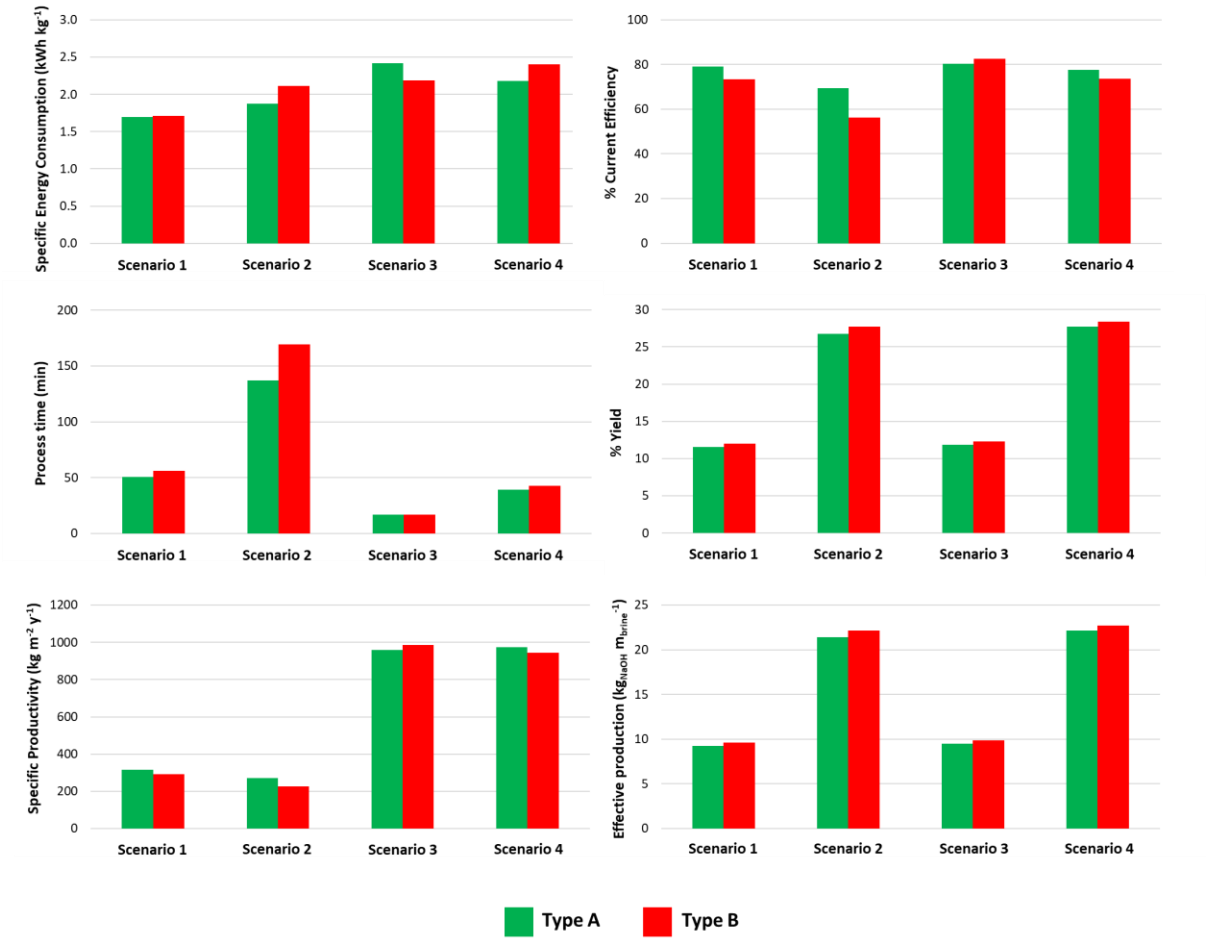

Figure 16. Comparison between the two types of membranes A and B in terms of Specific Energy Consumption, % Current efficiency, Process time, Yield, Specific Productivity and effective production for each investigated scenario.

The results indicate that the membranes behave differently depending on the applied current and NaOH concentration target. Specifically, when operating at a lower electric current (i.e., at 100 A m^{-2} in this case), the performance of the two types of membranes was similar at 0.4 M NaOH. This can be observed by comparing the SEC values with a 6% SEC for Type A membranes, which can be related to the lower impact of non-ideal phenomena, such as species diffusion and water transport across the membranes. Overall, the higher stack voltage offset the higher CE of membranes A, resulting in a very similar SEC as previously mentioned.

However, the performance varied in favour of type A membranes at a target of 0.8 M NaOH, as better SEC, CE, SP, and process time were obtained. Specifically, compared to scenario 1, process times were 2.7 and 3 times longer for membranes A and B, respectively. However, the required process time was not precisely double as expected theoretically. Indeed, this resulted from non-ideal phenomena occurring during the EDBM process, especially water transport (i.e., osmosis and electro-osmosis), which tends to dilute the alkaline solution. The increased SEC is primarily due to a lower CE caused by the above-mentioned non-ideal phenomena. Furthermore, the applied electric potential decreased during the process due to the reduction of the electrolytic solutions' ohmic resistance. In contrast, the Nernst potential increased as the concentration of acid and base increased as well. Overall, the reduction in ohmic resistance prevailed, thus determining a downward trend of the electric potential during the process. Therefore, since in this study, the experiments were carried out in a closed-loop configuration, the higher the target concentration, the lower the resulting average electric potential. Finally, the effective production was 21.4 $kg_{NaOH}\ m_{brine}^{-3}$ and 22.2 $kg_{NaOH}\ m_{brine}^{-3}$, respectively; hence, more than doubled compared to the values obtained at the target of 0.4 M.

When operating at 300 A m^{-2} and targeting 0.4 M NaOH, the best-performing membranes were type B because all indicators except for the processing time were better than those obtained for type A. The increase in current density to 300 A m^{-2} had a clear impact on the processing time since the (at least theoretical) acid/base production rate was increased [84]. Moreover, as expected, the SEC was higher when operating at 300 A m^{-2}. Indeed, the SEC is related to the CE and the electric potential, as mentioned before. The electric potential is partly related to the applied current according to the first Ohm's law (Ohmic contribution) and partly to the Nernst

potential. The results showed a predominant effect of the Ohmic contribution, thus increasing the electric potential with a consequent rise in SEC to 2.4 kWh kg^{-1} for membranes A and 2.2 kWh kg^{-1} for membranes B.

Finally, at 300 A m^{-2} and a target NaOH concentration of 0.8 M, the best-performing membranes were type A, as SEC, process time, CE, and SP were higher than those of type B membranes. Compared to scenario 2, in scenario 4 process time was lower because of the more significant current efficiency. Indeed, the current efficiency in scenario 4 was 9% and 17% higher than those obtained in scenario 2 for types A and B, respectively. Unlike scenario 3, there was no clear trend for the SEC, resulting in 2.28 kWh kg^{-1} for membranes A and 2.4 kWh kg^{-1} for membranes B. The SEC values were more affected by CE and less by electrical potential. Indeed, regardless of the membrane type used, when targeting 0.8 M, the electric potential decreased by less than 5% compared to that found in scenario three at 0.4 M NaOH. On the other hand, the CE varied by only 3% for membranes A and 11% for membranes B when passing from 0.4 M (i.e., scenario 3) to 0.8 M (i.e., scenario 4) of the target, thus indicating better selectivity of type A than B. In comparison to the corresponding scenario at 100 A m^{-2} (i.e., scenario 2), the yield (27.7-28.4%), specific productivity (974-943 kg m^{-2} y^{-1}), and effective production (22.2-22.7 kg_{NaOH} m_{brine}^{-1}) did not differ significantly for membranes A and B, hence demonstrating that diffusion and water transport phenomena did not have a significant influence on performance.

2.4 Conclusion and final remarks

The EDBM experimental inter-laboratory campaign generated HCl and NaOH from brines using new CEMs and AEMs (Suez) that incorporated thin and ultrathin non-woven polyester and polypropylene supports. The campaign demonstrated high reproducibility, as evidenced by the ANO-VA analysis.

The current density was directly affected by the HCl and NaOH final concentrations. For instance, by working at concentrations of 2 M NaCl, it was possible to reach NaOH concentrations higher than 1 M working with both membranes at 300 A/m^2 after two hours of experiment processing duration. Similarly, under the same conditions, HCl concentrations were higher than 1 M, reaching a maximum value of 1.7 M.

The experiment showed a decrease in current efficiency over time, with the current efficiency for membranes incorporating thin-polypropylene (Type A) decreasing to 72%, 55% and 48% working at 100, 200, and 300 $A \cdot m^{-2}$, respectively, after 120 min of processing. This may be due to higher acid and base diffusion towards the salt compartment and the non-ideal perm selectivity of the bipolar membranes. Although the ultra-thin structure of the AEM was claimed to have improved properties as proton-blocking for limiting the transfer of protons through the membrane, no statistically significant results were measured in this study. The opposite effect was observed regarding SEC, with higher values as time passed. Type A reported lower SEC values than Type B, and the final SEC values for Type A were 1.80, 2.63, and 3.29 kWh/kg working at 100, 200, and 300 $A \cdot m^{-2}$, respectively. Type A also showed higher SP than ultra-thin polyester (Type B), with values of SP between 942.58 and 314.43 kWh kg m^{-2} y^{-1} when working at 300 $A \cdot m^{-2}$.

This work provides a general overview to investigate further the effect of a monovalent salt mixture on the EDBM unit regarding SEC, acid-base production, and current efficiency.

Chapter 3

Innovative solution for sustainable chemical production by Electrodialysis with Bipolar Membranes for saltwork brine treatment

Graphical abstract

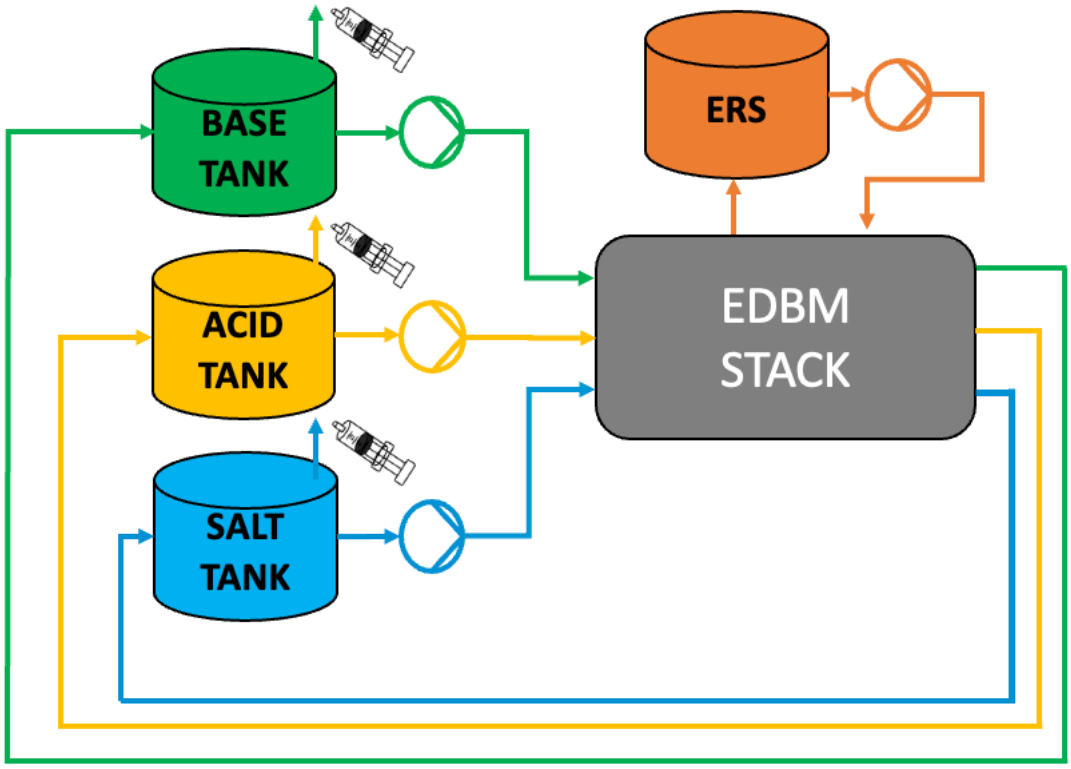

Abstract

Electrodialysis with Bipolar Membranes (EDBM) is a promising technology with the potential to address environmental and economic challenges associated with waste brine streams. This chapter investigated the performance of five compartments of electrodialysis with Bipolar Membrane (EDBM) when treating a synthetic solution of mixed salts of NaCl and Na_2SO_4 that mimics waste brine from an integrated process for the valorization of saltworks bitterns. The lab-scale EDBM unit was assessed using SUEZ ion exchange membranes (IEMs) and operated at 100 and 300 A/m^2 current density. This study also investigated the effect of the initial monovalent salt (NaCl)-feed solution and mixed salts (NaCl and Na_2SO_4) solution in feed compartments on the performance of the EDBM unit. The results highlighted that a higher initial NaCl concentration was favoured to reach the NaOH target concentration in less process time. The presence of the mixed solution in the feed compartments beneficially, yet slightly influenced the production of sodium hydroxide solution.

3.1 General Overview

In various industrial processes, such as the production of chemical fibre, Oxalic acid, penicillin, and formic acid, as well as the flue gas desulfurization process, Na_2SO_4 is a significant component of the wastewater [85]. To fulfil ever-stricter environmental requirements, a lot of waste salts, including Na_2SO_4, are produced during the so-called "zero-liquid discharge" (ZLD) process of high-salinity wastewater treatment [86],[87]],[88]. The high-salt wastewater was concentrated using evaporation [88], nanofiltration, reverse osmosis, electrodialysis (ED) [89], membrane distillation [90], or forward osmosis [91] in a typical ZLD process. The concentrated wastewater was then crystallized to generate salt and desalted water. Most manufacturers need to dispose of waste Na_2SO_4 as hazardous waste due to its low economic worth. Each year worldwide produces more than 20 million tons of waste Na_2SO_4 [85] . Therefore, it is desirable to convert Na_2SO_4 into commonly used products to prevent the buildup of waste salts.

Recently, there has been much interest in using electrodialysis with bipolar membrane electrodialysis (EDBM) to treat hypersaline wastewater [92]. EDBM is an electro-membrane process technology that can generate precious chemicals from the hypersaline stream [93]. Incorporating EDBM technology could result in advanced brine chemical recovery systems that offer a considerable financial return from the treatment chain and increase sustainability compared to conventional ZLD systems. The in-situ generation of chemical reagents needed by the treatment chain, such as acid solutions for membrane cleaning pre-treatments and alkaline solutions for reactive crystallization and the potential pH adjustment of output currents, is a potential with EDBM. In work conducted by Reig et al. [94], different process brines composed of Na_2SO_4 and NaCl were treated by EDBM and selectrodialysis techniques and obtained pure NaOH in both cases. Liu et al. [95] reported the production of 0.97 M H_2SO_4 and 1.56 M NaOH by removing the Na_2SO_4 from the wastewater via the EDBM process.

In practice, the operation parameters would affect the performance of the EDBM system in converting the mixture of NaCl and Na_2SO_4. The single and salt mixture on the ion exchange membrane, initial feed concentration and produced solutions, and current density were investigated. The current efficiency and specific energy consumption under different operation parameters were examined to verify the EDBM system's feasibility to convert NaCl and Na_2SO_4.

3.2 Material and Methods

3.2.1 Reagents and ion exchange membranes

NaCl (99.7% chemSolute), HCl (37% Merck), NaOH (98-100% Honeywell Flute), and Na_2SO_4 (99-100% Honeywell Flute) were used to prepare the synthetic solutions. All the reactants were of analytical grade.

Ion exchange membrane Type A (AR118U, CR61N, AR103tr.), provide by Suez were selected as described in chapter 2 of the thesis. The general properties of the membranes are mentioned in **Table 1**.

3.2.2 Experimental setup

The laboratory EDBM experimental setup is illustrated in Figure 17. Suez, France company provided the EBDM stack (Electromat MKI ED stack), and experiments were performed in a laboratory scale unit. The feature of the EDBM stack is detailed in section 2.2.2 of Chapter 2.

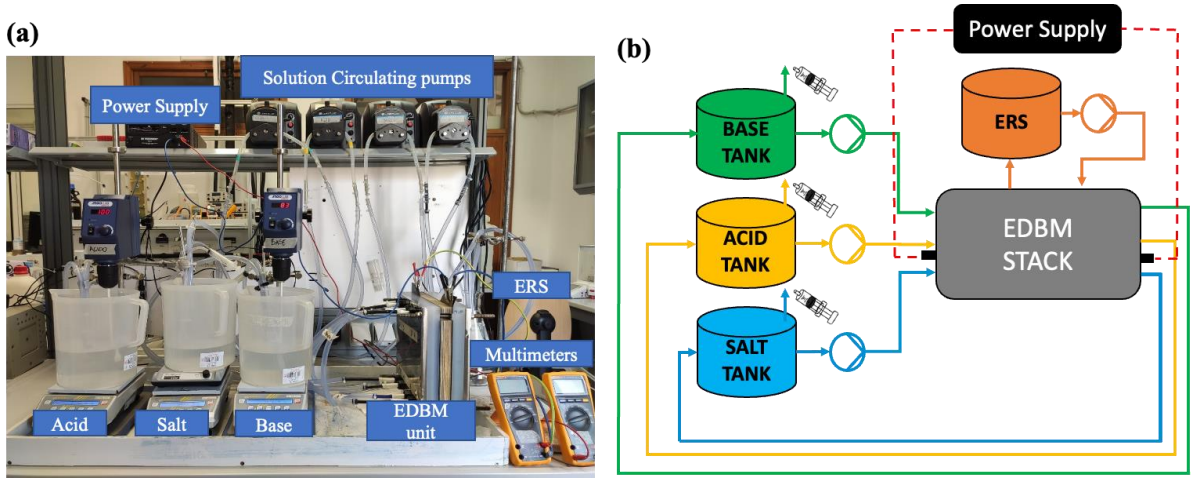

Figure 17. (a) Picture of the EDBM experimental setup and (b) Sketch the EDBM experimental apparatus.

3.2.3 Analytical Methods and Calculations

The voltage and current were acquired from the power supply (BK Precision 1902B). Samples from the acid (HCl) and base (NaOH) solutions were taken at specific time intervals for analysis. The acid and base concentrations in the collected samples were determined by acid and base titration using standard HCl 0.10 M and Na_2CO_3 0.05 M solutions and methyl orange as a pH indicator.

We monitored the pH and conductivity evolution using conductivity meters (3320, Xylem Analytic Germany FmbH D-82362 Weilheim) and pH meters (3320, Xylem Analytic Germany FmbH D-82362 Weilheim; Crison pH Basic 20).

3.2.4 Data analysis

The performance of the EDBM unit to produce HCl and NaOH from the mixture of NaCl and Na_2SO_4 was evaluated in terms of the current efficiency (CE), acid and base concentrations and specific energy consumption. For more details, the reader must look at section 2.2.5 of chapter 2.

3.2.5 Experimental Procedure

The experiments were performed under a constant current, mean channel flow velocity and initial salt, acid and base solution, as shown in **Table 6**. The electrode solution was 0.25 M of Na_2SO_4. The system was operated during all experiments with a fixed volume ratio of acid salt and base (1:1.5:1).

Table 6. *Operational conditions adopted in EDBM experiments include current density, initial concentrations of the different streams, and flow velocity.*

Case	Salt concentration (salt channel)	HCl concentration (acid channel)	NaOH concentration (base channel)	Applied current density (A/m^2)	Flow velocity (cm/s)
Reference	1M NaCl	0.05M	0.05M	100	7*
Type I	1M NaCl 2 M NaCl	0.05M	0.05M	100-300	7*
Type II	2MNaCl+ 0.1M Na_2SO_4				
Type III	2MNaCl+ 0.5M Na_2SO_4				

* Corresponding to a mean channel flow rate of 50 Lh^{-1}

To investigate the effect of the current density on the performance of the EDBM unit, the system was operated with different current densities of (100-300 A/m^2).

3.3 Results and Discussion

3.1.1 Effect of initial salt concentration on EDBM unit

To examine the influence of the initial NaCl concentration on the base compartment in a lab-scale EDBM system, the experiment was performed with different concentrations of 1 M and 2 M of salt solution in the salt-feed compartment, as shown in **Table 6.** Operational conditions adopted in EDBM experiments include current density, initial concentrations of the different streams, and flow velocity., respectively. The acid salt and base volume were 1:1.5:1, and the applied current density was 100 A/m^2.

Figure *18*a. Indicated that the base concentration generated from the simulated different concentrations of NaCl increased during the EDBM processes, as seen when the feed solution concentration containing 1 M and 2 M after continuously running for 240 min: NaOH concentrations up to 1 M and 0.8 M in the base compartment were obtained using the reference and type I tests. The concentration of NaOH obtained could meet the requirement of the magnesium and calcium recovery [96] from the waste brine. It was observed from **Figure *18***a, that the increase of base concentration at the beginning of the tests was quicker than that at the end later part of the test, which resulted from the reduction of NaCl concentration and from the increasing detrimental phenomena (such as thermodynamic potential to be won, diffusion, osmosis). The reduction of NaCl in the fed solution led less Na^+ and Cl^- ions to migrates to the neighbouring compartments. Moreover, along with the trans-membrane migration of ions, parts of the water existed in the form of hydrated ions that migrated from the salt compartment into the adjacent acid and base compartments through ion exchange membranes in a DC electric field (i.e., water electricity penetration) to lead to the increase of acid and base solution volumes, which delayed the increase of the concentration in the adjacent compartments. The results meant that the higher concentration of NaCl was favoured to generate a higher concentration of HCl and NaOH by the EDBM unit. The results suggested that the initial 2M fed salt concentrations can be considered appropriate for the BMED system in the next section.

The change of pH and conductivity of the solution with the different concentrations of NaCl in the salt compartment of the EDBM system was illustrated in **Figure *18***b: it was that the conductivity of the solution in the salt compartment reduced gradually during the processing time of the test, suggesting that NaCl in the salt compartment were almost depleted at the end of the experiments. It was also proved that EDBM could treat sodium chloride effluent to simultaneously realise the aim of acid and base production and desalination. The change in pH showed that the solution salt compartment was acidic after the initial period of the experiment. These results were observed in all the experiments. The pH decrease in the salt compartment is due to the leakage of H^+ ions from the acid compartment into the adjacent salt compartment during the EDBM process. This leakage phenomenon occurred because of the "tunnel effect" of H^+ ions , which led to the higher permeability of the anion exchange membrane for proton [97], [98].

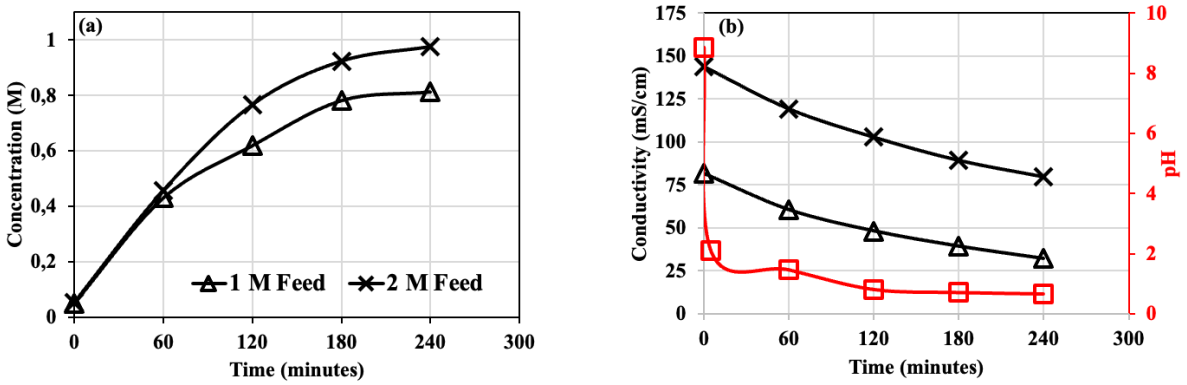

Figure 18. (a) Effect of the initial salt concentration on final NaOH amount and (b) conductivity and pH variation in feed compartment as a function process time.

3.1.2 Acid and base production for Mixed salt feed solution

The results in the section were conducted in a closed-loop configuration. These results enabled the evaluation of the EDBM unit performance to reach 60 minutes of the experiment duration, and the current density was 300 A/m^2. The effect of initial single and mixed solutions of NaCl and Na_2SO_4 are thoroughly discussed in this section.

Figure 19 (a), shows the acid and base product concentration at different initial concentrations of single salt (NaCl) and mixed salts of NaCl and Na_2SO_4 and a current density of 300 A/m^2. As it can be seen, adding Na_2SO_4 provides slight-to-negligible differences in the concentration of HCl and NaOH. The results were presented during the first 60 minutes run after the experiment.

Similar considerations can be inferred from

Figure 19 (b and c): the yield and the current efficiency do not seem to be affected by the additional presence of Na_2SO_4. Only a very slight increase of yield and CE is observable for the case of NaOH probably due to the higher concentration of Na^+ in the salt channel: as a matter of fact NaCl and Na_2SO_4 share the same cation. Notably, yield and CE are higher for NaOH compared to HCl in all cases, as expected, due to the high mobility of H^+ ions.

As far as SEC is concerned,

Figure 19 (d), shows no effect of the adoption of two salts in the salt compartment on the SEC of NaOH. This is in accordance with the information reported in

Figure 19 (a, b and c). Conversely, a slight increase in the SEC relevant to HCl was found, again probably related to the tunnel effect of H^+ ions.

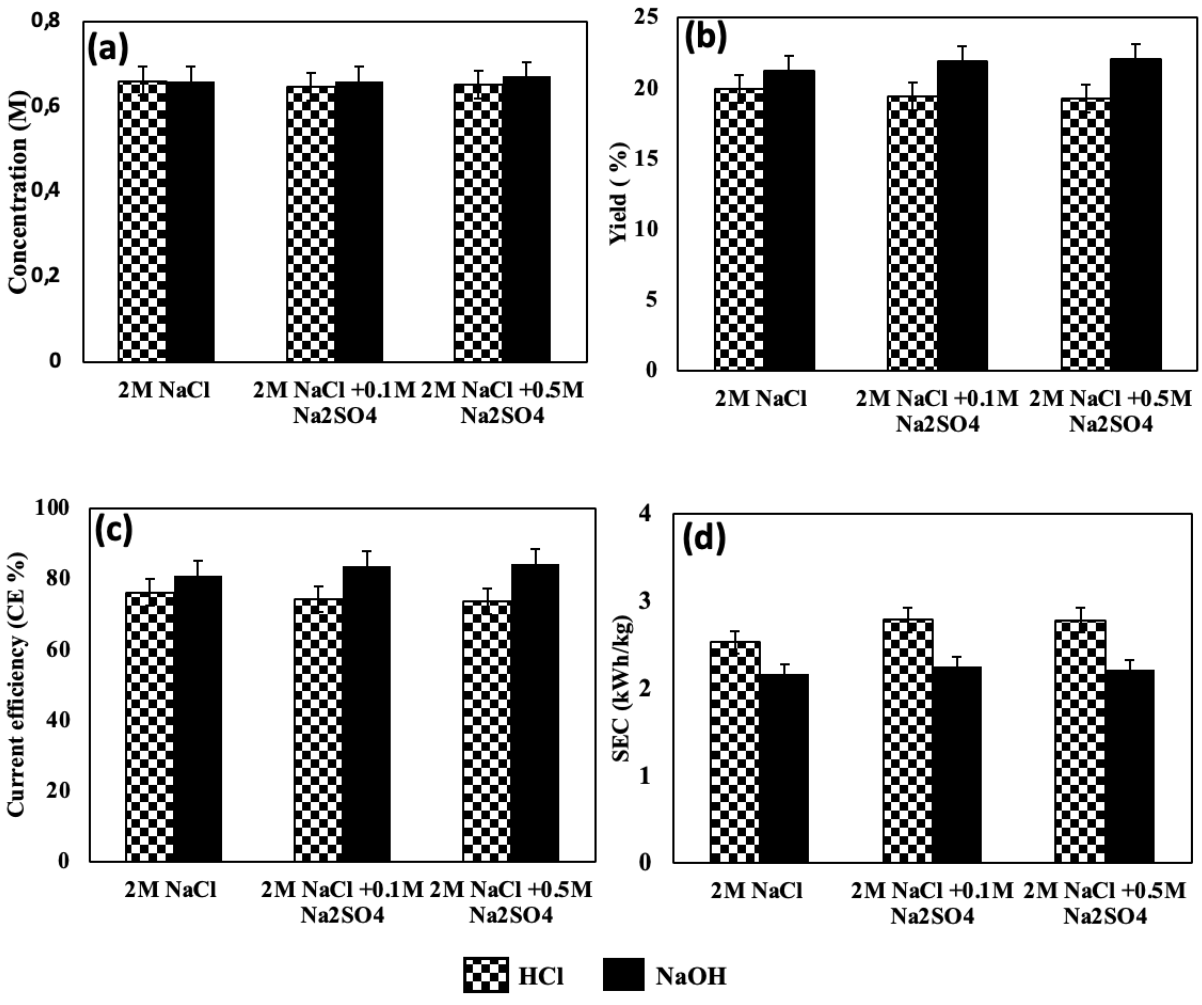

Figure 19. Effects of the initial single salt and NaCl & Na_2SO_4 mixed concentrations on the performance of the EDBM system. (a) EDBM stack voltage; (b) effect on product concentrations; (c) effect on current efficiency: and (d) effect on energy consumption and efficiency. Process time 60 minutes and applied current density 300 A/m^2.

3.1.3 Effect of current density on NaOH production

Two current densities (100 and 300 A/m^2) were applied to the EDBM unit to investigate the effect of current density in processing the Type (I, II, and III) compositions of experiments. The test was carried out in all the experiments for four hours. The performance of the EDBM unit was determined in terms of SEC, base concentration, and current efficiency. An initial solution of 0.05 M was used for the acid and base compartment inputs. In these experiments, the solution volume was 1:1.5:1 in acid salt and base tanks. In addition, to investigate possible performance differences, we carried out two different potential variation tests. **Figure 20**, shows the results obtained when applying a current density of 100 A/m^2 for the three investigated scenarios. The achievable concentration of NaOH was around 0.8 M. The feed salt content in the feed exceeded a level of adequacy, ensuring the successful attainment of the desired target. The yield at the target concentration was 26.9 %, 28.8% and 25.8 % for case type I, II and III experiments, respectively. A slight reduction in yield in cases II and III predominantly resulted from the large sodium ions in the feed compartment. Conversely, the target concentration's time duration was 133, 148, and 120 min for cases I, II and III, respectively. The current efficiency recorded for cases I, II, and III were 69.98%, 63.26% and 68.68%, respectively. The current efficiency showed a decreasing trend over the process duration, as illustrated in Figure 20c. The decline in the observed trend might be attributed to the noteworthy influence of non-ideal and adverse phenomena like diffusion, osmosis, and electro-osmosis. Similarly, there was a gradual rise in specific consumption as time progressed. The SEC at the target was 1.81, 2.10, and 1.83 kWh/kg for scenarios I, II and III, respectively. The sodium hydroxide purity of cases II and III was 99.8 and 98.5%, respectively, under the applied current density for the target concentration.

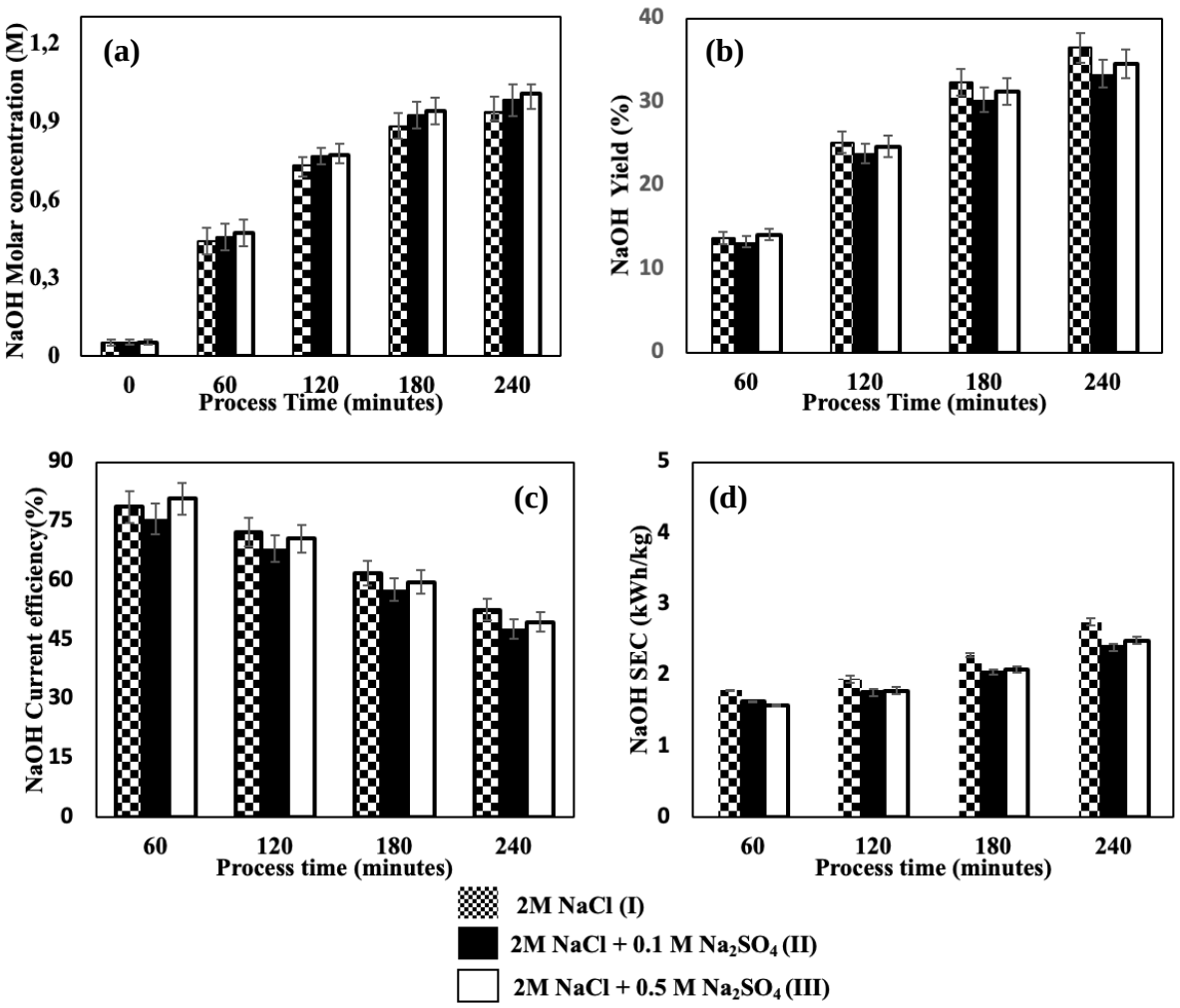

Figure 20. Time dependency of (a) Molar concentration, (b) Yield (%), (c)% Current efficiency, and (d) Specific energy consumption as a function of time and constant applied current density of 100 A/m^2 in closed loop EDBM setup.

Figure *21*, shows the results obtained for the three investigated cases (I, II and III) under the constant applied current of 300 A/m^2. The initial solution of 0.05 M was used in acid and base compartments as input.

As evident from the graph in **Figure *21***a, employing a high current density accelerated the water dissociation rate, increasing acid and base production and reducing the process duration: a concentration of NaOH higher than 1M was obtained in all cases. As indicated by **Figure *21***b, the yield was found to increase when an increasing value of sulfuric acid is added. This is likely related to the additional amount of Na^+ ions added to the salt channel. Furthermore, the theoretical proposition of tripling the existing current to 300 A/m^2 anticipates a proportional

reduction in process duration to approximately one-third of the timeframe observed at 100 A/m². The time required was found to be 40, 41, and 39 min for type I, II and III cases, respectively, thus resulting in a time that is about one-third of the time taken at 100 A/m². As shown in **Figure *21***c, the current efficiency is lower compared to the case of 100 A/m^2 due to the additional ohmic losses and to the higher NaOH concentrations achieved.

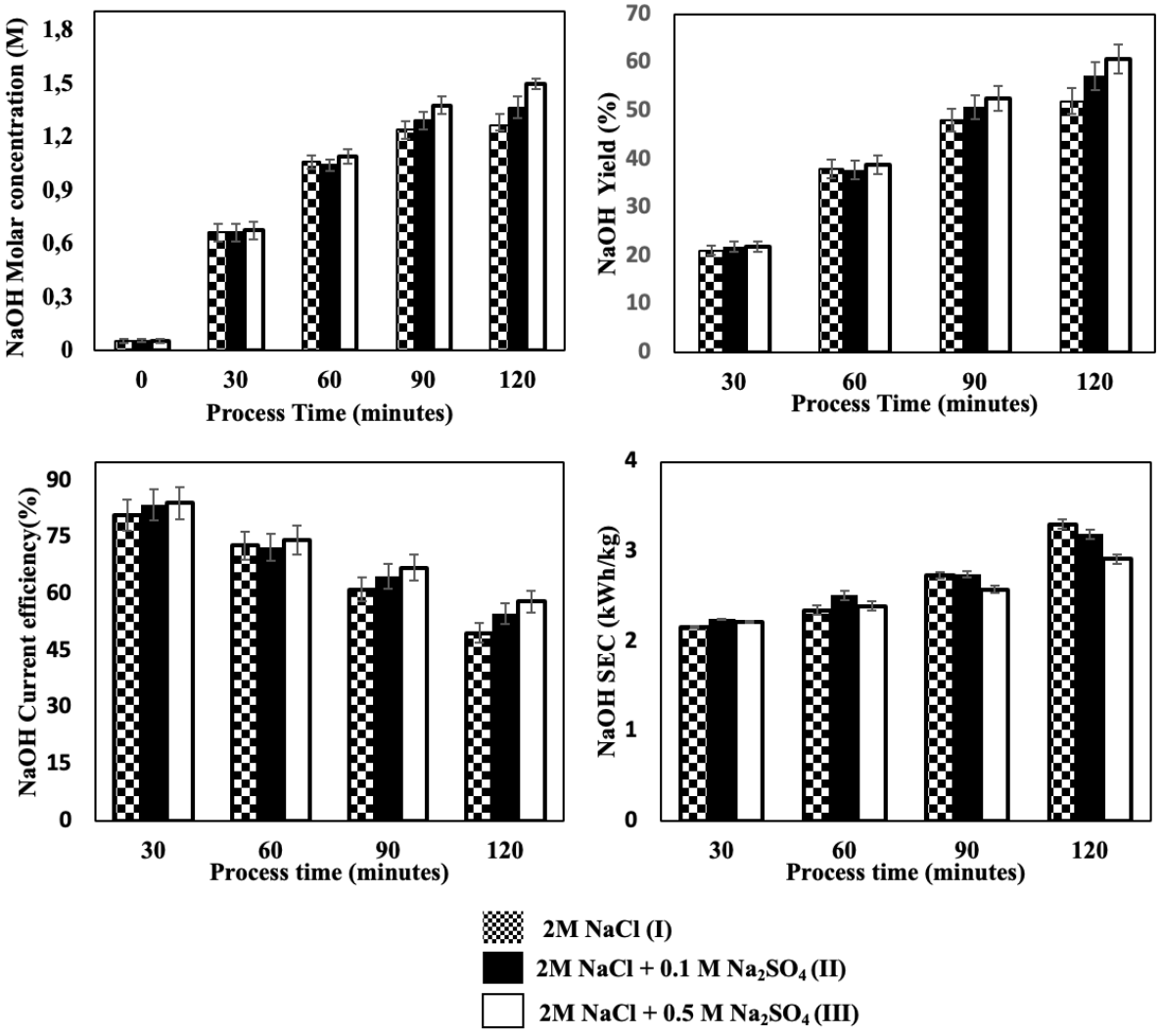

Figure 21. Time dependency of (a) Molar concentration, (b) Yield (%), (c)% Current efficiency, and (d) Specific energy consumption as a function of time and constant applied current density of 300 A/m^2 in closed loop EDBM configuration.

This is confirmed by the value of SEC reported in **Figure *21***d, which are higher than the corresponding ones relevant to the cases at 100 A/m² compared to the migrative flux when contrasted with the situation at 100 A/m².

Concerning the effect of adopting a mixture of NaCl and sulfuric acid in the salt-compartment, on overall, **Figure 20**, and **Figure *21***, suggest that this might be beneficial for the process, especially at high current densities.

3.4. Conclusion and final remarks

This work introduces a novel method for experimental characterisation of IEMs in the EDBM stack, particularly for feed streams containing a Sigle and mixed-ions solution in the feed compartment. Three different compositions containing (Na^+, Cl^- and SO_4^{2-}) with varying sulphate concentrations were analysed on SUEZ IEMs. The mixed ions solution barely affects the OH^- generation compared to the case of only 1 M and 2 M NaCl initial feed solution concentration. At a current density of 100 and 300 A/m^2, final OH concentrations of 1.0 and 1.5 M were achieved for the highly concentrated case (III). The energy consumption of 2.50 and 2.92 kWh/kg when operating in the 100 to 300 A/m^2 current density interval.

Furthermore, the EDBM system performance demonstrated improvement when mixed ions solution was used in a feed salt compartment.

This finding highlights the effectiveness of wastewater treatment using the EDBM system, producing highly pure sodium hydroxide. This sodium hydroxide can be utilised for magnesium recovery within the SEArularMINE project's treatment sequence or be commercially sold. Furthermore, the generated acid and base solutions have the potential for internal recycling within the system. Moreover, these acid and base solutions could be reutilised within the system. Beyond the chemical outputs, the process additionally yields desalinated water, enhancing the overall water efficiency of seawater desalination operations.

Chapter 4

Energetic Valorization of Saltworks Bitterns via Reverse Electrodialysis: A Laboratory Experimental Campaign

Graphical abstract:

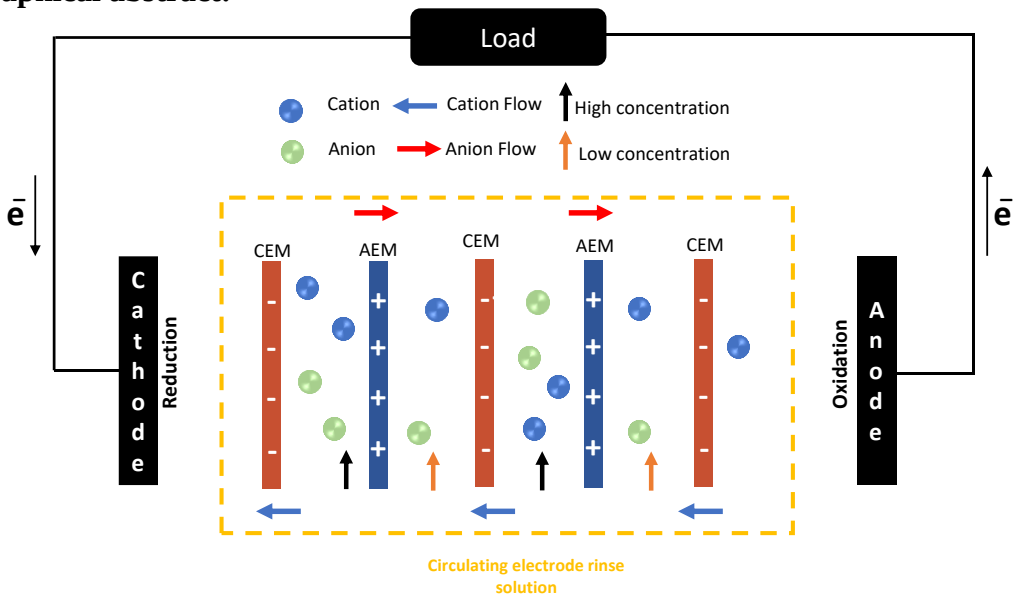

Abstract

Concentrated bitterns discharged from saltworks have incredibly high salinity, often up to 300 g/L. Thus, their direct disposal not only has a harmful effect on the environment but also generates a depletion of a potential resource of renewable energy. Here, reverse electrodialysis (RED), an emerging electrochemical membrane process, is proposed to capture and convert the salinity gradient power (SGP) intrinsically conveyed by these bitterns, aiming to reduce concentrated salty water disposal. A laboratory-scale RED unit has been adopted to study the SGP potential of such brines, testing ion exchange membranes from different suppliers and under different operating conditions. Membranes supplied by Fujifilm, Fumatech, and Suez were tested, and the results were compared. The unit was fed with synthetic hypersaline solution mimicking the concentration of natural bitterns (5 mol/L of NaCl) on one side and a variable concentration of NaCl dilute solutions (0.01–0.1 mol/L) on the other. The influence of several operating parameters has also been assessed, including solutions flow rate and temperature. Increasing feed solutions' temperature and velocity has been found to lower the stack resistance, enhancing the RED stack's output performance. The maximum obtained power density (corrected to account for the effect of electrodic compartments, which can be very relevant in five cell pairs laboratory stacks) reached around 10.5 W/m^{2}cellpair, with FUJIFILM Type 10 membranes, the temperature of 40 °C, and a fluid velocity of 3 cm s^{-1} (as an empty channel, considering 270 μm thickness). Notably, the present study results confirm the immense potential for SGP generation from hypersaline brines, thus providing helpful guidance for harvesting SGP in seawater saltworks worldwide.

Keywords: brine; salinity gradient power; RED; salty water

This chapter has been published as:

Abdullah Shah, Syed, Roberta Cucchiara, Fabrizio Vicari, Andrea Cipollina, Alessandro Tamburini, and Giorgio Micale. 2023. "Energetic Valorisation of Saltworks Bitterns via Reverse Electrodialysis: A Laboratory Experimental Campaign" *Membranes* 13, no. 3: 293. https://doi.org/10.3390/membranes13030293

4.1 General Overview

Brines produced from saltworks, desalination plants, and many other industrial activities contain high concentrations of total dissolved solids (TDS) and, depending on the process, can be released at a higher temperature than the environmental temperature. Directly discharging them into the ocean will deteriorate local marine ecology and the wider surrounding environment [99], [100].

Saltworks brine temperature is generally 30–40 °C [101], a kind of heat that can hardly be exploited and is generally classified as low-grade. In addition to the temperature gradient, a salinity one also exists in the saltworks, between the brine and seawater or locally available low-concentration streams such as wastewater treatment plant discharge.

Capturing this middle-temperature salinity gradient power (SGP) for energy generation might be essential for energy conservation, emission reduction, and coastal environmental preservation. Additionally, extracting renewable energy from brine can assist in achieving the seventh United Nations (UN) sustainable development goal (SDG7), affordable and clean energy.

At the moment, approaches for harvesting SGP include pressure retarded osmosis (PRO) [102][103], steam pressure energy (SPE)[104], and reverse electrodialysis (RED) [105], [106] [107], [108]. Among them, the RED technology has drawn the attention of many researchers due to the advantages of no moving components, excellent reliability, and simple eradication of membrane fouling concerns[109] .

As described in **Figure *22***, a RED device comprises a series of anion exchange membranes (AEMs) and cation exchange membranes (CEMs) forming adjacent channels in which hypersaline and dilute solutions flow without contacting one another. The intermembrane distance is maintained by placing a polymeric spacer between AEM and CEM, which provides mechanical stability to the compartment. The AEMs/CEMs permit ion transport across them, enabling the concentration gradient existing between the solutions to be converted into an ordered flux of ions which can ultimately be used to sustain electrochemical processes at the electrode and produce an external net flow of electrons. In other words, RED can directly produce electrical energy by directing the ion exchange between two solutions.

RED has been used to convert seawater and freshwater into electricity [106][110][111], but also for wastewater treatment [102], [112] and within a novel concept of a heat engine[113], [114].

However, technical issues in producing high net power densities still limit the RED industrial application. To tackle this issue, researchers have tried many different approaches. For example, Abdullah et al. demonstrated that combining multiple monovalent salts as feed solutions for RED could optimise power density, especially if compared with single salt solutions[105]. These findings are in line with those obtained by Micari et al., where the measured stack resistance for binary mixtures of salts was found to be lower than that of the pure salts in experiments, thus suggesting a potentially higher power density[115].

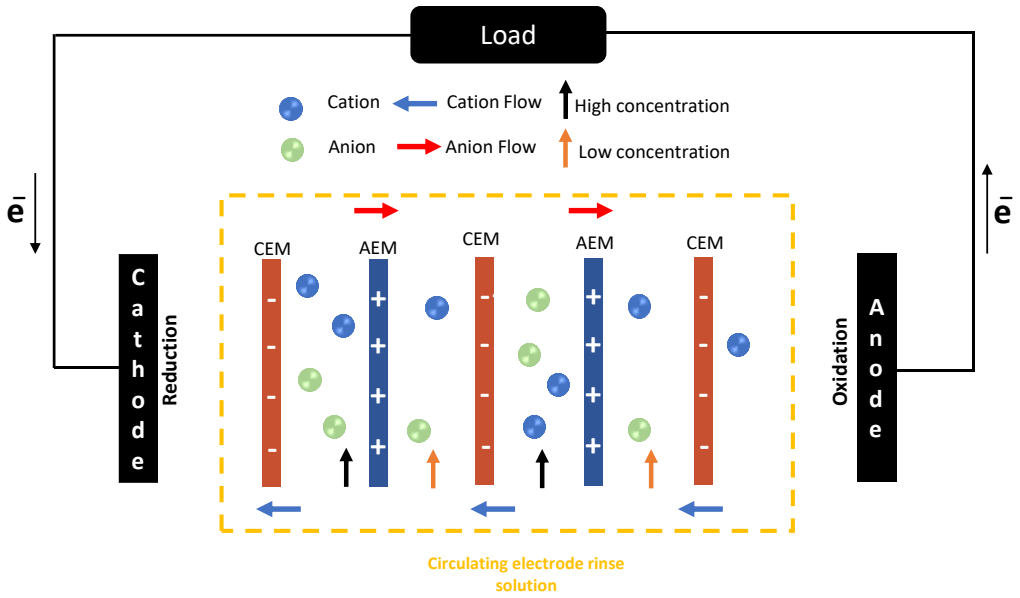

Figure 22. Schematic representation of the Reverse Electrodialysis RED (process). CEM: Cation Exchange membrane; AEM: Anion Exchange membrane.

Net power density is primarily influenced by the energy spent for pumping the solutions across the stack, which depends on membrane fouling in time. In this regard, Cosenza et al. [112] tested a RED unit run over 25 days utilizing effluents from crude oil extraction processes. During the long-run tests, a maximum power density of 2.5 W m^{-2}_{cp} was observed, and alternative anti-fouling techniques were investigated to manage the fouling occurrence.

Membrane fouling also inhibits ion migration, as highlighted by Kang and co-workers, who found that maximum power density and open circuit potential could be increased by 19% and 9.4%, respectively, just by filtering out sediments from the feed [116].

The maximum power density ever reported with RED is the one from Daniilidis, who examined the effect of solution concentration and temperature on the performance of a RED stack, obtaining a maximum power density of 10.6 W m^{-2}_{cp} and 13.4 W m^{-2}_{cp} at 40 °C and 60 °C, respectively [117].

Concerning high-salinity industrial streams, much work has been done for desalination brine management. As an example, Brauns and colleagues proposed a concept coupling RED with seawater desalination. After the desalination, the brine is released into a solar pond for additional concentration. Then, the concentrated brine and seawater are fed to the RED unit to generate electricity [118], [119].

Less attention has been devoted to the valorization of bittern; the peculiar industrial exhaust solution is obtained after sodium chloride production in the saltworks.

The first 1 kW RED pilot plant fed with real solutions in a natural environment was operated in a saltwork by Tedesco and colleagues, demonstrating the possibility of using bittern for as long as five months without losing performance[119].

Noteworthy, when the very same stack was fed with synthetic solutions containing NaCl of the same TDS as the real one, the power density produced almost doubled its value because of the absence of divalent ions [119]. In the framework of the SEArcularMINE project, following the scheme of a novel approach designed and patented by ResourSEAs SrL, the presence of divalent ions affecting performance has been solved by placing the RED unit at the end of a mineral extraction sequence, reducing the presence of magnesium and calcium to negligible values (see **Figure *23***)[120].

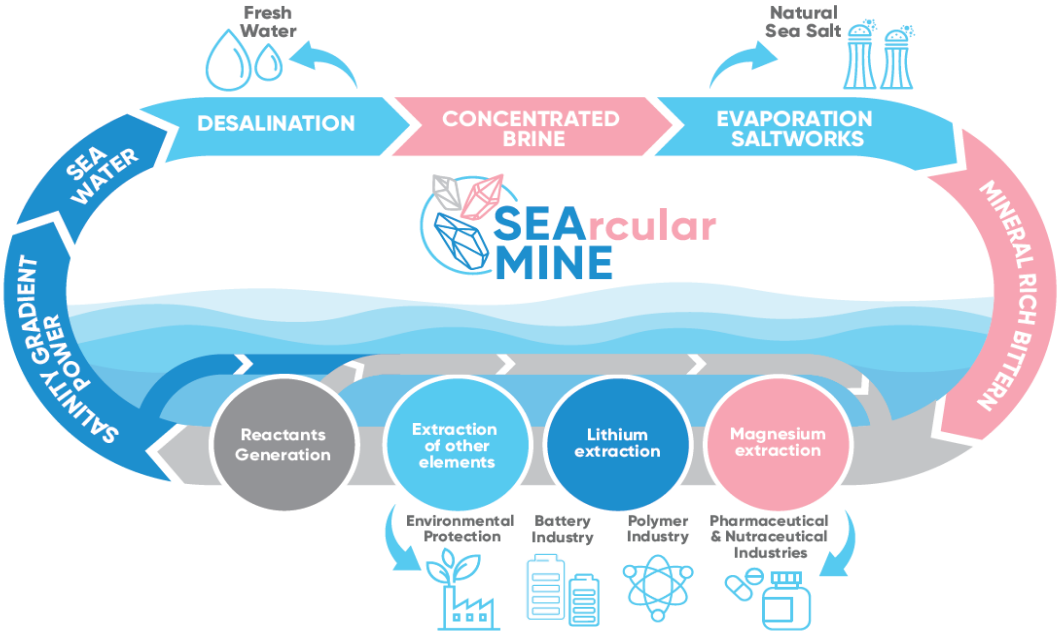

Figure 23. Schematic illustration of the SEArcularMINE project integrated process. Reprinted with permission from [120]

The present work conducted an extensive experimental campaign using a reverse electrodialysis unit. In particular, three different ion exchange membranes were tested for the

recovery of salinity gradient energy using artificial brines mimicking the expected features of brines in an actual application. More precisely, for the first time, RED units equipped with Fujifilm, Fumatech, and SUEZ IEMs were compared when operated with saltworks brine. The concentration and the temperature of the artificial feed were chosen based on the features of an actual brine examined in the framework of the SEArcularMINE project. Furthermore, the effect of feed velocity and dilute solution concentration was also studied. This study could guide harvesting salinity gradient energy from saltwork plants.

4.2 Experimental Setup and Procedure

4.2.1 RED stack configuration

Three RED stacks of the same size were built and assembled using different types of ion exchange membranes. In particular, the first RED stack was assembled with Fujifilm Type 10 AEMs/CEMs (Fujifilm Manufacturing Europe B.V., Tiburg, The Netherlands), a second stack was equipped with Fumatech AEM-FAB-PK-130/CEM-FKB-PK-130 (Fumatech BWT GmbH, Bietigheim-Bissingen, Germany). A third stack was built for further investigation using SUEZ membranes AEMs-AR103U/CEMs-CR67U (Suez, Paris, France). Membrane properties are reported in

Table *7*, for the sake of completeness. However, only some (i.e., perm-selectivity and electrical resistance) will be useful to discuss the results collected in Section 3. The three stacks were operated under the same experimental feed conditions. Each stack had an active area of 0.01 m^2 per membrane. The RED unit (REDstack B.V., Sneek, Netherlands) was equipped with five cell pairs separated by 270 μm spacers (Deukum, Frickenhausen, German); each cell pair is composed of one anion exchange membrane (AEM), one spacer, and one cation exchange membrane (CEM). Additional CEMs specifically selected for their high selectivity (Fumasep FKS-50, BWT GmbH, Bietigheim-Bissingen, Germany) were placed as shielding membranes next to each electrode compartment to prevent electrode rinse solution leakage into the high and low concentrations channels.

The end plates of each unit are made of poly-methyl-methacrylate (PMMA) and host two Ru-Ir oxides-coated titanium electrodes. The shielding membrane in the end compartments and endplate was separated using a silicon gasket, and the electrode compartments were filled with a woven spacer.

Table 7. Properties of the ion exchange membranes (IEMs) used in this work

Membrane	**Fujifilm**[121]		**Fumatech** [122]		**Suez**[123]	
	AEM	CEM	AEM	CEM	AEM	CEM
	Type 10	Type 10	FAB	FKB	AR103U	CR67U
Thickness dry (μm)	125	135	130	130	130	150
Electrical resistance (Ω cm^2)	1.7	2.0	< 8.5	< 5	1.4	2.0
Permselectivity	95	99	> 93	> 98	90	90
IEC (m_{eq} g^{-1})	1.8	1.5	-	-	2.37	1.92
Water permeability (mL bar^{-1} m^{-2} h^{-1})	6.5	6.5	-	-	-	-

The information in

Table 7, has been collected from the data sheets of membrane manufacturers, when available.

4.2.2 Experimental Setup

The laboratory RED experimental setup is illustrated in **Figure 24.** Synthetic feed solutions were prepared using sodium chloride (NaCl 99.7% ChemSolute Renningen, Germany), dissolved in deionized water. Five low-salinity feed solutions and one synthetic brine were prepared according to the requirements of the experimental campaign (**see Table 8).** The feed solution was heated to a desired temperature with a heating bath, and a heated magnetic stirring plate (LLG, uniStirrer7, Am Hambuch, Germany) was used for the electrode rinse solution to keep the required temperature constant. The synthetic brine was prepared to match the actual brine expected in the SEArcularMINE project closely. The ERS solution used for all the experiments contained 0.1 M of FeK3(CN)6/FeK4(CN)6 and 0.6 M NaCl as a supporting electrolyte.

A co-flow arrangement was adopted for the feed solutions. Peristaltic pumps were used to circulate feed and electrode rinse solutions to the stack (BT601S from Lead Fluid Technology, CO LTD, Hebei, China).

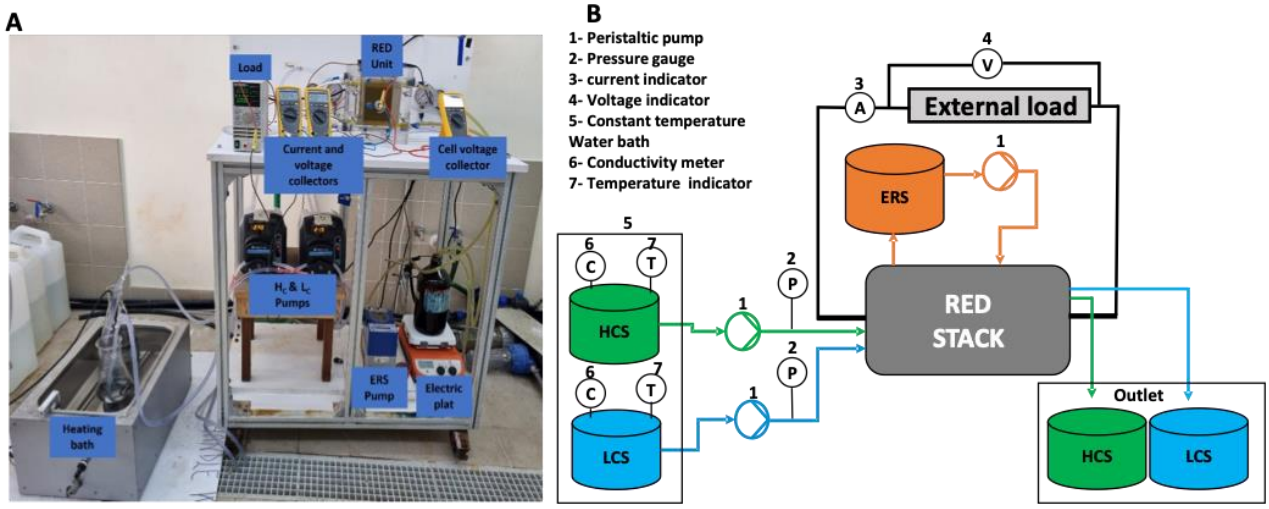

Figure 24. (A) Picture of the RED experimental setup. (B) shows the RED experimental diagram. HCS: high compartment solution; LCS: low compartment solution; ERS: electrode rinse solution.

Table 8. *Conditions selected for the experiments.*

Parameter	**Reference Test Value**
Dilute concentration	0.01–0.1 M NaCl
Concentrate concentration	5 M NaCl
Fluid velocity	1–3 cm s^{-1}
Spacer thickness (µm)	270

Temperature	20–40 °C
Effective area of membrane (m^2)	0.01
ERS solution composition	0.1 M of FeK3(CN)6/FeK4(CN)6 and 0.6 M NaCl
Conductivity	105 mS/cm
Pumping efficiency	90%
Temperature	20–40 °C

4.2.3. Experimental Procedure

Before each set of experiments, leakage tests were performed after the assembly of RED stack pumping only deionized water in high, low, and ERS compartments at a flow velocity of 1 cm s^{-1}. For example, to quantify high channel leakage, water was circulated in low, and ERS channels while the inlet of the high channel was maintained closed, and the outlet was left open. The percentage of leakage was determined by the volume $(V_{mL})_{leak}$ from the high compartment divided by the test duration (minutes) and flow rate (Q = 81 mL/min), as indicated in Equation (1) below. The test was carried out to ensure that the stack was assembled well and that there was no internal mixing of the feed and ERS solution. The results of the leakage tests are shown in ***Table 9***.

$$Leakage\ (\%) = \frac{(V_{mL})leak}{t \times Q} \quad (1)$$

Table 9. Leakage test results using deionized water in all channels.

Stack	**Fujifilm**	**Suez**		**Fumatech**
AEM	Type-10	AR103U		FAB-PK-130
CEM	Type-10	CR67U		FKB-PK-130
Flow velocity (cm s^{-1})	1	1		1
Internal leakage	< 0,1%	HC	LC	0%
		6%	12%	

Artificial sodium chloride solutions of various concentrations were used as the feed solutions. The concentrations of diluted solutions ranged from 0.01 M to 0.1 M with a constant concentrated solution of 5 M. Feed solutions were injected into the stack continuously at a fixed flow rate of 1, 2, and 3 cm s^{-1}. The electrode rinse solution consisting of 0.1 M potassium ferricyanide $K_3Fe(CN)_6$, 0.1 M potassium ferrocyanide $K_4Fe(CN)_6$ (Honeywell Flute, Seelze,

Germany), and 0.6 M sodium chloride (99.7% ChemSolute, Renningen, Germany), was recirculated through the electrode compartments of the stack. The electrode rinse solution was in a black bottle to avoid light exposure. All the solutions were prepared in deionised water. The temperatures of the feed solutions (ranging from 20 °C to 40 °C) were controlled by a water bath and were continuously monitored using a temperature meter. A conductivity meter (3320, Xylem, Weilheim in Oberbayern, Germany) and pressure gauges (Cewal, Camponogara, Italy) monitored the compartments' solution conductivity and pressure losses. Multimeters (Fluke-175 True RMS, Everett, WA, USA) and an external load (BK Precision,8540, Yorba Linda, CA, USA) were employed to collect the polarization curves (i.e., current versus electric potential over the stack curves).

4.2.4 Performance Indicators

The performance of a RED unit can be expressed based on some performance indicators, which can be easily derived from the measured experimental information:

Stack electrical potential, V_{stack}:

$$V_{stack} = OCV - I\,R_{stack} \qquad (2)$$

Where V_{stack} is the output potential of the RED stack, *OCV* is open circuit voltage (measured when the external electrical load is disconnected), *I* is the electrical current (measured by an amperometer), and R_{stack} is the electrical internal resistance of the stack which can be ideally expressed as:

$$R_{stack} = R_{blank} + N_{cell}\,(AEM_R + CEM_R + High_R + Low_R) \qquad (3)$$

Where R_{blank} represents the resistance of electrodic compartments and can be measured by assembling the RED stack with only one cation exchange membrane (Fumasep FKS-50, BWT GmbH, bietigheim, Germany) and feeding the electrode compartment with the above-mentioned rinse solution only. From Equation (2), it is clear how the internal resistance of the RED stack can be obtained from the slope of the output voltage (*V*) to current (*I*) curve (the so-called “polarization curve”), as shown in **Figure 25,** with three examples of polarization curves obtained with each of the membrane sets adopted in this study.

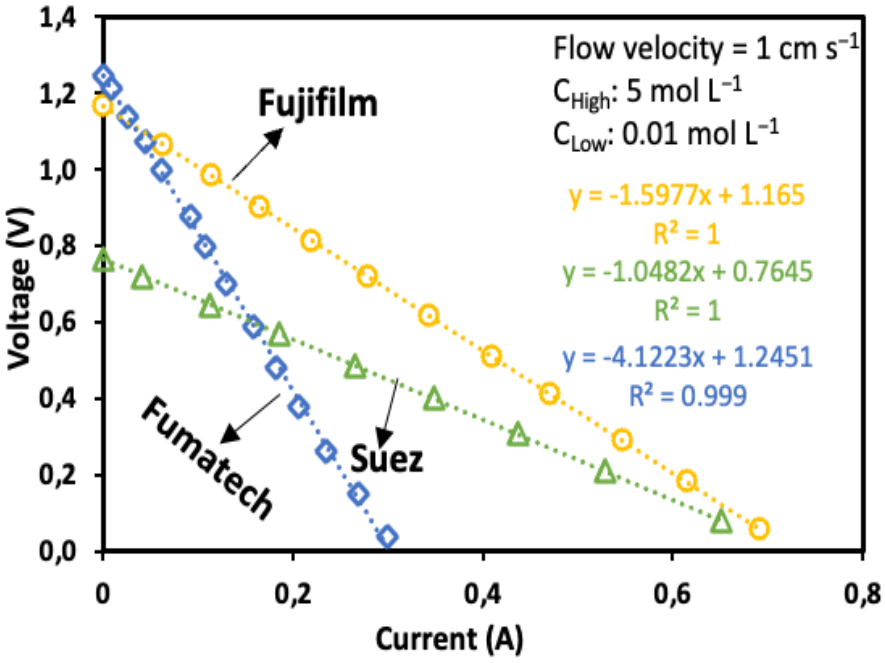

Figure 25. Polarization curves were obtained with each IEMs set adopted in the study. The equation reported in the box shows, concerning Equation (2), the values of R_{stack} (angular coefficient), and OCV (y−intercept).

Figure *26*, instead, shows the polarization curve with a one-membrane stack to determine R_{blank}, as the slope of the resultant linear trend, eventually determined to be 0.27 **Ω**.

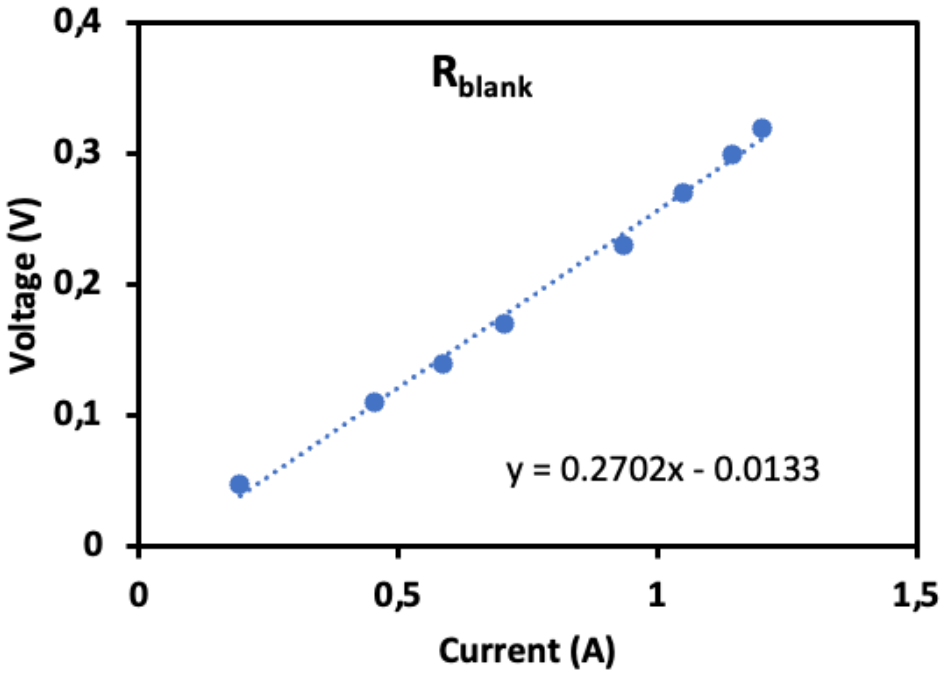

Figure 26. R blank as the slope between voltage and current under the experimental condition of 0.1 M FeK3(CN)6/FeK4(CN)6, and 0.6 M NaCl in the electrode compartment, 20 °C temperature, and 180 mL min−1 of flow rate.

The output power, P is given by:

$$P = V_{stack} \times I \quad (4)$$

The power generation per unit cell pair area is defined as power density:

$$PD = \frac{P}{NA} \quad (5)$$

N is the number of cell pairs (5) and A is the active area of membranes (0.01 m2).

Once the value of R_{blank} is identified, the measured value of PD can be corrected (PD_{corr}) starting from Equation (5), to determine the power density corresponding to an ideally large number of cell pairs (e.g., in a full-scale stack), where the contribution given by electrode compartments to total stack resistance (R_{blank}) becomes negligible. In particular, the PD_{corr} is calculated by subtracting the R_{blank} from the stack resistance R_{stack} and redetermining the main electrical variables according to [3]:

$$PD_{corr} = \frac{OCV^2}{N\ A\ R_{load}\left(1 + \frac{R_{cells}}{R_{load}}\right)^2} \quad (6)$$

Where$R_{cells} = R_{stack} - R_{blank}$

Other than PD_{corr} also, the $PD_{net,cover}$, was calculated, subtracting from the power density the power consumed by the pumps (PD_{pump}), theoretically estimated as the product of pressure drops and flow rate, then normalized by the total cell pair area:

$$PD_{net,cover} = PD_{corr} - PD_{pump} \quad (7)$$

$$PD_{pump} = \frac{\Delta P_{high} \times Q_{high}^{tot} + \Delta P_{low} \times Q_{low}^{tot}}{N.A} \quad (8)$$

Please, note that the power needed to heat the solutions to 30–40 °C is not considered because bitterns can achieve these temperature values in summer when discharged after the

salt collection. Where ΔP_{high}, ΔP_{low}, and Q_{high}^{tot}, Q_{low}^{tot} respectively, the pressure drops and flow rates for the concentrate and dilute compartments.

The mean fluid velocity inside a single spacer-filled compartment, *v*, has been calculated as:

$$v = \frac{\mathrm{Q}}{60 \times \mathrm{N} \times \mathrm{W} \times \mathrm{T}} \quad (9)$$

Where *Q* is the flow rate of the feed solutions (mL min^{-1}) in a single compartment, N is the number of cell pairs (5), *W* is the channel width (10 cm), and *T* is the spacer thickness (0.027 cm).

4.3 Results and Discussion

Membrane features, flow rates in the compartment channels, dilute solution concentration, and feed solutions temperature are the primary variables influencing the RED process[124], [125]. Therefore, considering these parameters, experiments were implemented to study the influence of all these parameters on the performance of the RED stack equipped with different ion exchange membranes.

4.3.1 Temperature Influence of RED Performance

Figure *27*a, illustrates the variation of PD_{corr} at different feed temperatures under the experimental conditions of C_{High} = 5 mol L^{-1}, C_{low} = 0.06 mol L^{-1}, and a flow velocity of 1 cm s^{-1}.

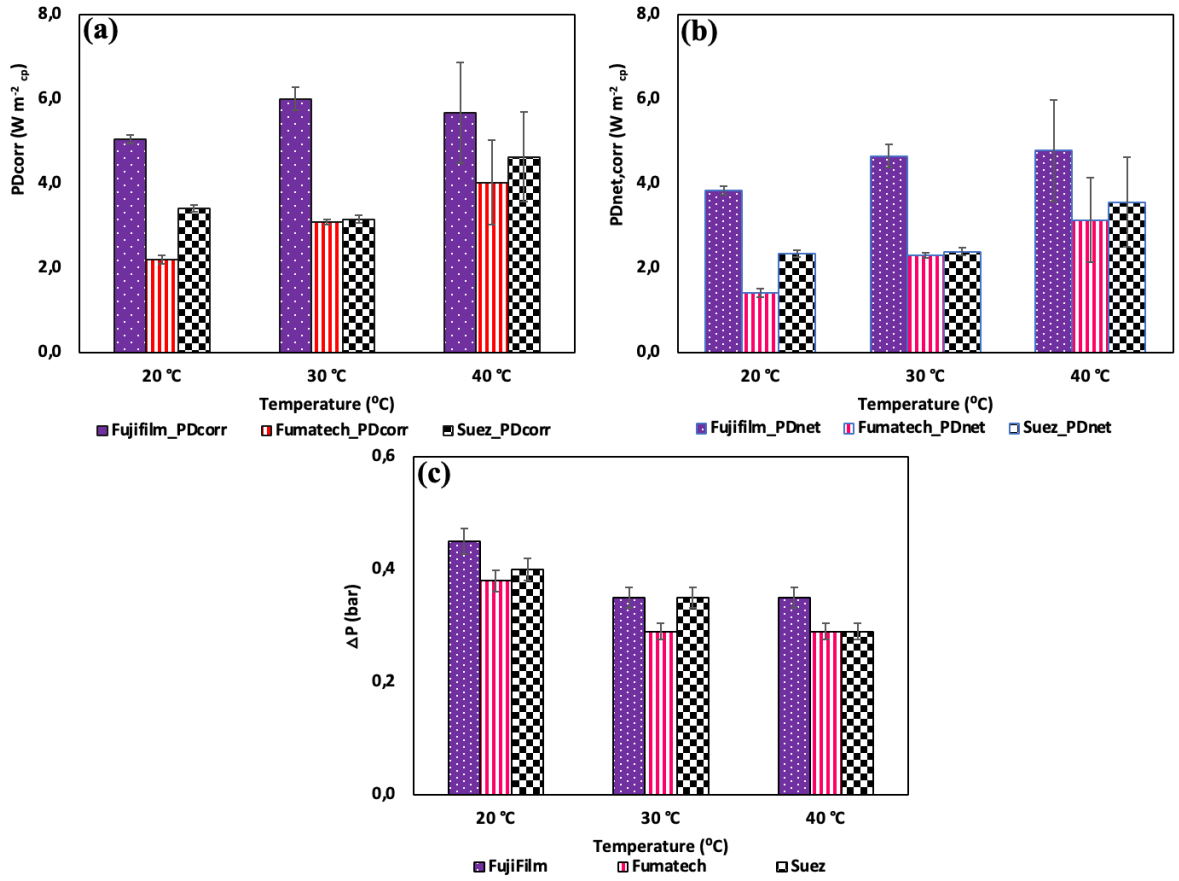

Figure 27. The influence of temperature on (a) power density, (b) Net power density and (c) average pressure drop in high and low compartments for the different IEMs under the experimental conditions of C_{High} = 5 mol L−1, C_{low} = 0.06 mol L^{-1}, and flow velocity of 1 cm s^{-1}.

The corrected power density increases with inflations at 20 to 40 °C. As already reported in the literature[124], [126], [127], the temperature has a beneficial effect on power density, so that when increasing it from 20 °C to 40 °C, the PD_{corr} increases for every membrane tested, though at different rates: from 5.0 W m^{-2}_{cp} to 6.0 W m^{-2}_{cp} for Fujifilm, from 2.2 W m^{-2}_{cp} to 4.0 W m^{-2}_{cp} for Fumatech, and from 3.4 W m^{-2}_{cp} to 4.6 W m^{-2}_{cp} for Suez stack.

Figure *27*b, shows a decreasing trend with a power density of three ion exchange membranes; these results agree with equation 8. On the other hand, with an increase in temperature, there has been a reduction in pressure drop in the channel of the whole RED stack assembled with different types of IEMs, as depicted in **Figure *27***c; the reduction of pressure drop is due to several effects such as membrane properties, viscosity, of the feed solution and transport numbers of the ions. The viscosity of the solution changes with temperature. Higher temperature leads to lower viscosity, which can affect the flow at the higher temperature, and thus can reduce the pressure drop. The ion-selective membranes are sensitive to temperature

changes. Temperature variations can influence selectivity, permeability, and electrical conductivity. These factors can affect the transport of ions and water through the membranes, impacting overall system performance and pressure drop. Other factor which can affect the pressure drop in RED system the thickness the of the IEMs as mentioned in **Table *7***.

In order to better explain the behavior of the system, the trends of OCV and R_{stack} have been monitored, as illustrated in **Figure 28**. Overall, the OCV of the stacks assembled with different IEMs has not been dramatically affected by the increase in temperature, whereas the internal resistance was differently reduced with the increase in temperature, likely due to the increase in ionic conductivity of the feed solutions and the membrane. The temperature rise has been found to enhance the degree of swelling and enlarges the size of the pores in the membranes, which helps ion migration through the membranes[128]. The resistance reduction effect is particularly evident for the Fumatech stack, where there is a variation from 2.39 Ω to 1.58 Ω, which eventually resulted in the increasing trend of PD for all membrane types [129].

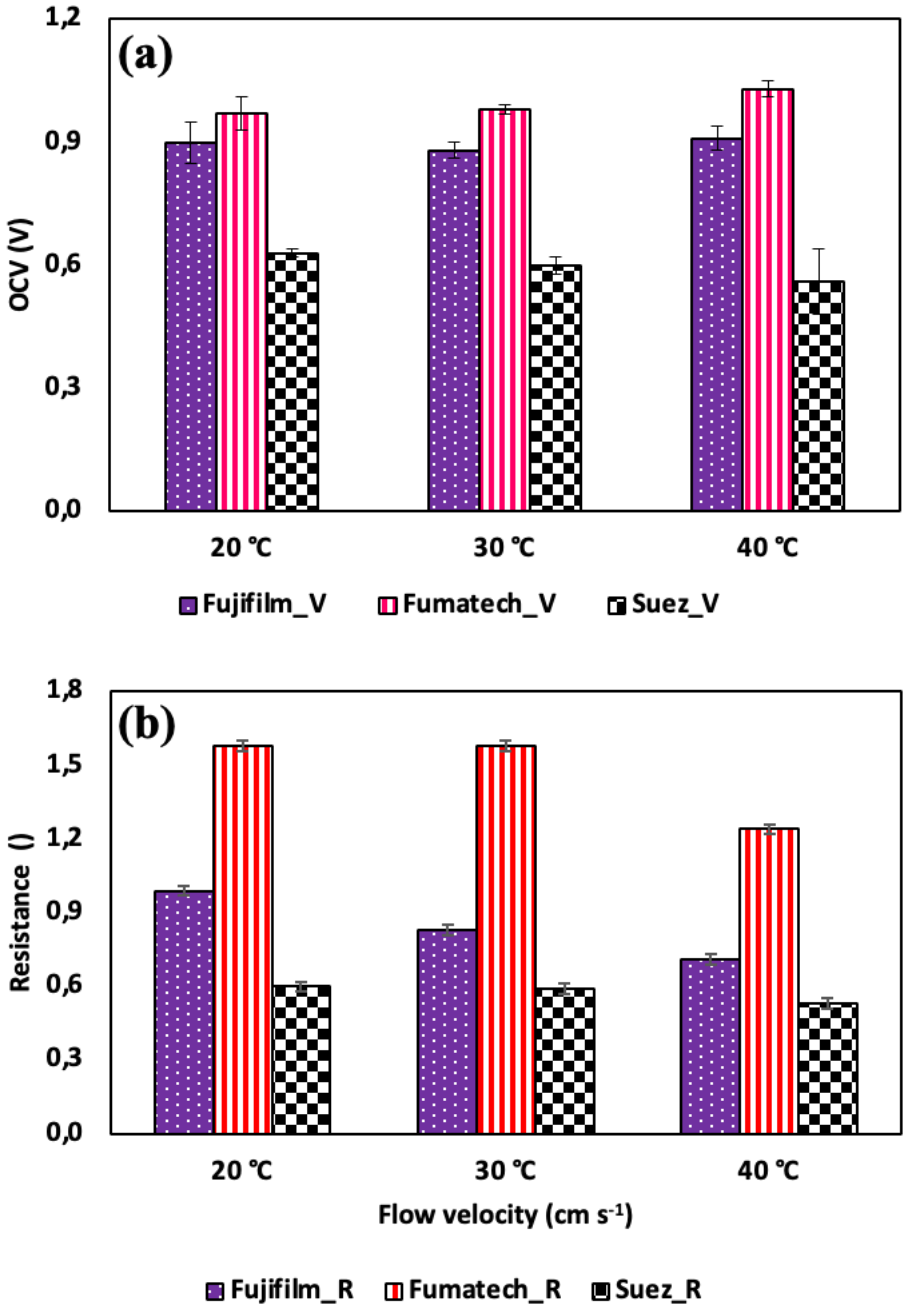

Figure 28. Variation of (a) Open circuit voltage and (b) stack resistance with temperature under the experimental conditions of 5 mol L^{-1} C_{High}, 0.06 mol L−1 C_{Low}, and 1 cm s^{-1} flow velocity.

The output power density of the RED system is related to the perm selective of ion exchange members during the test; this means that the higher the selectivity of the membranes, the more significant will be the system's output power. A perm-selective test was carried out at 30 °C . A fixed concentration of 5M and 0.06 M were circulated on both sides of the membranes during these experiments. The solution was circulated at a 200 mL/min flow rate for about 1 hour. The permselective measured by the given equation as given below.

$$\alpha = \frac{V_{thro}}{V_{Exp}} \quad (10)$$

Where V_{thro} is the voltage measured by equation 11 as theoretical and V_{Exp} is the voltage measured experimently.

As can be seen in ***Figure 29,*** the Fumatech IEMs illustrate the higer perm-selectivity and cell potential but due the higher resistant as mentioned in **Table *7***, and **Figure *28***b. On the other side, the SUEZ IEMs showed a very low cell voltage and perm-selectivity but observed a slight hiher power density than Fumatech membrane. This result suggested that membrane resistance and perm-selectivity are crucial for the RED system.

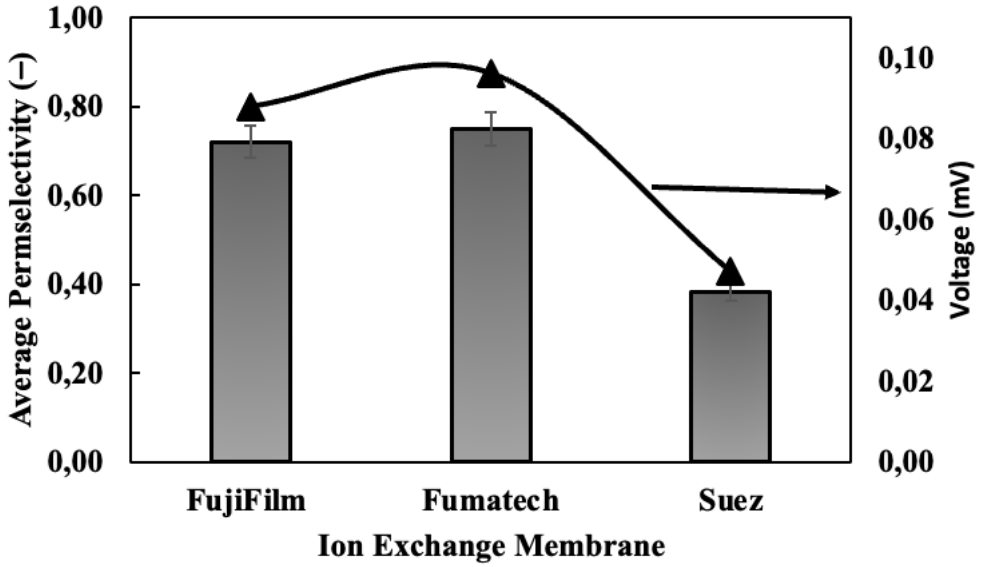

Figure 29. Ion Exchange membrane perm-selectivity using feed solution of HC= 5M and LC=0.06 M at 30 C°.

4.3.2 Influence of Dilute Solution Concentration

The influence of feed TDS has been evaluated at a fixed temperature of 20 °C by varying the concentration of the dilute solution for the stacks equipped with the three different membrane sets.

The concentration of the dilute solution (C_{Low}) has been studied in the range of 0.01–0.1 mol L^{-1}, which can be expected to be found at the outlet of a wastewater treatment plant [30].

It is clear how, for every concentration explored, the maximum PD_{corr} for the RED is always obtained with the membranes provided by Fujifilm, followed by Suez membranes and Fumatech membranes (see ***Figure 30*** a).

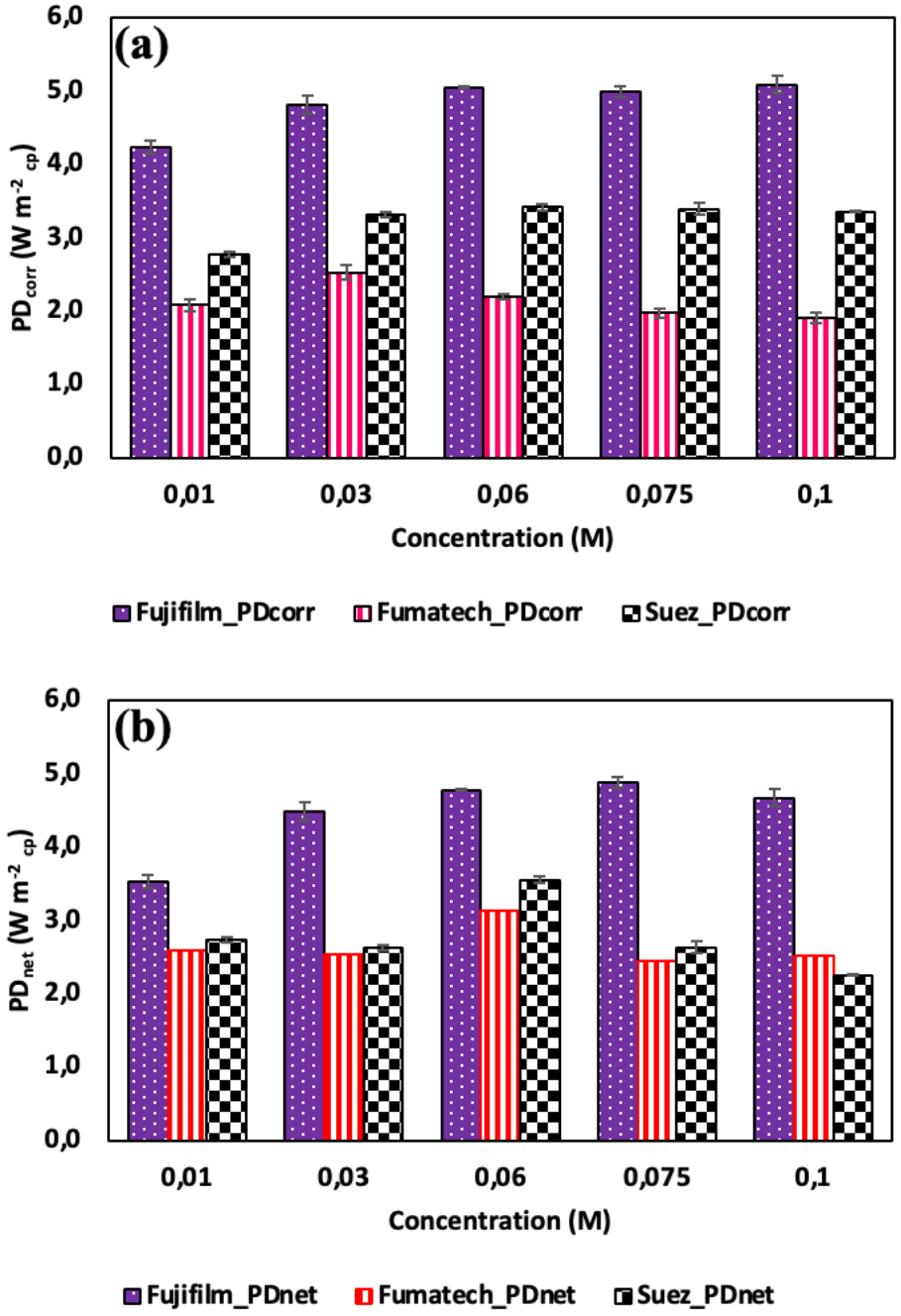

Figure 30. Influence of TDS concentration in the low salinity stream (CLow) on the three configurations' a) power density and b) Net power densitt using the fixed CHigh = 5 mol L−1, 20 °C temperature and flows velocity 1 cm s −1.

On the other hand, the maximum OCV is obtained with Fumatech membranes (0.97 V) rather than Fujifilm (0.9 V) or Suez (0.63 V) (see **Figure 31**). These two discordant results can be

explained by the different characteristics of the membrane under investigation; first of all, the average permselectivity of membranes αm, whose value determines the OCV according to Equation (11) [130] .

$$OCV = 2N\alpha_m \frac{RT}{zF} \ln\left(\frac{a_c}{a_d}\right) \quad (11)$$

Where R is the ideal gas constant (8.314 J(mol K^{-1}), T is the temperature (K), z is the valance number of ions (−), F is Faraday constant (96,485 C mol^{-1}), and a_c/a_d is the ionic activity of concentrated and diluted solution, respectively (mol $m^{-}3$).

Hence, the OCV is significantly enhanced by the high perm selectivity of both anion and cation Fumatech membranes and affected by the low values of SUEZ membranes (**Table *7***).
The advantage of a high perm selectivity comes with the cost of a higher membrane resistance, which increases stack resistance R_{stack} (see Equation (3)) and, in turn, in a reduction of the total producible power *P* according to Equation (6).

Since Suez membranes have the lowest internal resistance among the three providers compared, even in the absence of a high OCV, they succeed in achieving a higher power density than the Fumatech stack.

As a consequence of this delicate equilibrium between membrane resistance and perm selectivity, Fujifilm membranes, which have intermediate values of both parameters, result in the higher power density produced.

In the investigated range, increasing the concentration of the dilute compartment enhanced power production for Fujifilm and Suez stack, whereas in the last case (Fumatech membranes), the maximum power density was achieved for the intermediate concentration of C_{Low} = 0.03 mol L^{-1} (see ***Figure 30***).

This result can be interpreted as the different relative weights on stack resistance of the different membranes (see Equation (3)). Adopting SUEZ and Fujifilm membranes, dilute compartment resistance is always the limiting factor in power production for the explored C_{Low} concentration range. Conversely, Fumatech membranes resistance is so high that it limits power production for every concentration greater than 0.03 M.

Fumatech membranes outperformed the other in terms of OCV at various concentrations, as shown in **Figure 31**a**.** As expected, the general trend is a reduction of OCV moving C_{Low} from 0.01 mol L^{-1} to 0.1 mol L^{-1} because of the reduction in the salinity gradient.

A particular behavior observed in **Figure 31**b, is the distance between the two curves representing the internal resistance of Fujifilm and SUEZ stacks, which is not constant and tends to become negligible at higher concentrations. This occurrence is probably due to the membranes behaving differently in the presence of highly concentrated solutions among both sides of CEM/AEM, which can result in swelling and ion sorption phenomena that affect the IEC of the IEMs [131] and ultimately contribute to lower the actual resistance of the thinner membranes.

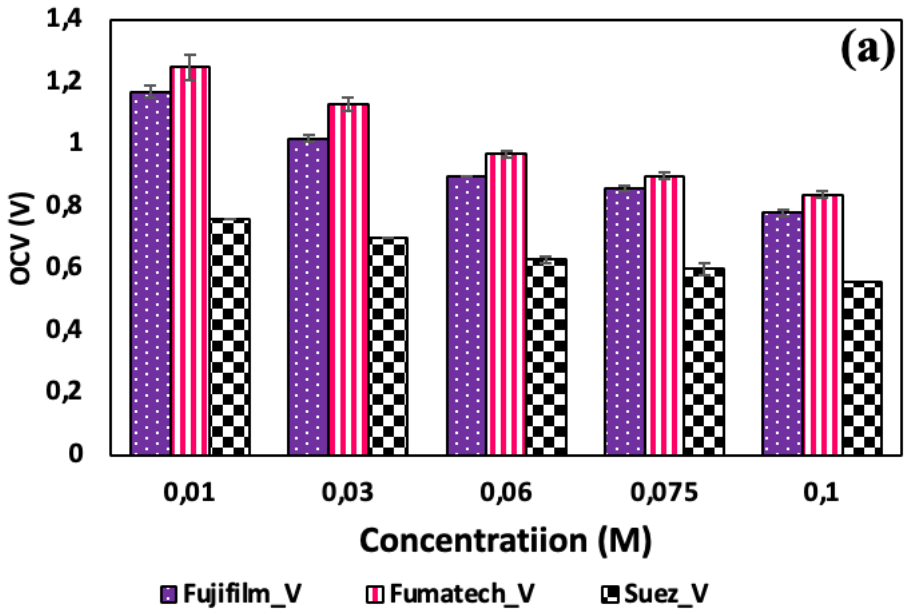

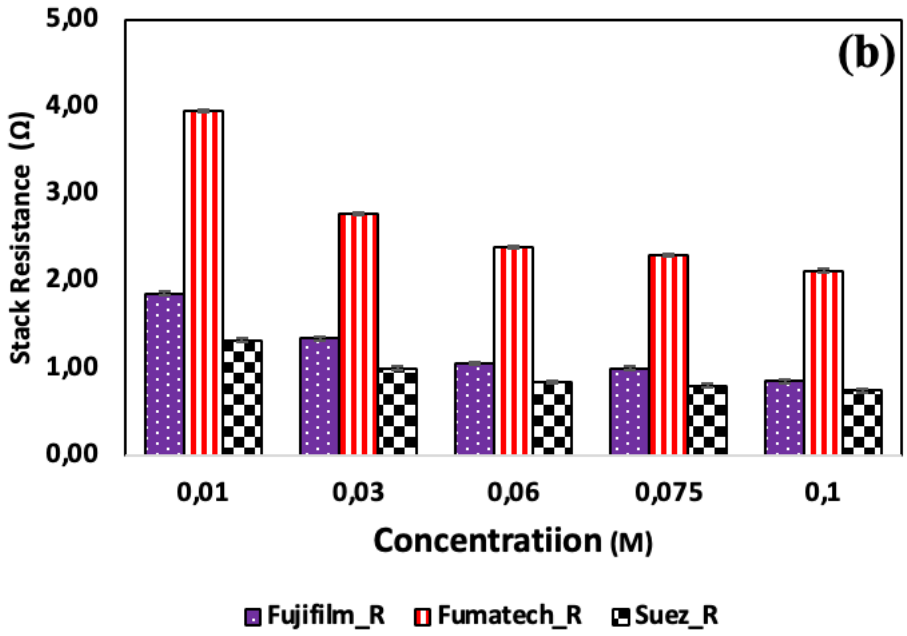

Figure 31. Variation of a) open circuit voltage (OCV), and (b) stack resistance with dilute concentration under the experimental conditions of 5 mol L−1 CHigh, 20 °C temperature and 1 cm s −1 flow velocity.

4.3.3 Influence of Feed velocity

The linear flow velocity of the streams running through the RED stack is strongly linked to net power density, and therefore, a specific working range is widely suggested. In this section, the RED stack was investigated between 1 and 3 cm s^{-1}. In this sense, three different IEMs were studied using a five-cell pairs stack. **Figure 32**, demonstrates the corrected power and net power density achieved for various flow velocities. The maximum $PD_{,corr}$ increases by 46% (Fujifilm stack), 29% (Fumatech stack), and 51% (Suez stack) as the velocity increases from 1 to 3 cm s^{-1}, allowing it to reach almost 10.5 W $m^{-2}{}_{cp}$ for the Fujifilm stack. However, the increase in $PD_{,corr}$ from 2 to 3 cm s^{-1} is much more limited than the one obtained from 1 to 2 cm s^{-1}. Even if the corresponding OCVs have shown modest improvement, stack internal resistance is reduced by the increased flow velocity (see **Figure 33**), thus improving power density. The increase of feed velocity on net power output is more evident due to the dramatic increase in hydraulic losses. In particular, the net power density becomes negative for the RED unit assembly with Fumatech IEMs, at the flow velocity of 3 cm s^{-1}, whereas Fujifilm exhibits the highest net power density of 5.8 W $m^{-2}{}_{cp}$, and Suez showed 3.20 W $m^{-2}{}_{cp.}$

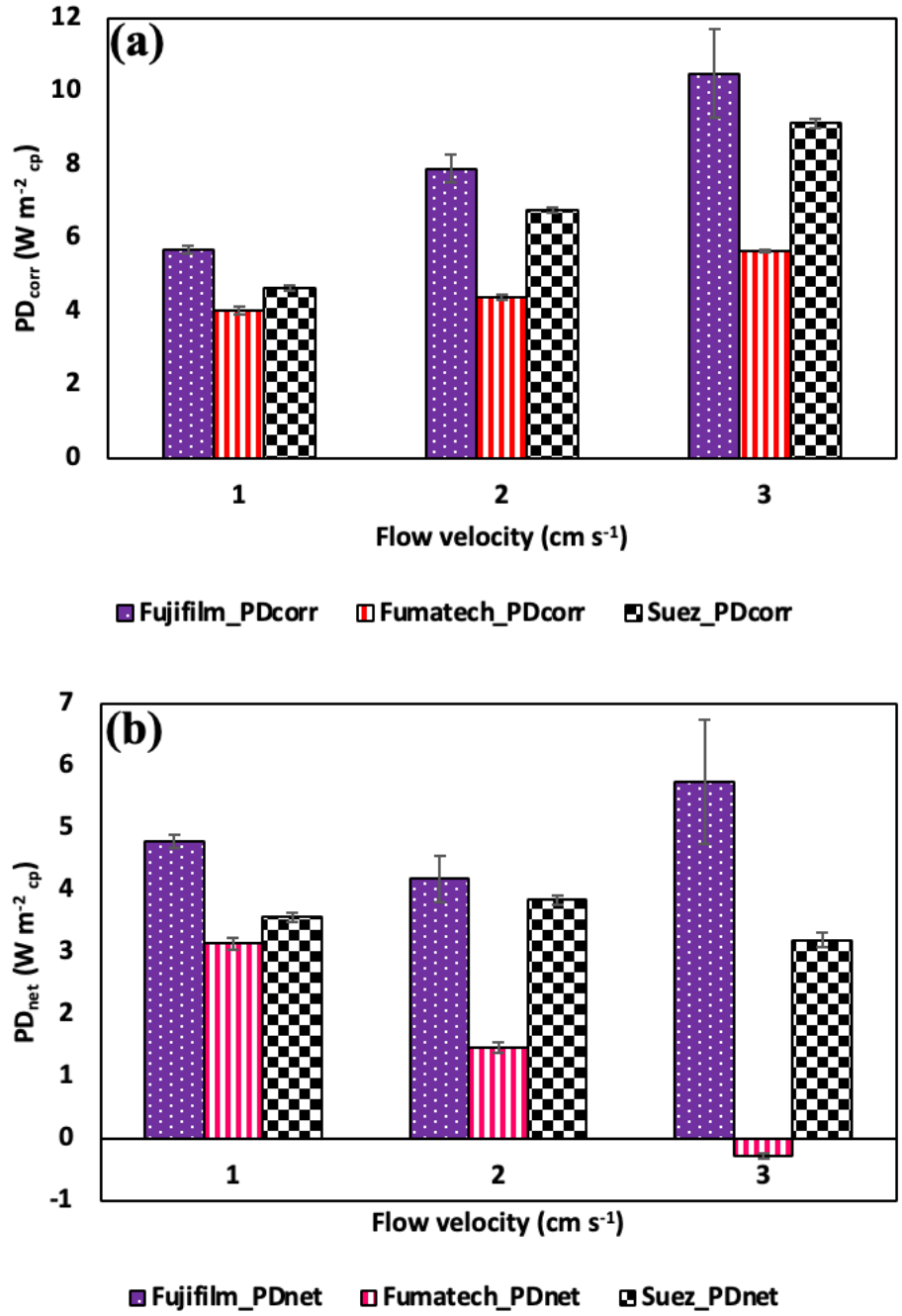

Figure 32. Influence of fluid velocity on (a). power density and (b) Net power desity for the different configurations under the experimental conditions of 5 mol L^{-1} C_{High}, 0.06 mol L^{-1} C_{Low}, and 40 °C temperature.

Regardless of the type of IEMs used, identical dependencies of *OCV* and stack resistance on stream velocity were observed. *OCV*, for instance, generally increases with velocity, whereas resistance decreases with velocity (**Figure 33**a). The *OCV* increase with velocity is due to the lower residence time in the stacks: the shortened residence duration results in a lower salinity gradient change between C_{High} and C_{Low} compartments and in a driving force that decreases

poorly along the streamwise direction [132]. The increase in flow rate increases the salinity gradient energy entering the RED stack per unit of time. The higher *OCV*, when using higher flow velocity, may be attributed to the lower effect from concentration polarisation phenomena. The output power of all the stacks assembled with different IEMs is considerable, with a high flow rate. The excessive flow velocity will enhance the hydrodynamic loss in the stack.

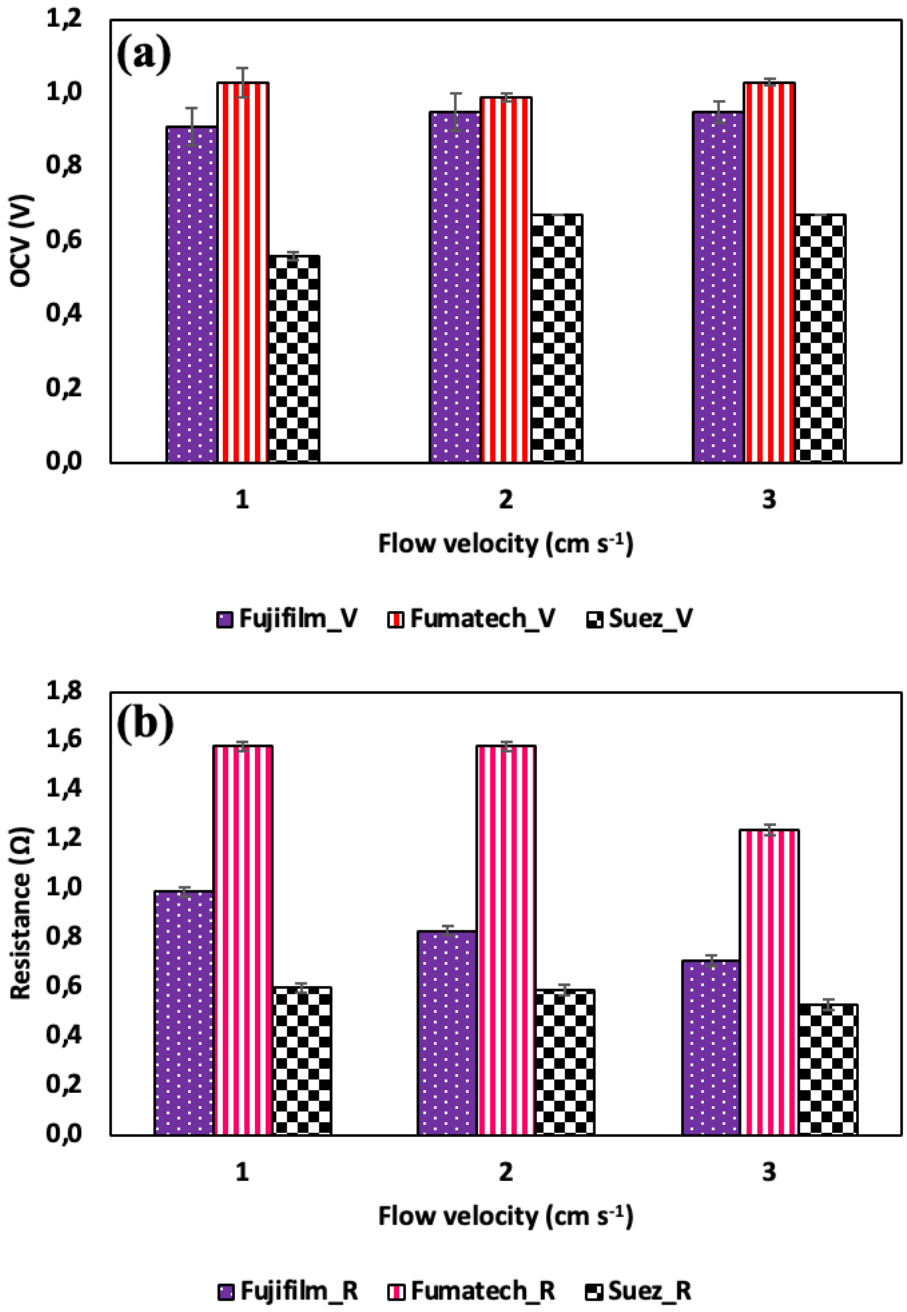

Figure 33. OCV and stack resistance variation with flow velocity under the experimental conditions of 5 mol L^{-1} CHigh, 0.06 mol L^{-1} CLow, and 40 °C temperature.

Finally, the best results collected in the present work were compared with other relevant results in literature. As can be seen in **Table 10** where all data are summarized, the power density achieved in the present work with the RED unit equipped with Fujifilm membranes (i.e., first row in the table) was the highest for feed solutions at 40 °C. Only a RED unit provided with Neosepta membranes and operated at 60 °C achieved a higher power density. Of course, this temperature is difficult to obtain naturally (i.e., bittern discharged in summer); instead, a solar or waste heat recovery would be needed to achieve such power.

Table 10. Comparison of present data to those previously reported in scientific literature.

Membrane	**Experimental Conditions**				**Concentration (mol L^{-1})**		**Performance**	**Reference**
Supplier	N° pairs	Flow velocity (cm s^{-1})	Area (cm^2)	Temp (°C)	C_{High}	C_{Low}	Power density (W m^{-2})$_{CP}$	
Fuji Type 10	5	3	10 × 10	40	5	0.06	10.5	This work
Fuji- Type II	-	8.7 mm s^{-1}	-	50	3	0.6	0.26	[127]
Fumasep	50	4	10 × 10	40	5	0.5	12	[101]
Neosepta®	4	0.81	10 × 10	40	0.513	0.017	1.88	[132]
YDS	8	0.717	17 × 7	40	66.70 g L^{-1}	0.66 g L^{-1}	0.88	[133]
Fuji-Type II	10	8.55 mm s^{-1}	0.118 × 0.065 m^2	50	3	0.06	0.2	[116]
Neosepta®	5	25 mL min^{-1}	10 × 10	60	5	0.01	13.4	[117]

4.4 Conclusion and Final Remarks

This work is a fundamental step towards the application of Reverse Electrodialysis for high salinity industrial brines valorisation, with particular reference to the operational scheme developed within the SEArcularMINE concept, where saltworks bitterns can be used to generate electricity via RED, using as a low salinity stream reclaimed water from other processes. Parametric analysis on stacks equipped with different IEMs has allowed us to assess the influence of ion exchange membranes produced by multiple manufacturers, temperature and flow velocity on converting chemical energy to electrical energy.

More than permselectivity, membrane resistance plays a significant role in SGP recovery. Indeed, the RED unit employing Fujifilm Type 10 membranes has shown a maximum $PD_{,corr}$ of 5.1 W m^{-2}_{cp} using 1 cm s^{-1} flow velocity at room temperature (20 °C) due to the fact that the membrane combines lower resistance and high permselectivity. On the other hand, working

with Fumatech membranes, characterised by higher permselectivity and resistance, resulted in only 1.9 W m^{-2}_{cp} for the same flow velocity, while SUEZ reached 3.4 W m^{-2}_{cp}.

It has been confirmed that temperature has a beneficial effect on power density $PD_{,corr}$, that raised from 5.06 W m^{-2}_{cp} to 6.01 W m^{-2}_{cp} (Fujifilm stack) with increasing temperature from 20 °C to 30 °C.

In conclusion, a maximum power density of 10.5 W m^{-2}_{cp} using C_{High} 5 mol L^{-1} and C_{Low} 0.06 mol L^{-1} and a flow velocity of 3 cm s^{-1} has been achieved in this study when using Fujifilm type 10 IEMs.

Chapter 5

Harvesting renewable energy from saltworks waste brines via reverse electrodialysis

Graphical abstract:

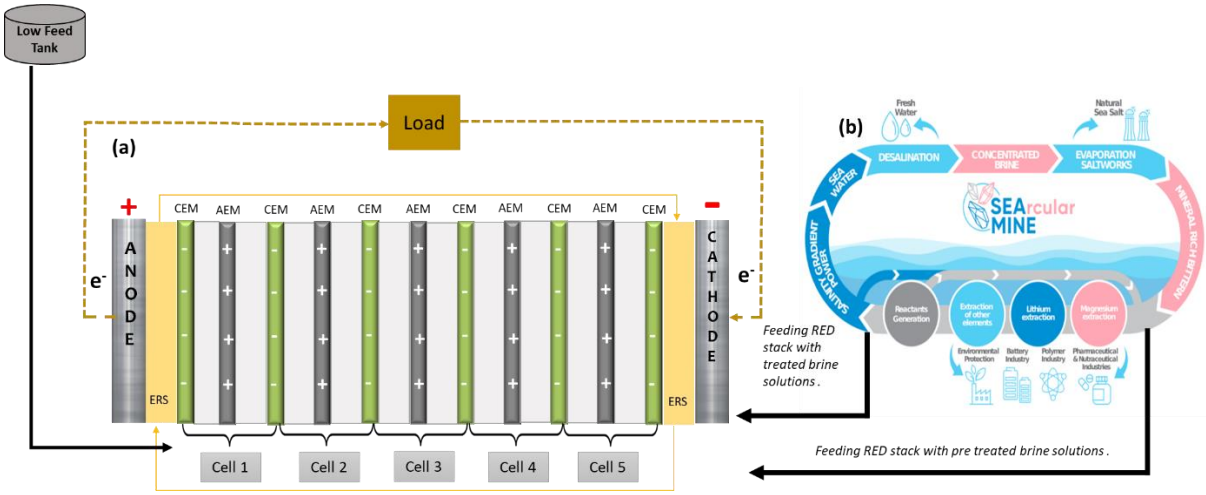

Abstract

As the world faces a climate emergency and a growing population, it is essential for us to discover cost-effective and sustainable methods of producing energy from renewable and continuous sources. This research presents an experimental campaign to investigate the possibility of harvesting electric power from saltworks waste brines (named bitterns and located in Trapani, Italy) by employing a laboratory scale reverse electrodialysis (RED). Two saltworks bitterns were tested depending on the basin location: Margi and Nubia saltworks. Two different homogeneous Ion Exchange Membranes IEMs, developed by (I) Fujifilm Manufacturing Europe BV (The Netherlands) and (II) Suez (France), were investigated under several experimental conditions. The membranes were characterized by ions sorption, membranes fixed charged, water uptake and permselectivity. Both real/pre-treated brine and artificial solutions (5 M of NaCl comparable to sodium chloride concentration in real brine) were investigated as feeds solution at 30 °C. The reinformed Fujifilm IEMs resulted in high electrical resistance, yet exhibiting high permselectivity.

Interestingly, the monovalent ions sorption and counter ion concentration of Fuji IEMs were higher than Suez membranes, while the co-ion concentration in both IEMs were comparable. The RED application with hypersaline Margi-A and Nubia-A brine (TDS; 364.60 g/L and 359.28 g/L) showed a power density of 3.57 W/m^2 and 4.32 W/m^2 for Fujifilm IEMs, respectively, while Suez (ultra- thin nonwoven polyester cloth) IEMs demonstrate a significantly lower power density of 0.77 W/m^2 and 0.69 W/m^2, respectively.

Keywords: Brine; Ion exchange membranes; Ion sorption; Reverse electrodialysis, Salinity gradient energy.

This Chapter under internal Revision

Syed Abdullah Shah, Enrica Fontananova, Andrea Cipollina, Alessandro Tamburini, Alberto Figoli, Giorgio Micale, “Harvesting Renewable Energy from saltworks waste brine via Reverse Electrodialysis”.

5.1 Introduction

According to the US Energy Information Administration, total worldwide power production is predicted to grow from 20 trillion to above 40 trillion kWh by 2040; among all energy sources currently rising demand, renewable energy is the fastest growing by 2.8% ramp up per year [134]. Salinity Gradient Power (SGP) is a novel blue energy source due to its architectural and technological advancement. SGP originally proposed by Pattle in 1954 by mixing of seawater and river water [135]. SGP has tremendous potential to meet global energy necessity, and the overall evaluated technical natural salinity potential energy is 647 GW, which is corresponding to 23% of the global power consumption [111], [136]. Suitable SGP application sites are estuaries where river water (freshwater) meet into the seawater [106], [137], [138], saltworks and salt mining [139], [140], hypersaline stream from desalination plant [141], [142] and saltwater lakes [143].

The most promising membrane-based technologies for SGP harvesting are reverse electrodialysis (RED) [105], [106] and pressure- retarded osmosis (PRO) [144], [145] compared to other techniques [146], [147]. Usually, a RED stack consists of alternating cation exchange membranes (CEMs) and anion exchange membranes (AEMs) between the cathode and anode, as described in **Figure *34***. The ion exchange membranes (IEMs) are kept apart from one another by placing a spacer in between. The resulting channels host the feed saline. During the process, the ions move through the IEMs from the High Concentration Compartment (HCC) to the Low Concentration Compartment (LCC) due to the salinity difference across the membranes. This ion flux is converted into electricity in the electrodic channels via suitable reversible redox reactions occurring on the electrode surface when an external load resistance is connected to the circuit [105].

In the framework of the SEArcularMINE project, which is focused to the sustainable valorization of brine for valuable minerals recovery and the harnessing of renewable energy through innovative technologies, a strategic approach has been implemented to address the complexities associated with divalent ions during the operation of a Reverse Electrodialysis (RED) system. Specifically, the RED unit has been fed with both untreated brine and brine that has undergone a treatment process within a Magnesium Hydroxide Crystallization Reactor (Mg-CGCR) [148]. This innovative approach is poised to revolutionize the field by mitigating the impact of divalent ions, thereby enhancing the efficiency and effectiveness of the RED unit within the broader objectives of the SEArcularMINE project[120].

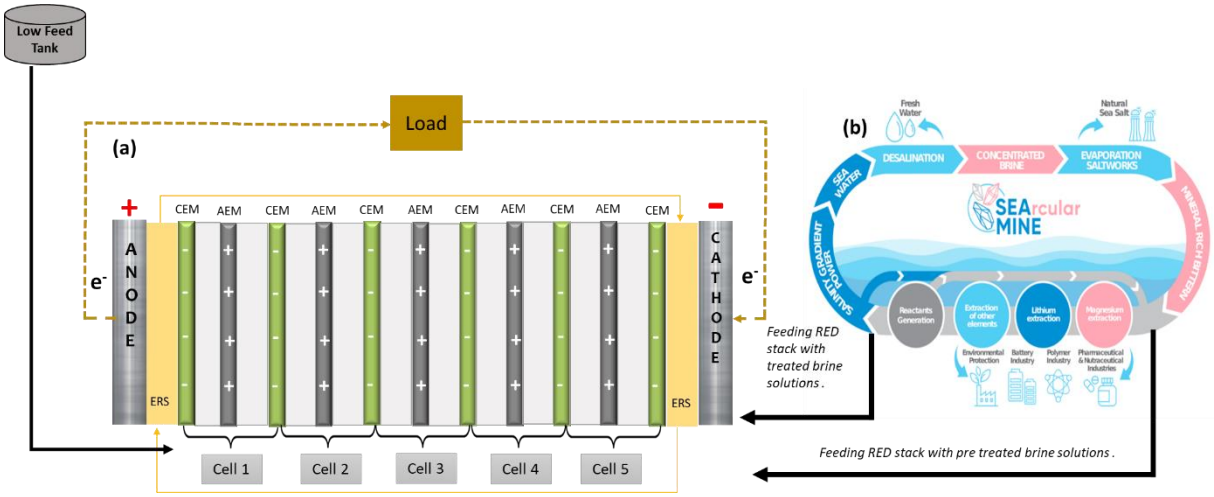

Figure 34. a) Schematic representation s of the Reverse Electrodialysis (RED) and, b) Searcular Mine project process [120]. CEM: Cation exchange membrane; AEM: Anion exchange membrane.

The most widely available natural source of salinity gradients are seawater and river water. In ideal situation the theoretical calculated SGP is very high e.g., 1 m^3 seawater (30 kg. m^{-3}) completely mixed with the same amount of river water (pure water) generate 1.7 MJ energy at 298 K, that can increase up to 6.1 MJ by volumetric ratio pure water/seawater is 10:1 [149]. By R.E Pattel in (1954), the power density of 0.20 W/m^2 was first determined via RED [135]. Currently, significant breakthroughs in membrane technology and membrane engineering led to a rise in the power density. RED units equipped with commercially available IEMS have shown a maximum power density of 6.7 W/m^2 and 12 W/m^2 on laboratory scale experimental study respectively [101], [117]. Kim et al. developed a lab scale pore filling IEMs and obtained a power density of 2.4 W/m^2 [150]. The same author reported the resistance of homemade IEMs was lower than commercially available IEMs such as AMX/CMX (Tokuyama Co., Japan), FAS/FKS (Fumatch GmbH, Germany) and AMV/CMV (Asahi Glass Co. Ltd, Japan). Choi et al. studied the effect of ion exchange capacity of lab made membrane in RED and reported a maximum power density of 0.69 W/m^2 using a single cell pair RED stack [107]. Shah et al. observed 27 mW/m^2 maximum power density by modified Nafion nanocomposite membrane (CEM) combined with FAA3 (AEM) at 75 mL/min flow rate in a single cell pair RED unit [106].

Aforementioned literatures are carried out using only NaCl as a feed solution in the RED process. However, a diverse spectrum of monovalent and multivalent ions are available in the natural feed stream. The presence of divalent ions, such as (Ca^{2+}, Mg^{2+}, and SO_4^{-2}), in natural seawater and river water applications has been studied through experiments: the gross power density of the process was affected by the multi-ion solutions compared to artificial NaCl

solutions [111], [151]. The most notable effects of the presence of divalent ions included an increase in IEM resistance, uphill transport, and a decrease in Nernst potential. Simoes et al. (2022) operated a RED unit for one month with natural water, at the Afsluitdijk, the Netherlands, and measured the gross power density between 0.3 to 0.4 W/m^2 [152]. Avci et al reported a power density of 0.46 W/m^2 and a stack resistance of 30.5 Ω using natural feed solution at 60 ºC, whereas artificial feed solution at the same temperature indicated a power density of 1.41 W/m^2 and a stack resistance of 12.8 Ω [111]. All of these studies focused on river-water – seawater, while a very few efforts have been devoted to the investigation of multi-ion feed streams at higher concentrations (i.e. brines). With this respect, the analysis of natural feed solution discharged from saltworks is essential for a comprehensive comprehension of RED potential.

In this study, we investigated two distinct types of commercial membranes (Fujifilm and Suez), focusing on counter-ions with charges opposite to those of the fixed charge groups and co-ions with charges matching those of the fixed charge groups. These ion exchange membranes were sourced from manufacturers and subjected to desorption techniques.

The membranes were equilibrated by exposure to external solutions containing NaCl concentration (0.5, 1 and, 5 M) and real Margi brine solutions. Additionally, we also explored the water uptake and permselectivity, shedding light on the behavior of both membranes across a range of salt concentrations and in the presence of real brine solutions.

The performance of a lab-scale RED unit was evaluated in a real environment by testing two real brine discharge for distinct origin and salinities, but both coming from the saltworks: Margi saltwork brine and Nubia saltwork brine as feed solutions.

5.2 Experimental part

5.2.1 Material

Two different homogeneous Ion Exchange Membranes IEMs, developed by Fujifilm Manufacturing Europe BV (The Netherlands) and Suez (France) were investigated: Fujifilm-AEM-Type 10 and Fujifilm-CEM-Type 10, Suez AEM (AR103) and CEM (CR67U) [153].

Fujifilm membranes were supplied in the dry form before the use and were activated in 0.5 M of NaCl while Suez membranes were received in wet form (Deionized water) and were immersed in 0.5 M of NaCl for activation. All the experiments were repeated twice, and medium values were reported.

5.2.2 Water Uptake

Square ion exchange membrane samples (3.5 *3.5 cm^2) were pre-soaked for 48 hours in di-ionized water (DI) to remove residual solvents not associated with the fixed-charged group. They were then immersed in artificial aqueous solution of NaCl only at 0.5 M, 1M, 5M and in real Margi A brine, in both cases in a volume of 30 mL for 48 hours. These membranes were then put on a scale to obtain their wet mass (W_{wet}). The membranes were dried in an oven at 50 ºC for 24 hours to measure the dried mass (W_{dry}). Water uptake can be calculated as:

$$W_u = \frac{W_{wet} - W_{dry}}{W_{dry}} X\ 100 \quad (1)$$

5.2.3 Ion Sorption

Following water pre-soaking these membranes were then immersed in 30 mL of an artificial aqueous solution 0.5 M, 1M, 5M NaCl and real Margi brine for 48 h to reach equilibrium, after which the membranes were transferred to water of a known volume 30 mL for a further 48 hours. During the second soaking period, the absorbed co-ions were released into the water. The concentration of co-ions in these water samples were later measured by ion chromatography.

The cation exchange membranes were moved to 0.5 M HNO_3 solution and anion exchange membranes were transferred to 0.5M of NaOH solution of a known volume (30 mL) for a further 48 h to release the adsorbed counter-ions. The solution was changed after each 48 hours to make sure that all counter-ions are released. During this soaking period, the adsorbed ions were released into the HNO_3 and NaOH. The concentration of counter-ions in HNO_3 and NaOH were later measured by ion chromatography.

The concentration of ions in CEMs and AEMs was measured by ion chromatography. One time desorption procedure was sufficient to extract all co-ions from the membranes: as a matter of fact, a negligible co-ions concentration was found in the second desorption solution.

The co-ion and counter-ion concentration in the membrane was calculated from:

$$C^m_{co-ion_i}[\frac{mol}{kg_{water}}] = \frac{10^{-3} * m_i^{sol}[ppm] * M_{sol}[g]}{MW_i * W_u * M_{dry}[g]} \quad 2$$

$$C^{m}_{counter-ion_i}[\frac{mol}{kg_{water}}] = \frac{10^{-3} * m_i^{sol}[ppm] * M_{sol}[g]}{MW_i * W_u * M_{dry}[g]} \quad 3$$

where $C^{m}_{co-ion_i}$ is mole of ions per kg of membranes (i.e., water and ions in the volume of the swollen membrane), m_i^{sol} is part per million of ions (ppm), M_{sol} is volume of desorption solution, and MW_i is molar weight of the ion and M_{dry} is dry mass of the membrane in grams.

5.2.4 Perm selectivity

A two-compartment cell was operated at a temperature of 30 °C to determine the membrane potential as shown in **Figure 35**. The membranes were conditioned in a 0.5 M NaCl solution overnight before measurements were taken. After that, the membrane was placed between the compartments where two solutions at different concentrations were fed, and the membrane potential was measured using Ag/AgCl reference electrode connected to a multimeter (Fluke 289).

To facilitate the measurement process, the solutions were continuously recirculated through the compartments using two gear pumps, operating at a flow rate of 2 cm s^{-1}, and maintained temperature at 30 °C. Finally, the permselectivity (α) was calculated by taking the ratio between the measured membrane potential (V) and the theoretical membrane potential (V), as outlined in equation 4.

$$\alpha = \frac{\Delta V_{measured}}{\Delta V_{theoretical}} \quad (4)$$

$\Delta V_{theoretical}$ is measured by the Nernst equation which is reported in equation 5 for the case of saline solutions composed of NaCl only.

$$\Delta V_{theoretical} = \frac{RT}{zF} \ln\left(\frac{a_c}{a_d}\right) \quad (5)$$

where R is the universal gas constant (J mol^{-1} K^{-1}), T is the absolute temperature (K), F is the Faraday constant (C mol^{-1}), a_c and a_d is the activity of the concentrated and diluted solution (mol L^{-1}), respectively, and z is the ion valence (-). The extended Debye-Huckel equation can be used to determine the activity coefficient [154].

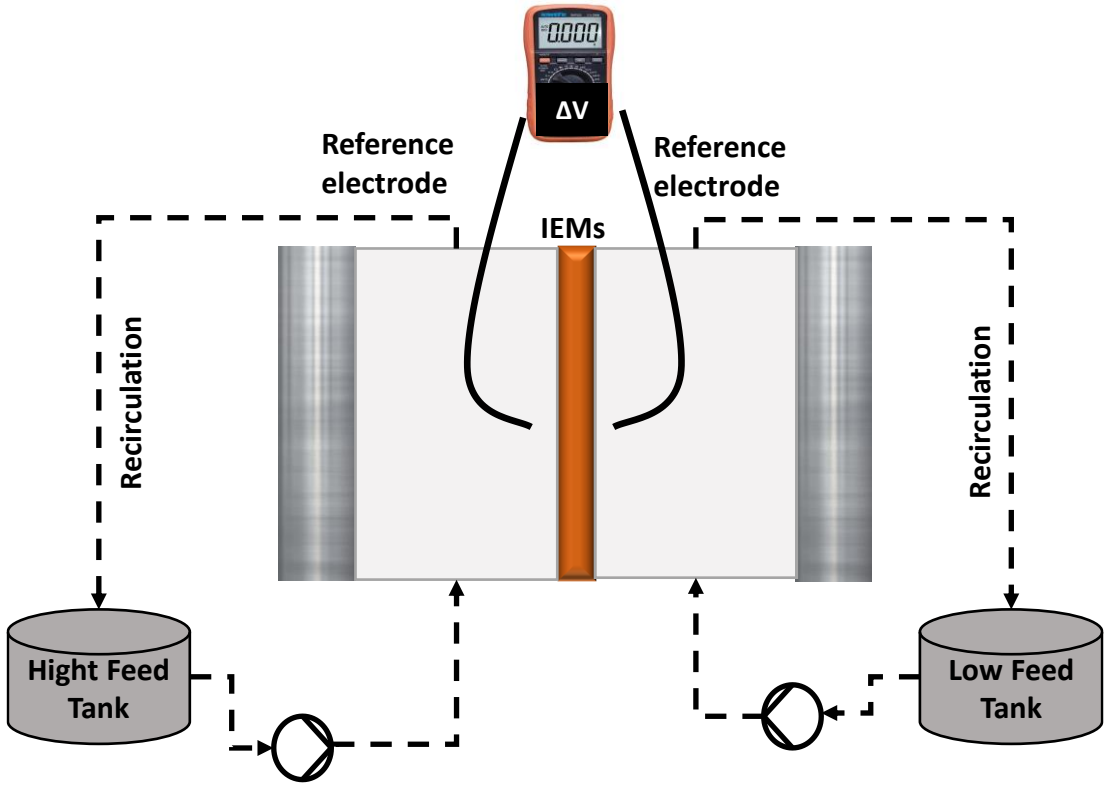

Figure 35. Characterizing perm selectivity in a two-compartment system.

For real brine solution $OCV_{theoretical}$ was calculated by the following equation.

$$\Delta V_{theorectical} = \frac{RT}{F} ln \prod_i \frac{(\gamma_{\pm}^{c} C^{c})^{\frac{1}{z_i}}}{(\gamma_{\pm}^{d} C^{d})^{\frac{1}{z_i}}} \quad (6)$$

where $\gamma_{\pm}^{c}$ and $\gamma_{\pm}^{d}$ represent the activity coefficient of the ion while C^{c} and C^{d} represent the high and low concentration solution respectively.

5.2.5 Reverse electrodialysis stack

A conventional lab scale RED stack (REDstack B.V., Netherlands) comprised of five piled cell pairs (see Error! Reference source not found.), with an active membrane area of 10×10 cm^2, as described in our previous paper [153], was investigated. The IEMs were separated by placing a polyamide woven spacer 270 μm thick (Deukum, Frickenhausen, German) to create the feed channels. At the end-plates, a pair of 10×10 cm^2 two Ru-Ir oxides coated titanium electrodes

(Magneto Special Anodes BV) were used as a cathode and anode. Before each RED test, a pre-treatment process was used to condition the membranes by keeping the stack in the solutions to be tested overnight.

RED experiments were carried out at different flow velocity (1- 3 cm/s), as detailed in Table 11. High H_c and Low L_C feed solutions were fed to the stack at the same temperature 30 ºC. 0.1 M of $K_3Fe(CN)_6$/ $K_4Fe(CN)_6$ and 0.6 M NaCl is used as electrolyte rinse solution. The feed solutions were fed to the stack by Masterflex L/S peristaltic pumps (BT601S from Lead Fluid Technology, CO LTD, China). A custom-made heating bath was employed to keep the feed solutions at the desired temperature. The solutions conductivity was monitored by a conductivity meter (3320, Xylem). To quantify measurement uncertainty, all experiments were repeated three times, and experimental results were averaged.

As feeds, two different saltworks bitterns were investigated (i.e. Margi and Nubia). In addition, in accordance with SEArcularMINE project idea, these brines might be either directly sent to a RED unit for electricity production or pretreated by removing Mg^{+2} ions in an upstream crystallizer and reducing the brine salinity. The former case is hereafter regarded as untreated brine, case A; the latter is hereafter regarded as treated brine, case B. Relevant compositions are reported in section 5.2.7. Moreover, for comparison purposes, an artificial Ca^{+2} and Mg^{+2}-free brine solution having a conductivity being similar to that Margi-A solution was also investigated. This solution was named Margi-S feed. Its composition is also reported in section 5.2.7.

Table 11. Scenarios configuration for the experimental campaign

Scenario	**Flow velocity (cm/s)**	**Temperature (°C)**
Margi A		
Margi B		
Nubia A	1 to 3	30
Nubia B		
Margi S		
Synthetic solution	1	

"A" means untreated brine, "B" means treated brine, and "S" Spiked brine.

5.2.6 Polarization curve and power measurements

The measurements were done by connecting two multimeters (Fllike-175) one in series and one in parallel to the RED stack (the range varying from 0-10 A). They are used to measure the polarization curve, i.e. the current-voltage (I-V) curve and the corresponding power *P* produced. In order to do so, a variable load resistance R_{load} (BK Precision, 8540) was employed. Power generation per unit cell pair area is defined as power density (W/m^2):

$$P_d = \frac{P}{NA} \tag{7}$$

where N is the number of cell pairs (5) and A (0.01 m^2) is the active area of membranes.
The blank resistance R_{blank} has a significant effect on the power density when a small-scale RED unit composed of a few cell pairs is adopted. However, using a large number of cell pairs (e.g., in a full-scale stack) where the contribution given by electrode compartments to total stack resistance (R_{blank}) becomes negligible on the power density. The R_{blank} was measured by mounting the RED unit with only one end membrane and electrode compartments were fed with electrode rinse solution (ERS) only. Once measured, a corrected power density ($P_{d,corr}$) can be computed by subtracting R_{blank} from the stack resistance R_{stack} according to equation 8. The resistance used to calculate the power density is the relevant to the cell pairs only and it is named R_{cells} ($R_{cells} = R_{stack} - R_{blank}$). R_{stack} is inferred from the slope of the measured I-V curves. [101]. The resulting

$$P_{d,corr} = \frac{OCV^2}{N\ A\ R_{load}\left(1 + \left(\frac{R_{cells}}{R_{load}}\right)\right)^2} \tag{8}$$

where OCV is the open circuit voltage.

5.2.7 Ion chromatography

Ion chromatography (Metrohm, Italy) analysis was employed to quantify the ions present in real and treated brine at the inlet of RED unit operated under the experimental conditions shown in **Table** 12. The samples were analyzed at room temperature at which ion chromatography was calibrated. 3.2 mM Na_2Co_3 + 1 mM $NaHCO_3$ was used as eluent for anion column (882

compact IC flex), whereas 5.5 mM phosphoric acid solution was used as eluent for the cation column (930 compact IC flex). The measured compositions are reported in Table 12

Table 12. Composition of real treated brine of salt works.

Type of Brine	Composition (g/L)							TDS (g/L)	Conductivity (mS/cm)
	Na^+	K^+	Mg^{2+}	Ca^{2+}	Cl^-	Br^-	SO_4^{2-}		
Margi A	56.10	13.27	49.40	0.05	181.69	2.48	61.59	364.60	162
Margi B	27.48	1.87	0.00	0.00	24.20	0.00	8.073	62.28	104
Nubia A	72.59	11.02	38.65	0.00	186.29	2.18	48.55	359.28	184
Nubia B	28.40	1.59	0.01	0.00	26.65	0.31	7.30	64.26	125
Margi-S	96.07	0.69	0.01	0.00	102.46	0.05	26.07	225.35	218

5.3 Results and discussion

5.3.1 Water Uptake and membrane fixed charge concentrations

Figure 36, presents the water uptake behavior of ion exchange membranes (IEMs) after equilibration with artificial NaCl solutions of different concentrations: 0.5 M, 1 M, 5 M, and the real Margi brine solution. Membrane swelling by the water absorption into the charged polymer has a direct effect on the absorption behavior of the IEMs. Water permeated the polymer matrix to hydrate both the fixed charged group and their counter-ions. The hydration of the IEMs resulted in the expansion and elongation of the polymer network. The crosslinking of the polymer creates elastic forces that push back against expansion, preventing too much water from infiltrating the network [155]. The water uptake of IEMs is affected by several factors, such as (I) counter-ions concentration, (II) counter-ions hydration and (III) how they interact with the fixed charged group. The water uptake is also related to fixed charged group, external concentration, and degree of crosslinking [156].

Figure 36, presents water uptake as a function of artificial aqueous solution of NaCl only and real brine solution for Fuji and Suez IEMs. Water uptake values present in **Figure 36,** which clearly shows that the two membranes having considerably different water uptake values. The water uptake value is 0.34 and 0.71 (wet mass / dry mass) for Fujifilm CEM and Suez CEM respectively. For all monovalent salt external solution, the water uptake values decreased for both IEMs membranes due to osmotic deswelling [157] [158]. The osmotic deswelling depend on polymer crosslinking [159]. Fuji IEMs has the largest amount of polymer crosslinking and

the lowest amount polymerization solvent. Higher crosslinking favors lower water uptake and less osmotic deswelling at higher external salt concentrations. The opposite trend was observed in the case of brine external solution for both IEMs.

The backing fabric is changed from Fujifilm IEMs is polyolefin and polyester cloth for Suez IEMs as described by the manufacturers. The percentage water uptake for Fujifilm CEM membranes is a bit lower at 5 M NaCl only solution (0.34 g/g) compared to 0.5 M and 1 M salt solutions (0.31 g/g). The swollen Suez cation exchange membranes are greater in both water uptake and thickness. The water uptake appears to be identical between 0.5 M and 1 M using Suez AEM and declined 5% in 5 M salt concentration while in case of Suez CEM the decrease is more pronounced (17% from 0.5M to 1M and 31% from 1M to 5M). An increase in both IEMs water uptake was observed for the case of real bitterns. This is probably due to the presence of divalent ions in the brine streams.

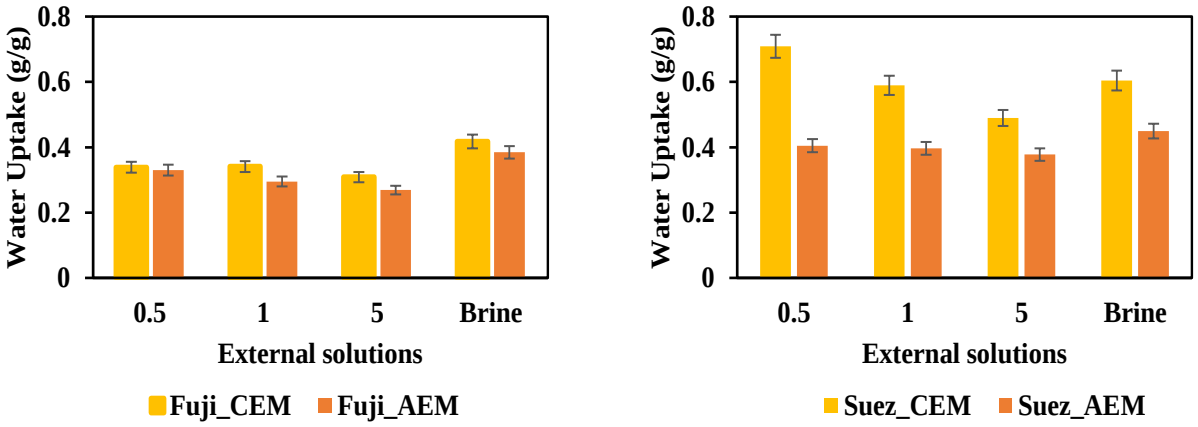

Figure 36. Influence of external salt concentration and brine solution on water uptake in Fuji and Suez IEMs.

5.3.2 Co- ion concentration in membranes

The concentrations of both counter-ions and co-ions within the ion exchange membranes (IEMs) were quantified. Predominantly, the counter-ions found within the membrane are closely linked to the fixed charges residing within the polymer matrix. However, a minute fraction of counter-ions is necessary to neutralize any co-ions that may have been sorbed within the membrane.

The presence of co-ions is effectively blocked from permeating the membrane, primarily because they face repulsion from the fixed charge groups. These charge groups create an

electric potential, referred to as the Donnan potential, at the interface between the membrane and the surrounding solution, as described initially by Donnan in 1924 [160]. As the concentration of external salt increases, this electric potential diminishes due to the screening effect of charged species, thereby enabling a greater intake of co-ions. Thus, as expected, the concentration of co-ion (i.e., Cl^-) in Fujifilm CEM and Suez CEM and (i.e., Na^+) in both membranes AEMs, increase with increasing external salt solution concentration in **Figure 37**.

The Donnan potential exhibits an inverse relationship with the valence of counter-ions [161]. Consequently, the introduction of divalent counter-ions, such as magnesium in Anion Exchange Membranes (AEMs) and sulphate in Cation Exchange Membranes (CEMs), serves to diminish the Donnan potential. This reduction, in turn, contributes to an augmented co-ion concentration within the membrane. Furthermore, the similar behavior of the Cl^- in both CEMs is due to the higher water uptake of Suez membrane as shown in **Figure 36**. The co-ion Na^+ in Suez AEM were ~22% and Mg^{2+} were ~62% higher than the Fujifilm AEM.

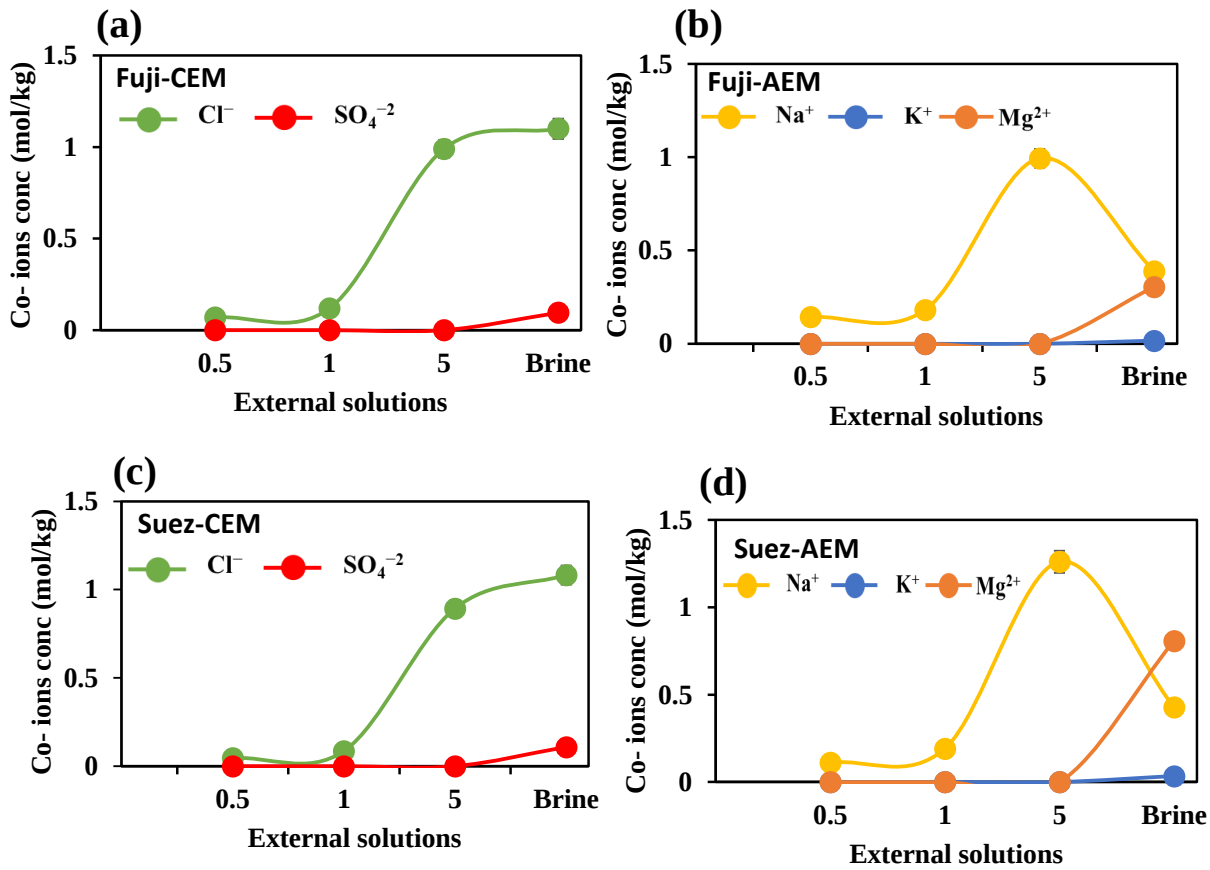

Figure 37. Concentration of co-ion (expressed in mol/kg) in Fuji and Suez cation exchange membranes and anion exchange membranes as function external salt and real Margi brine solution.

5.3.3 Counter ion in cation exchange membrane

Counter-ions in the cation exchange membranes (swollen membranes) are reported in moles per kg in **Figure 38**, CEMs were pre-soaked in water. At 0.5 M and 1 M the measured counter-ions concentration was similar and low compared to 5 M solution because at high external solution concentration all fixed charge groups are occupied. Moreover, more counter-ions are sorbed in Fujifilm CEM than in Suez CEM, resulting from a better IEMs but a smaller swollen membrane for fuji CEM. When a bittern is adopted as saline solution, the concentration of magnesium in Fuji CEM is 2.27 mol/kg which is half of that of sodium due to its double charger (**Figure 38** (a)). The Suez CEM exhibits a magnesium ion concentration of 1.42 mol/kg while the sodium ion concentration is 1.96 mol/kg which is 26% less than the Mg^{2+} (**Figure 38** (b)). Notably, the concentration of Na^{+} in the membranes approached that of magnesium. This phenomenon arises due to the screening effect of the accumulating ions in the solution, leading to a decrease in the strength of electrostatic forces. Consequently, the Donnan exclusion effect is reduced, particularly for monovalent ions. It should be noted that the Mg^{2+} concentration in Suez CEM is very close to the single salt concentration, although the magnesium concentration in brine external solution was low. While the hydrated radii of Mg^{2+} is larger than that of sodium, the presence of the former ion leads to a stronger bound with the fixed charged group of Suez CEM.

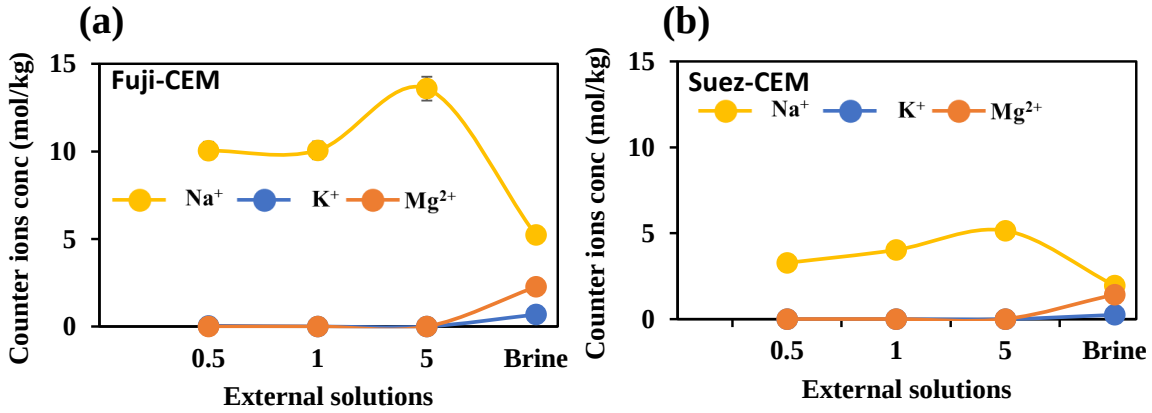

Figure 38. Counter ion concentration in (a) Fujifilm and (B) Suez cation exchange membranes with concentration variation from 0.5 M to 5 M and real Margi brine.

5.3.4 Counter ions in Anion Exchange membranes

Similar tests were performed to obtain the concentration of counter-ions in the Fuji and Suez anion exchange membranes. The counter ion concentration of Cl^- in both AEM Fujifilm and Suez somehow increases when the artificial aqueous solution of NaCl only increases from 0.5 M to 5 M, expressed in mol/kg swollen membranes **Figure 39**. The trend is reversed when the amount of fixed charged concentration is taken into consideration **Figure 40**. The fixed charge concentration is noticeably lower for Suez AME in comparison with Fuji AEM. It is also apparent that Cl^- is preferably absorbed when the membranes were equilibrated in brine solution. The concentration is Fujifilm AEM from 0.5 M to 1 M is not changed with increase in the concentration compared to slightly increase in the external 5M solution concentration while in case of the Suez AEM the change is plateau 0.5 M to 1 M and 5 M to brine solution concentration. The counter ion Cl^- in Fuji AEM appeared to be greater than that observed in Suez AEM. These results are agreement with the fixed charge group concentration in membranes as illustrated in **Figure 40**.

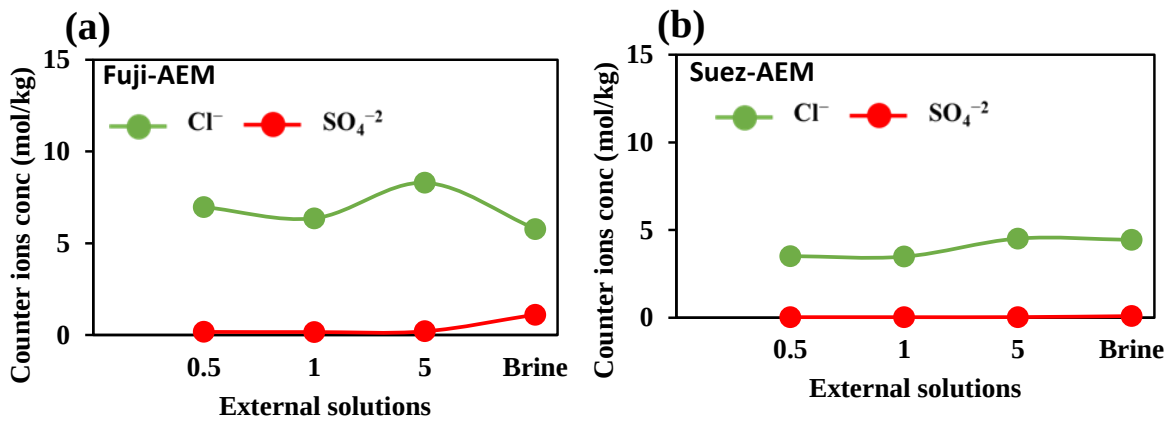

Figure 39. Membrane's counter-ion concentration as function of external salt and brine solution: (a) Fujifilm AEM and (b) Suez AEM.

5.3.5 Fixed charged concentration in membranes

Based on experimentally determined the fixed charge group concentration in the membrane was determined (Via $C_{fix}^{m} = C_{counter\ ions}^{m} - C_{co-ions}^{m}$) and it is shown as a function of external salt and real brine solution in **Error! Reference source not found.**. The fixed charge group concentration values were 10.02, 9.95, and 12.60 mol/kg for Fuji CEM at 0.5 M, 1 M, 5 M of salt external solution respectively while in case of Fuji AEM these values were 7.00, 6.34, and

7.50 mol/kg respectively. For the case for real brine the measured number were limited to 6.99 and 6.17 mol/kg for CEM and AEM respectively. Interestingly, the Suez IEMs demonstrated 68-60% lower value for CEM and 45-55% for AEM. The fixed charge group concentration often increases as external salt solution increases, and this is due to the reduction in water uptake. For Suez CEM, the membrane fixed charge group concentration increases by ~ 18% in going from 0.5 M to 1M, and ~24% in going from 1M to 5 M. Likewise, for the AEM, the membrane fixed charge group concentration were comparable in going from 0.5M to 5M. Consequently, these membranes were more sensitive to shrinking with respect to Fujifilm ion exchange membranes.

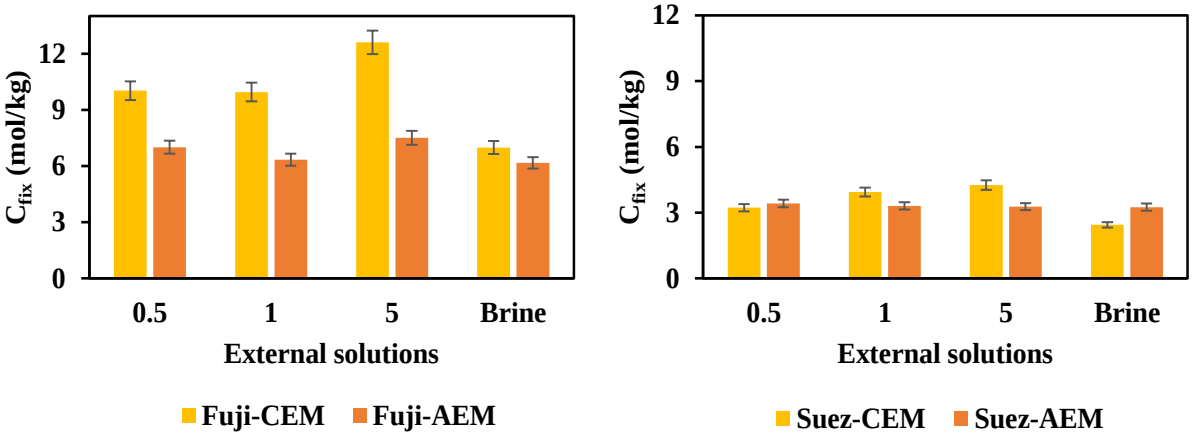

Figure 40. Influence of external salt concentration and brine solution on fixed charge group concentration in Fuji and Suez IEMs. The fixed charge group was measured as difference between the co-ion and counter ion in membranes.

5.3.6 Perm selectivity

Membrane permselectivity is a crucial indicator of its ability to selectively transport counter-ions over co-ions. It is noteworthy that the majority of commercially available ion exchange membranes exhibit a permselectivity exceeding 0.90. However, prior research has demonstrated that the permselectivity of these membranes is notably influenced by the concentration of the test solutions. While the permselectivity can approach the ideal value of 1.00 in diluted solutions, it tends to decrease in more concentrated solutions or brines [162]. Consequently, we conducted tests on Cation Exchange Membranes (CEMs) and Anion

Exchange Membranes (AEMs) across two hypersaline concentration gradients, specifically, in (I) 0.06M/5M, and (II) 0.06M/ Margi real brine solution pairs.

Figure 41, provides a comparative analysis of permselectivity data for Fujifilm and Suez IEMs, illustrating their responses to NaCl and brine solution concentration gradients while maintaining a constant temperature of 30 °C. In solution (0.06/5 M NaCl), the measured perspectivity for Fuji CEM and AEM was around (α = 0.75) and (α = 0.72) respectively, while for Suez CEM (α = 0.07) and AEM (α = 0.24). The high charge density of Fuji CEM and AEM leads to a good co-ion repulsion and permeates the counter-ions, while the lower charge density of Suez CEM and AEM cause a larger co-ion transport from the high to the low concentration compartment. Furthermore, in real brine solution the value reduces for Fuji CEM to 65% and AEM to 52% while the Suez permselectivity significantly reduces of 79% for CEM and 47% for AEM. The reduced permelectivity of Suez IEMs can be ascribed to its porous structure, which leads to inefficient Donnan exclusion, possibly due to the presence of defects or the occurrence of interstitial concentration polarization. To justify the equation 6, the open circuit values of real brine at 2 cm/s were considered (see

Figure 44), and were compared with the average perm selectivity as shown in **Figure 41**. The values were α= 0.31 and α = 0.12 for Fujifilm and Suez IEMs respectively, these obtained number are comparable to values of **Figure 41**.

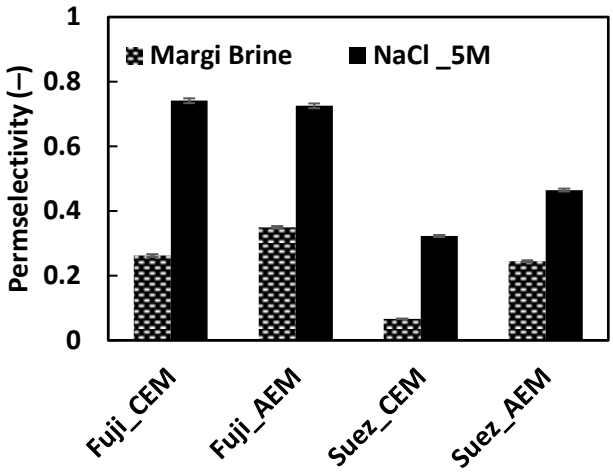

Figure 41. Perm selectivity of Fujifilm and Suez IEMs at 5M NaCl and real Margi brine solution (temperature: 30 °C and flow velocity: 2 Cm/s.

5.3.7 RED studies performance with distinct origin brine.

This section is devoted to the experiments carried out with the laboratory scale RED unit. The higher compartment of the RED stack was fed by natural brine discharged from two distinct origin (Margi and Nubia) brines under investigation containing 364.60 and 359.28 g/L of total dissolved solid (TDS), respectively. The lower compartment was fed by synthetic solutions (i.e., NaCl only) of 0.06 M equivalent to natural fresh water.

Figure 42, Illustrates current (A) versus open circuit voltage (V) and current versus power density curves for the RED unit assembled with the two different IEMs (Fujifilm and Suez) for both brine and artificial solution at constant temperature 30 ºC and at 1 cm/s flow velocity.

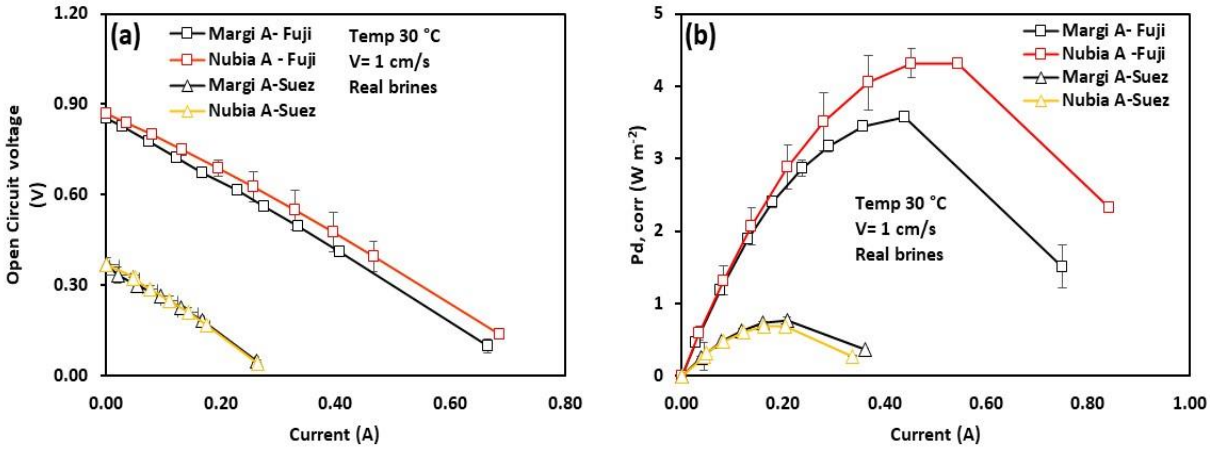

Figure 42. RED studies performance of two different IEMs at 30 ºC: a) open circuit voltage vs current; b) corrected power density vs current.

The maximum corrected power density was obtained by the RED stack feeding with Nubia real brine and Fujifilm membranes: $P_{d,corr}$ reached a maximum of 4.32 W m^{-2} at current of 0.40 A (OCV was 0.87Vand Stack resistance R_{stack} was 1.14 Ω). On the other hand, the poorest performance was detected by the stack fed with real Nubia brine and Suez IEMs: maximum $P_{d,corr}$ and current fell down to 0.69 W m^{-2} and 0.17 A. This difference is due to the much lower OCV (=0.37 V, 58% lower compared) because R_{stack} was found to be similar in the two cases (R_{stack} = 1.25 Ω). The average permselectivity α_m, of both IEMs can be calculated by dividing the measured OCV to the theoretical one [163].

5.3.8 Influence of IEMs on RED performance

The influence of the two different ion exchange membranes is studied. Membranes are critical components of the RED stack that limit SGP recovery performance. The electrical membrane resistance, perm selectivity, ionic resistance, membrane swelling degree (SD), and ion exchange capacity (IEC) are all critical properties of ion exchange membranes. Prior studies highlighted the importance of commercially available IEMs designed specifically for RED applications with superior physical and electrochemical features that boost energy efficiency and promote the wider implementation of the technology [164]. In this sense, **Figure 43**, depicts the results accomplished, indicating the better performance obtained by Fujifilm Type 10 membranes. The open circuit voltage (OCV) of 0.85 and 0.87 V feeding the RED stack with real stream of Margi-A and Nubia-A brine, respectively. On the other hand, the OCV of 0.37 and 0.61 V was obtained by Suez membranes. The performance behavior of membranes is totally different to the brine streams collected from distinct origin. The reason for higher OCV of Fujifilm membranes indicates higher selectivity of ions than that of Suez membranes.

The effect of divalent ions on stack internal resistant and power density in **Figure 43**, before the treatment and after treatment has been investigated using the IEMs mentioned in [153]. The stack composed of Fujifilm/Suez IEMs fed with streams of Margi (A & B) brine showed a very significant difference in terms of stack internal resistance. This is due to the reduction of Na^{+} and Cl^{-1} ions, as illustrated in above Table 12. Alternatively, the interior stack resistance was comparable when the RED stack was fed with Nubia (A & B) brine. The stack constructed with Fuji membrane demonstrates higher stack resistance for both real and treated brine. Due to the treatment of brines, the concentration of ions in brines has decreased, which has increased stack resistance.

The maximum corrected power density for the spot tests operation are shown in **Figure 43**, for stack with Fujifilm and Suez membranes, as a function of Margi (left) and Nubia (right) brines from one side of IEMs and lower feed stream of 0.06 M from the other side of IEMs at temperature of 30 ºC. The dramatically decreasing trend in power density for the case of the RED unit assembled with Suez IEMs compared to the Fujifilm membranes are reflected in the obtained open circuit voltage (V). This finding can be explained by the fact that the pore size of IEMs makes it more challenging to transport divalent ions across the membrane. Furthermore, the lower permselectivity of cation and anion ions within Suez AEMs, and lower mobilities of divalent cations within the Suez CEMs limit the cell potential of stack. Other explanation for the observed phenomenon includes the following point: (1) divalent ions with a strong affinity for the fixed functional groups of IEMs, (2) divalent counterions with a high valence, (3) Divalent ions have lower activity coefficients than monovalent ions, and (4) larger

hydrated radii for divalent ions than for monovalent ions[165]. Another possible explanation could be membrane swelling by water absorption into the fixed charged polymer affects IEMs absorption and ions mobility properties. Water molecules penetrate the polymer matrix to hydrate both fixed charged and their counter ions, altering the polymer network [166]. Water uptake is further influenced by the hydrated radius of the counter ions, the valency of the counter ions, and fixed charge group interaction to these ions. The hydrated radius of cations ions such as Na^{+} (3.58 Å), K^{+} (3.31 Å), Mg^{2+} (4.28 Å) and Ca^{2+} (4.12 Å) while in the case of Cl^{-} and SO_4^{2-} are 3.24 Å and 3.79 Å, respectively [167], [168].

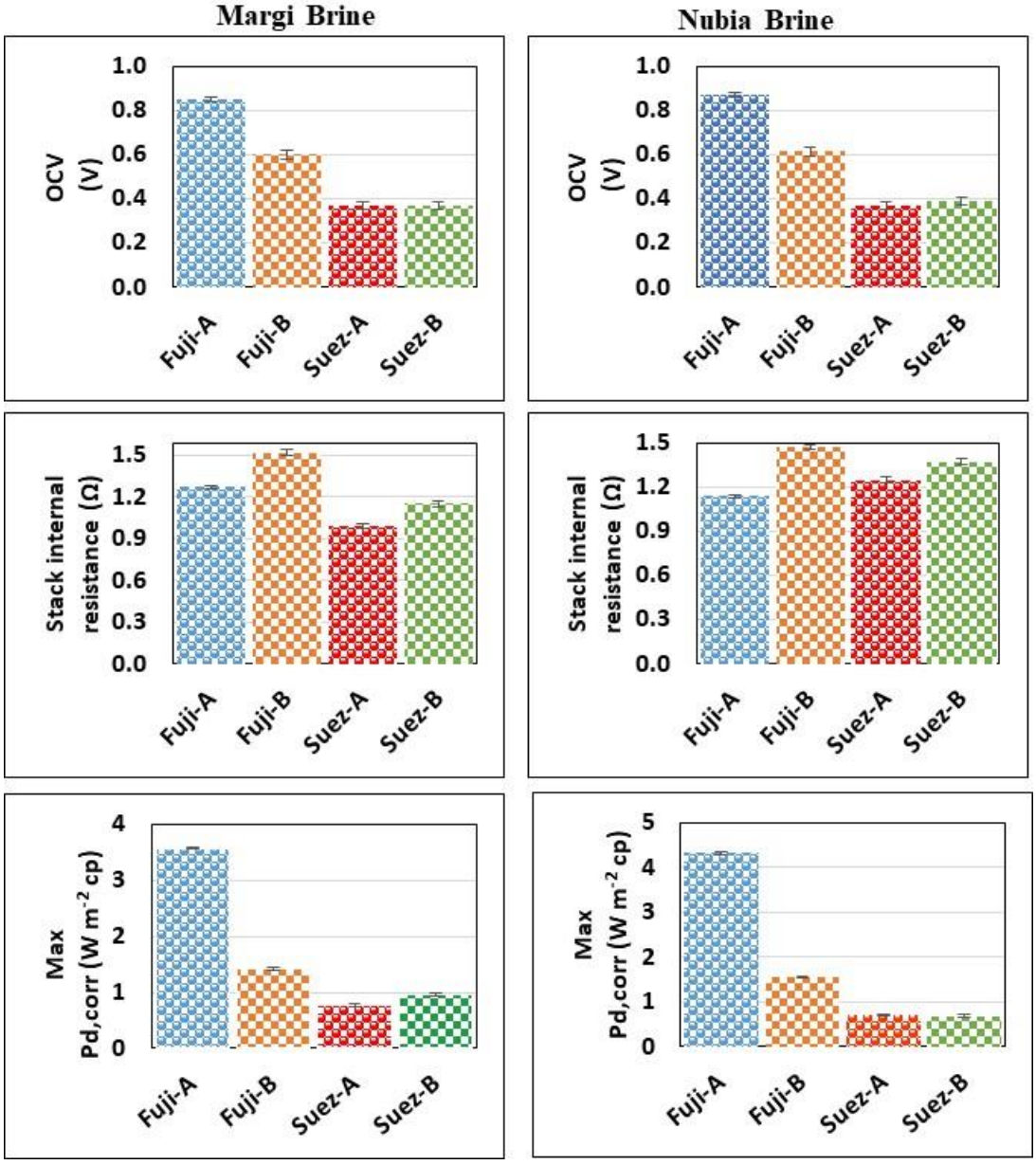

Figure 43. Experimental OCV, R_{stack} and Max Pd, $_{corr}$ as functions of Fuji / Suez IEMs, and real/purified brines. 5 cell pairs stack fed with solutions Margi brine (left column) and Nobia brine (right column), $V_{low} = V_{high} = 1$ cm. s^{-1}, and T = 30 ºC.

5.3.9 Effect of flow rate on RED stack

The flow velocity of streams in the RED channels can alter the rate of ion migration through ion exchange membranes, hence affecting the performance of the RED stack.

Figure 44, shows the effect of the flow velocity on OCV (

Figure 44a), and max $P_{d,corr}$ (

Figure 44b), for the different investigated brines (dilute concentration equal to 0.06 M, T=30 ºC).

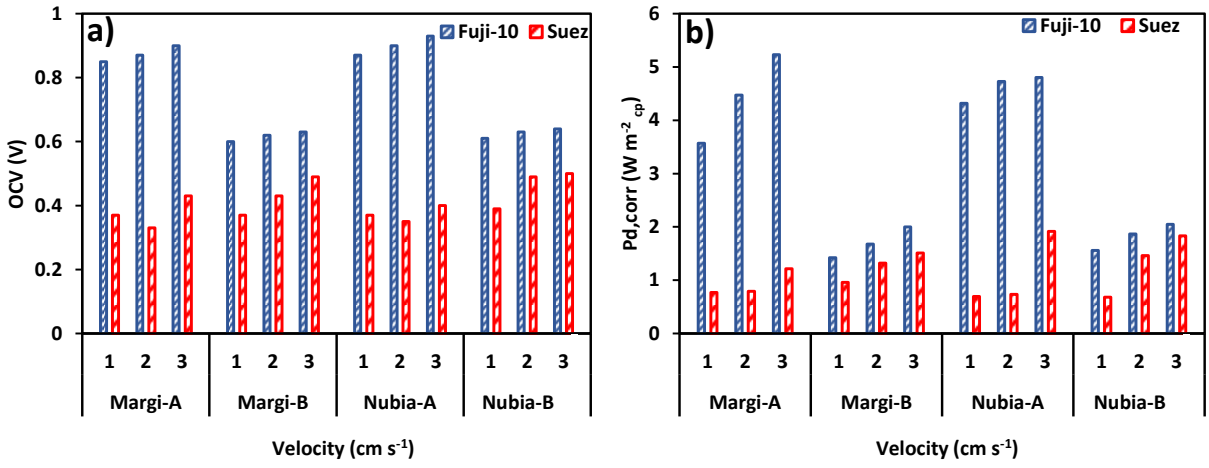

Figure 44. Effect of flow velocity on performance of RED stack.

Figure 44 (a), shows that as the flow velocity of brine (A & B) released from the Margi or Nubia increases, the open circuit voltage of the RED stack assembled with Fujifilm/Suez IEMs initially increases and then practically remains unchanged, while the stack internal resistance decreases. The decreasing trend of internal stack resistance with increasing flow velocity is attributable to the fact that rate of ion migration and concentration between the high and low

channels decreases slowly with the increase of flow velocity, the potential on the side of channel increase, and the corresponding Open- circuit voltage of the RED stack also increase. When the flow velocity varies from 1 to 3 cm s^{-1} for Margi (A) brine the internal resistance of reduced 18.2% and 11.3% for fuji and Suez IEMs respectively. These were limited to 22.4% and 7.5% for purified Margi (B) brine for both membranes. The change of the stack resistance is very small. This is due to the fact that when the flow velocity reaches a certain limit, the variation of cation and anion ions between the channels is small, and lower compartment concentrations decrease less. More precisely, flow velocity of the stream solution mainly affects both the ohmic and non-ohmic resistance to lower compartment solution resistance [169], [170]. Other parameters also affect the internal stack resistance of the RED stack; the composition ions in the channels called compartment solution resistance, the resistance of ion exchange membranes.

It can be found in **Figure 43** (b), that the max $P_{d,corr}$ increases 32% from 3.57 W m^{-2} to 5.32 W m^{-2} for the Fujifilm membrane with virgin Margi (A) brine, while in case Nubia virgin brine the increase was observed only 10%. It is also worth noting that the pattern of rising power density for actual and purified brine with respect to flow velocity is observable for Suez IEMs. Furthermore, in the case of higher TDS the Suez membranes showed the similar performance in terms of OCV and PD at flow velocity of 1 and 2 cm s^{-1}. Moreover, the performance of Suez membranes while facing the flow stream containing less TDS exhibits much better with increasing flow velocity. This finding explain the Suez membranes were more sensitive compared to the fuji IEMs facing the divalent ions present in the working solution. Another possible explanation could be the pore size within the Suez IEMs are smaller, preventing the passage of divalent ions with large radii. However, after the purification of brines, the Fujifilm ion exchange membranes demonstrated a significant reduction in terms of OCV and PD. This decline in PD can be explained by the reduction of ions in the working solution, which results to lower conductivity of brines and increases the stack internal resistance compared to the real brine stream.

5.3.10 Spike brine RED test performance

In this section, the RED stack equipped with Fujifilm / Suez membranes was investigated using spike brine, in which additional salt was mixing in Margi brine during the purification (treatment) in order to somehow achieve the real Margi (A) conductivity without Mg^{2+} and Ca^{2+} ions. Magnesium and calcium divalent ions have significant negative effects on the

performance of RED unit. The tests were conducted at 1 cm s^{-1}, 2 cm s^{-1} and 3 cm s^{-1}. Variations of PD and OCV are shown in **Figure 45**.

Figure 45, shows the variation of output voltage of the RED stack assembled with two different types of IEMs under different flow velocity. The increase of OCV has a total increase of 25% for Fujifilm membrane at flow rate of 1 cm s^{-1} compared to Margi (B), and it increase about 33% for Suez membrane, while increases between the same brine among the fuji and Suez IEMs was only 47% at flow rate of 3 cm s^{-1}. Due to the accumulation of salt on one side of the IEMs the obtained OCV of Suez stack is lower than the Fuji membranes. It was found that the stack resistance is almost unchanged, only decrease by 11% and 14% for both Fujifilm and Suez membrane respectively. The maximum power corrected density showed in

Figure **44** also has increasing trend with the increasing flow velocity of both membranes. When the flow velocity, the corresponding Max. Pd corrected for Fuji IEMs is 2.97 Wm^{-2}, 3.34 Wm^{-2}, 4.29 Wm^{-2} respectively, with an increase of 32%, 49% and 57% with respect to Margi (b) purified brine. The Max. Pd corrected value were observed for Suez IEMs is 1.55 W m^{-2}, 2.36 W m^{-2}, and 4.00 W m^{-2} under the same flow velocity.

***Table 13**. Performance of the RED unit fed by the Spike brine as concentrate and 0.06 NaCl solution as dilute.*

Spike Brine						
	Fujifilm Type 10			Suez		
Velocity Cm/s	Pd,corr W/m^2	OCV V	R_{stack} Ω	Pd,corr W/m^2	OCV V	R_{stack} Ω
1	2,97	0,80	1,34	1,55	0,55	1,25
2	3,34	0,85	1,36	2,36	0,61	1,05
3	4,29	0,87	1,14	4,00	0,64	0,78

The residence time of the stream in the RED stack becomes shorter as flow velocity increases, implying a large salinity gradient between the high and low compartments at the stack's exit. The increase of power output of the RED stack is due to the increase of both current and voltage. Under the same experimental parameters, the change of internal stack resistance mainly depends on the lower concentration solutions and membrane physical properties. The power density, OCV and stack resistance are illustrated in

Table 13 . Furthermore, while a high flow rate can result in higher power density, it also increases hydraulic loss.

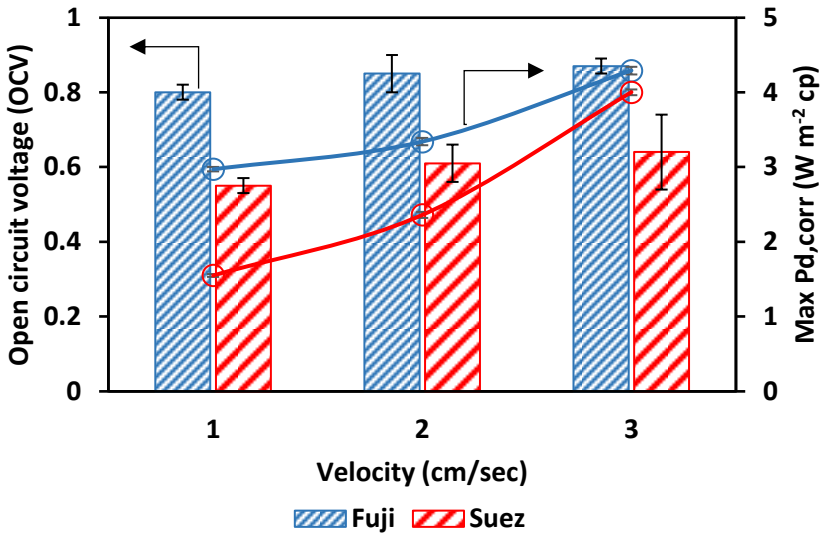

Figure 45. Effect of spike brine on power density of RED stacks.

5.3.11 Comparative Evaluation of Synthetic, Spiked, and Margi Brine Approaches

In this section the power densities of both membranes were compared under 1 cm/s feed solution velocity. The synthetic solution of 5 M of salt was used as a high concentrated solution. The low compartment of the RED stacks composed of Fujifilm, and Suez IEMs were fed with 0.06 M of concentration under the same above temperature 30 °C.

The synthetic solution demonstrated a very high-power density of 6.01 W/m^2 and 3.16 W/m^2 for Fujifilm and Suez IEMs respectively. The power density obtained with synthetic solution was higher ~ 40% form Margi brine using RED stack assembled with Fuji membranes while in case of Suez IEMs stack the difference were ~75% in power density compared to synthetic solution obtained power density. The performance of Suez IEMs improved going from Margi real brine solution to spike and to synthetic solution. The trend of power density is (synthetic sol> Spike brine sol>Margi brine sol) while on the other hand the fuji IEMs showed a slight decline in Spiked brine solution this due to the increase internal stack resistance.

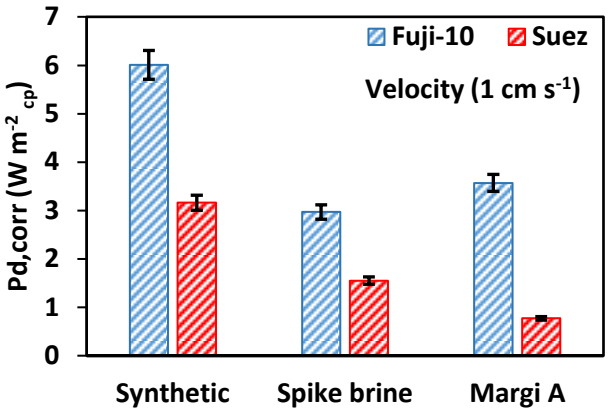

Figure 46. Power density comparison using synthetic, Spike and Margi solutions.

5.4 Conclusions and final remarks

This study quantifies the performance of ion exchange membranes from two manufacturers concerning parameters such as water uptake, fixed charge density, and perm selectivity. The electrochemical performance of these ion exchange membranes was assessed within a RED (Reverse Electrodialysis) system, measuring power generation, stack resistance, and open cell potential.

In this article, we investigate the behavior of various types of solutions, including synthetic 5M NaCl, spiked brine, real brine collected from saltworks, and purified brine. When exposed to NaCl and real brine solutions, we report the equilibrium ion concentrations in commercially available Fujifilm Type 10 and Suez ion exchange membranes. This evaluation allows us to understand water uptake, fixed charge concentration, and ion sorption within the membranes.

Notably, the presence of real brine significantly impacts the water uptake in Ion Exchange Membranes (IEMs). When subjected to salt and real brine external solutions, the Suez Cation Exchange Membrane (CEM) exhibited the highest water uptake value. Co-ion sorption was consistent across the membranes, primarily due to the higher water uptake value observed in the Suez membrane. Ion sorption decreased with increasing fixed charge concentration due to Donnan exclusion. Furthermore, both membranes' fixed charge and counter-ion concentrations increased in tandem with higher fixed charge group concentrations.

The perm selectivity results clarify the significant difference in the RED performance of both IEMs. These findings underscore the direct correlation between potential difference and membrane perm selectivity. Consequently, optimizing ion exchange membrane by balancing

perm selectivity and resistance is anticipated to lead in power production per unit membrane area.

Finally, based on the above-mentioned study, the RED tests were carried out using synthetic 5 M NaCl solution, real brine discharged from two different salt work namely (Margi and Nubia) before and after the treatment. Notably, the RED power density observed for Fujifilm CEM and AEM membrane pairs consistently outperformed the Suez membrane across all tested solutions.

General Conclusions

In light of the escalating global challenges posed by the climate emergency and the increasing global population, the intensified utilization of desalination plants for potable water provision has become a prominent trend. However, these plants face a consequential challenge in generating brine, a concentrated solution with elevated salinity, presenting notable environmental concerns. Addressing this challenge necessitates the development of a cost-effective and environmentally friendly brine management system for responsible disposal. This research has strategically investigated membrane-based technologies, specifically electrodialysis and reverse electrodialysis, as potential solutions to manage brine concentration effectively while recovering valuable resources and enhancing renewable energy recovery.

The research commenced with an experimental inter-laboratory campaign employing Electrodialysis with Bipolar Membranes (EDBM). This campaign successfully generated hydrochloric acid (HCl) and sodium hydroxide (NaOH) from brines using innovative ion exchange membranes (CEMs and AEMs) with thin and ultrathin non-woven polyester and polypropylene supports. The findings indicated a high level of reproducibility, validated by statistical analyses.

The impact of current density on HCl and NaOH final concentrations revealed the direct influence of current density on the resulting concentrations. Notably, working at 2 M NaCl concentrations demonstrated the feasibility of achieving NaOH concentrations exceeding 1 M with both membranes at 300 A/m2. However, a decrease in current efficiency over time was observed, potentially attributed to the non-ideal perm selectivity of the bipolar membranes and higher acid and base diffusion towards the salt compartment. The study also underscored the importance of membrane composition, with thin-polypropylene membranes exhibiting decreased current efficiency and specific energy consumption over time.

Expanding the investigation, the research explored the effect of a monovalent salt mixture on the EDBM unit. The study introduced a novel method for characterizing ion exchange membranes within the EDBM stack under various feed compositions. The results indicated that mixed-ion solutions did not significantly affect OH^- generation, providing a foundation for further understanding the system's behavior.

Furthermore, the study delved into applying reverse electrodialysis (RED) for high-salinity industrial brine valorization. Parametric analysis involving different ion exchange membranes, temperature, and flow velocity demonstrated the influence of these factors on converting chemical energy to electrical energy. Notably, the study highlighted the significance of membrane resistance in salinity gradient power (SGP) recovery, showcasing the superiority of Fujifilm Type 10 membranes in achieving higher power density due to lower resistance and high permselectivity.

Additionally, the research quantified the performance of ion exchange membranes from different manufacturers concerning water uptake, fixed charge density, and perm selectivity. Evaluating these membranes within a RED system provided insights into power generation, stack resistance, and open cell potential. The results emphasized the direct correlation between potential difference and membrane perm selectivity, underscoring the importance of optimizing ion exchange membranes for enhanced power production.

In conclusion, this research signifies a significant stride towards addressing the challenges of brine management in desalination processes. Using membrane-based technologies, specifically EDBM and RED, has demonstrated promising outcomes in resource recovery, renewable energy generation, and efficient brine concentration management. The findings contribute valuable insights into optimizing ion exchange membranes and process parameters for sustainable and economically viable solutions. This scientific endeavor holds implications for advancing environmentally responsible practices in desalination and brine management, aligning with the imperative for sustainable water and energy solutions in the face of global challenges.

Future Work

Building upon the insights gained from the current research, several avenues for future exploration and development emerge, focusing on advancing the practical applications and scalability of electro-membrane technologies for sustainable energy production, saline wastewater treatment, and chemical regeneration. The following areas present promising directions for future work.

1. **Optimization of Operational Parameters**

Conduct further research to optimize the operational parameters of bipolar membrane electrodialysis (BMED) and reverse electrodialysis (RED) to enhance their efficiency in treating real salt brine and extracting valuable resources. This includes investigating current density, temperature, and flow rate variations to maximize energy production and resource recovery.

2. **Membrane technology advancements**

Explore and develop advanced ion exchange membranes (IEMs) with improved properties, such as higher perm selectivity, electrical resistance, low cost, and durability. Investigate novel materials and manufacturing techniques that enhance membrane performance, leading to more effective and sustainable electro-membrane processes.

3. **Scale-up and Integration**

Investigate the scalability of the electro-membrane technologies for widespread implementation. Explore possibilities for integrating BMED and RED systems into existing industrial wastewater treatment plants and salt production facilities, ensuring a seamless transition to sustainable practices on a larger scale.

4. **Economic Viability and Cost-Effectiveness**

Conduct economic feasibility studies to assess the cost-effectiveness of electro-membrane technologies compared to conventional methods. Analyze the potential return on investment, considering membrane costs, energy consumption, and revenue generated from recovering valuable products.

5. **Environmental Impact Assessment**

Conduct comprehensive life cycle assessments to evaluate the overall environmental impact of implementing electro-membrane technologies. Assess factors such as carbon footprint, water usage, and potential environmental benefits, providing a holistic understanding of the technologies' sustainability.

References

[1] “https://unesdoc.unesco.org/”

[2] E. Jones, M. Qadir, M. T. H. van Vliet, V. Smakhtin, and S. Kang, “The state of desalination and brine production: A global outlook,” Science of The Total Environment, vol. 657, pp. 1343–1356, Mar. 2019, doi: 10.1016/j.scitotenv.2018.12.076.

[3] S. P. Maurya, P. K. Singh, A. Ohri, and R. Singh, “Identification of indicators for sustainable urban water development planning,” Ecol Indic, vol. 108, p. 105691, Jan. 2020, doi: 10.1016/j.ecolind.2019.105691.

[4] G. Cipolletta et al., “Policy and legislative barriers to close water-related loops in innovative small water and wastewater systems in Europe: A critical analysis,” J Clean Prod, vol. 288, p. 125604, Mar. 2021, doi: 10.1016/j.jclepro.2020.125604.

[5] M. O. Mavukkandy, C. M. Chabib, I. Mustafa, A. Al Ghaferi, and F. AlMarzooqi, “Brine management in desalination industry: From waste to resources generation,” Desalination, vol. 472, p. 114187, Dec. 2019, doi: 10.1016/j.desal.2019.114187.

[6] T. Hoepner and S. Lattemann, “Chemical impacts from seawater desalination plants — a case study of the northern Red Sea,” Desalination, vol. 152, no. 1–3, pp. 133–140, Feb. 2003, doi: 10.1016/S0011-9164(02)01056-1.

[7] O. Ogunbiyi et al., “Sustainable brine management from the perspectives of water, energy and mineral recovery: A comprehensive review,” Desalination, vol. 513, p. 115055, Oct. 2021, doi: 10.1016/j.desal.2021.115055.

[8] S.-Y. Pan, A. Z. Haddad, A. Kumar, and S.-W. Wang, “Brackish water desalination using reverse osmosis and capacitive deionization at the water-energy nexus,” Water Res, vol. 183, p. 116064, Sep. 2020, doi: 10.1016/j.watres.2020.116064.

[9] “D. Acuña Mora, A. de Rijck, Blue energy: salinity gradient power in practice, global sustainable development report. (2015) 1–8.”

[10] V. M. Ortiz-Martínez et al., “A comprehensive study on the effects of operation variables on reverse electrodialysis performance,” Desalination, vol. 482, p. 114389, May 2020, doi: 10.1016/j.desal.2020.114389.

[11] J. Jang, Y. Kang, J.-H. Han, K. Jang, C.-M. Kim, and I. S. Kim, “Developments and future prospects of reverse electrodialysis for salinity gradient power generation: Influence of ion exchange membranes and electrodes,” Desalination, vol. 491, p. 114540, Oct. 2020, doi: 10.1016/j.desal.2020.114540.

[12] C. Cassaro, G. Virruso, A. Culcasi, A. Cipollina, A. Tamburini, and G. Micale, “Electrodialysis with Bipolar Membranes for the Sustainable Production of Chemicals from Seawater Brines at Pilot Plant Scale,” ACS Sustain Chem Eng, vol. 11, no. 7, pp. 2989–3000, Feb. 2023, doi: 10.1021/acssuschemeng.2c06636.

[13] T. León, S. A. Shah, J. Lopez, A. Culcasi, A. Cipollina, J. L Cortina A. Tamburini, G.Micale “Electrodialysis with Bipolar Membranes for the Generation of NaOH and HCl Solutions from Brines: An Inter-Laboratory Evaluation of Thin and Ultrathin Non-Woven Cloth-Based Ion-Exchange Membranes,” Membranes (Basel), vol. 12, no. 12, p. 1204, Nov. 2022, doi: 10.3390/membranes12121204.

[14] M. O. Saeed, M. M. Ershath, and I. A. Al-Tisan, “Perspective on desalination discharges and coastal environments of the Arabian Peninsula,” Mar Environ Res, vol. 145, pp. 1–10, Mar. 2019, doi: 10.1016/j.marenvres.2019.02.005.

[15] S. Lattemann and T. Höpner, “Environmental impact and impact assessment of seawater desalination,” Desalination, vol. 220, no. 1–3, pp. 1–15, Mar. 2008, doi: 10.1016/j.desal.2007.03.009.

[16] “chrome-extension://efaidnbmnnnibpcajpcglclefindmkaj/https://www.jccp.or.jp/international/conference/docs/3-1SWCC.”

[17] M. Ahmad, B. Garudachari, Y. Al-Wazzan, R. Kumar, and J. P. Thomas, “Mineral extraction from seawater reverse osmosis brine of Gulf seawater,” Desalination Water Treat, vol. 144, pp. 45–56, 2019, doi: 10.5004/dwt.2019.23679.

[18] L. Bilińska, K. Blus, M. Gmurek, and S. Ledakowicz, “Brine Recycling from Industrial Textile Wastewater Treated by Ozone. By-Products Accumulation. Part 1: Multi Recycling Loop,” Water (Basel), vol. 11, no. 3, p. 460, Mar. 2019, doi: 10.3390/w11030460.

[19] D. Bhatia, N. R. Sharma, R. Kanwar, and J. Singh, “Physicochemical assessment of industrial textile effluents of Punjab (India),” Appl Water Sci, vol. 8, no. 3, p. 83, Jun. 2018, doi: 10.1007/s13201-018-0728-4.

[20] Dresel, P.E., Rose, A.W., 2010. Chemistry and Origin of Oil and Gas Well Brines in Western Pennsylvania. Open-File Report OFOG, v. 10-01.0, Pennsylvania Geological Survey, Harrisburg, PA.

[21] A. Justo et al., “Pharmaceuticals and organic pollution mitigation in reclamation osmosis brines by UV/H2O2 and ozone,” J Hazard Mater, vol. 263, pp. 268–274, Dec. 2013, doi: 10.1016/j.jhazmat.2013.05.030.

[22] S. A. Shah, R. Cucchiara, F. Vicari, A. Cipollina, A. Tamburini, and G. Micale, “Energetic Valorisation of Saltworks Bitterns via Reverse Electrodialysis: A Laboratory Experimental Campaign,” Membranes (Basel), vol. 13, no. 3, p. 293, Feb. 2023, doi: 10.3390/membranes13030293.

[23] N. Ghaffour, T. M. Missimer, and G. L. Amy, “Technical review and evaluation of the economics of water desalination: Current and future challenges for better water supply

sustainability," Desalination, vol. 309, pp. 197–207, Jan. 2013, doi: 10.1016/j.desal.2012.10.015.

[24] A. Panagopoulos, K.-J. Haralambous, and M. Loizidou, "Desalination brine disposal methods and treatment technologies - A review," Science of The Total Environment, vol. 693, p. 133545, Nov. 2019, doi: 10.1016/j.scitotenv.2019.07.351.

[25] A. Giwa, V. Dufour, F. Al Marzooqi, M. Al Kaabi, and S. W. Hasan, "Brine management methods: Recent innovations and current status," Desalination, vol. 407, pp. 1–23, Apr. 2017, doi: 10.1016/j.desal.2016.12.008.

[26] "https://www.lenntech.com/processes/brine-treatment-ZLD.htm."

[27] D. Ariono, M. Purwasasmita, and I. G. Wenten, "Brine Effluents: Characteristics, Environmental Impacts, and Their Handling," Journal of Engineering and Technological Sciences, vol. 48, no. 4, pp. 367–387, Sep. 2016, doi: 10.5614/j.eng.technol.sci.2016.48.4.1.

[28] P. Loganathan, G. Naidu, and S. Vigneswaran, "Mining valuable minerals from seawater: a critical review," Environ Sci (Camb), vol. 3, no. 1, pp. 37–53, 2017, doi: 10.1039/C6EW00268D.

[29] S. Y. Alnouri, P. Linke, and M. M. El-Halwagi, "Accounting for central and distributed zero liquid discharge options in interplant water network design," J Clean Prod, vol. 171, pp. 644–661, Jan. 2018, doi: 10.1016/j.jclepro.2017.09.236.

[30] D. Brogioli, F. La Mantia, and N. Y. Yip, "Thermodynamic analysis and energy efficiency of thermal desalination processes," Desalination, vol. 428, pp. 29–39, Feb. 2018, doi: 10.1016/j.desal.2017.11.010.

[31] N. Bajraktari, C. Hélix-Nielsen, and H. T. Madsen, "Pressure retarded osmosis from hypersaline sources — A review," Desalination, vol. 413, pp. 65–85, Jul. 2017, doi: 10.1016/j.desal.2017.02.017.

[32] A. Subramani and J. G. Jacangelo, “Treatment technologies for reverse osmosis concentrate volume minimization: A review,” Sep Purif Technol, vol. 122, pp. 472–489, Feb. 2014, doi: 10.1016/j.seppur.2013.12.004.

[33] H. Bamufleh, F. Abdelhady, H. M. Baaqeel, and M. M. El-Halwagi, “Optimization of multi-effect distillation with brine treatment via membrane distillation and process heat integration,” Desalination, vol. 408, pp. 110–118, Apr. 2017, doi: 10.1016/j.desal.2017.01.016.

[34] K. W. Lawson and D. R. Lloyd, “Membrane distillation,” J Memb Sci, vol. 124, no. 1, pp. 1–25, Feb. 1997, doi: 10.1016/S0376-7388(96)00236-0.

[35] A. M. Karam, A. S. Alsaadi, N. Ghaffour, and T. M. Laleg-Kirati, “Analysis of direct contact membrane distillation based on a lumped-parameter dynamic predictive model,” Desalination, vol. 402, pp. 50–61, Jan. 2017, doi: 10.1016/j.desal.2016.09.002.

[36] P. Wang and T.-S. Chung, “Recent advances in membrane distillation processes: Membrane development, configuration design and application exploring,” J Memb Sci, vol. 474, pp. 39–56, Jan. 2015, doi: 10.1016/j.memsci.2014.09.016.

[37] F. Macedonio, C. Quist- Jensen, O.Al-Harbi, H. Alromaih,F.Al shaboung, E.Drioli “Thermodynamic modeling of brine and its use in membrane crystallizer,” Desalination, vol. 323, pp. 83–92, Aug. 2013, doi: 10.1016/j.desal.2013.02.009.

[38] C. Quist-Jensen, F. Macedonio, and E. Drioli, “Integrated Membrane Desalination Systems with Membrane Crystallization Units for Resource Recovery: A New Approach for Mining from the Sea,” Crystals (Basel), vol. 6, no. 4, p. 36, Apr. 2016, doi: 10.3390/cryst6040036.

[39] M. Reig, S. Casas, O. Gibert, C. Valderrama, and J. L. Cortina, “Integration of nanofiltration and bipolar electrodialysis for valorization of seawater desalination

brines: Production of drinking and waste water treatment chemicals," Desalination, vol. 382, pp. 13–20, Mar. 2016, doi: 10.1016/j.desal.2015.12.013.

[40] H. M. N. AlMadani, "Water desalination by solar powered electrodialysis process," Renew Energy, vol. 28, no. 12, pp. 1915–1924, Oct. 2003, doi: 10.1016/S0960-1481(03)00014-4.

[41] H. Strathmann, "Electrodialysis, a mature technology with a multitude of new applications," Desalination, vol. 264, no. 3, pp. 268–288, Dec. 2010, doi: 10.1016/j.desal.2010.04.069.

[42] S. A. Shah, S. Y. Choi, S. Cho, M. Shahbabaei, R. Singh, and D. Kim, "Modified single-wall carbon nanotube for reducing fouling in perfluorinated membrane-based reverse electrodialysis," Int J Hydrogen Energy, vol. 45, no. 55, pp. 30703–30719, Nov. 2020, doi: 10.1016/J.IJHYDENE.2020.08.111.

[43] "European Commission. Report on Critical Raw Materials for the EU, Report of the Ad Hoc Working Group on Defining Critical Raw Materials; Ref. Ares(2015)1819595-29/04/2015; European Commission: Brussels, Belgium, 2014; Volume 41."

[44] "European Commission. Communication from the Commission to the European Parliament, the Council, the European Economic and Social Committee and the Committee of the Regions Tackling the Challenges in Commodity Markets and on Raw Materials; European Commission: Brussels, Belgium, 2011; Volume 59."

[45] W. Rabe, G. Kostka, and K. Smith Stegen, "China's supply of critical raw materials: Risks for Europe's solar and wind industries?," Energy Policy, vol. 101, pp. 692–699, Feb. 2017, doi: 10.1016/j.enpol.2016.09.019.

[46] M. S. Diallo, M. R. Kotte, and M. Cho, "Mining Critical Metals and Elements from Seawater: Opportunities and Challenges," Environ Sci Technol, vol. 49, no. 16, pp. 9390–9399, Aug. 2015, doi: 10.1021/acs.est.5b00463.

[47] A. Panagopoulos and K.-J. Haralambous, “Minimal Liquid Discharge (MLD) and Zero Liquid Discharge (ZLD) strategies for wastewater management and resource recovery – Analysis, challenges and prospects,” J Environ Chem Eng, vol. 8, no. 5, p. 104418, Oct. 2020, doi: 10.1016/j.jece.2020.104418.

[48] M. Kieselbach et al., “Brines from industrial water recycling: new ways to resource recovery,” Journal of Water Reuse and Desalination, vol. 10, no. 4, pp. 443–461, Dec. 2020, doi: 10.2166/wrd.2020.033.

[49] H. Lassesson, A. Malovanyy, and A. Andersson, “Optimizing resource flow of industrial processes, with a case study of zero liquid discharge at a copper smelting plant,” J Clean Prod, vol. 286, p. 125452, Mar. 2021, doi: 10.1016/j.jclepro.2020.125452.

[50] A. Culcasi, L. Gurreri, A. Cipollina, A. Tamburini, and G. Micale, “A comprehensive multi-scale model for bipolar membrane electrodialysis (BMED),” Chemical Engineering Journal, vol. 437, p. 135317, Jun. 2022, doi: 10.1016/j.cej.2022.135317.

[51] “https://searcularmine.eu/about/project-overview.”

[52] G. Battaglia et al., “Analysis of particles size distributions in Mg(OH)2 precipitation from highly concentrated MgCl2 solutions,” Powder Technol, vol. 398, p. 117106, Jan. 2022, doi: 10.1016/j.powtec.2021.117106.

[53] H. M. Saif, R. M. Huertas, S. Pawlowski, J. G. Crespo, and S. Velizarov, “Development of highly selective composite polymeric membranes for Li+/Mg2+ separation,” J Memb Sci, vol. 620, p. 118891, Feb. 2021, doi: 10.1016/j.memsci.2020.118891.

[54] G. Battaglia et al., “Recovery of Lithium Carbonate from Dilute Li-Rich Brine via Homogenous and Heterogeneous Precipitation,” Ind Eng Chem Res, vol. 61, no. 36, pp. 13589–13602, Sep. 2022, doi: 10.1021/acs.iecr.2c01397.

[55] F. Vicari et al., “Mining minerals and critical raw materials from bittern: Understanding metal ions fate in saltwork ponds,” Science of The Total Environment, vol. 847, p. 157544, Nov. 2022, doi: 10.1016/j.scitotenv.2022.157544.

[56] “Consortium - SEArcular Mine.” Accessed: Mar. 03, 2022. [Online]. Available: ” https://searcularmine.eu/about/consortium/ (accessed Sep. 21, 2021).

[57] M. Badruzzaman, J. Oppenheimer, S. Adham, and M. Kumar, “Innovative beneficial reuse of reverse osmosis concentrate using bipolar membrane electrodialysis and electrochlorination processes,” J Memb Sci, vol. 326, no. 2, pp. 392–399, Jan. 2009, doi: 10.1016/j.memsci.2008.10.018.

[58] C. Huang and T. Xu, “Electrodialysis with Bipolar Membranes for Sustainable Development,” Environ Sci Technol, vol. 40, no. 17, pp. 5233–5243, Sep. 2006, doi: 10.1021/es060039p.

[59] E. Al-Dhubhani, R. Pärnamäe, J. W. Post, M. Saakes, and M. Tedesco, “Performance of five commercial bipolar membranes under forward and reverse bias conditions for acid-base flow battery applications,” J Memb Sci, vol. 640, p. 119748, Dec. 2021, doi: 10.1016/j.memsci.2021.119748.

[60] C. Huang, T. Xu, Y. Zhang, Y. Xue, and G. Chen, “Application of electrodialysis to the production of organic acids: State-of-the-art and recent developments,” J Memb Sci, vol. 288, no. 1–2, pp. 1–12, Feb. 2007, doi: 10.1016/j.memsci.2006.11.026.

[61] Y. Yang, X. Gao, A. Fan, L. Fu, and C. Gao, “An innovative beneficial reuse of seawater concentrate using bipolar membrane electrodialysis,” J Memb Sci, vol. 449, pp. 119–126, Jan. 2014, doi: 10.1016/j.memsci.2013.07.066.

[62] M. Reig, S. Casas, C. Valderrama, O. Gibert, and J. L. Cortina, “Integration of monopolar and bipolar electrodialysis for valorization of seawater reverse osmosis

desalination brines: Production of strong acid and base," Desalination, vol. 398, pp. 87–97, Nov. 2016, doi: 10.1016/j.desal.2016.07.024.

[63] M. Herrero-Gonzalez, P. Diaz-Guridi, A. Dominguez-Ramos, A. Irabien, and R. Ibañez, "Highly concentrated HCl and NaOH from brines using electrodialysis with bipolar membranes," Sep Purif Technol, vol. 242, p. 116785, Jul. 2020, doi: 10.1016/j.seppur.2020.116785.

[64] J. R. Davis, Y. Chen, J. C. Baygents, and J. Farrell, "Production of Acids and Bases for Ion Exchange Regeneration from Dilute Salt Solutions Using Bipolar Membrane Electrodialysis," ACS Sustain Chem Eng, vol. 3, no. 9, pp. 2337–2342, Sep. 2015, doi: 10.1021/acssuschemeng.5b00654.

[65] N. Yu. Ganchenko, E. N. Kalaydin, G. S. Ganchenko, and E. A. Demekhin, "Electrohydrodynamics of Bipolar Membranes," Doklady Physics, vol. 63, no. 1, pp. 28–32, Jan. 2018, doi: 10.1134/S1028335818010032.

[66] M. A. Blommaert, D. Aili, R. A. Tufa, Q. Li, W. A. Smith, and D. A. Vermaas, "Insights and Challenges for Applying Bipolar Membranes in Advanced Electrochemical Energy Systems," ACS Energy Lett, vol. 6, no. 7, pp. 2539–2548, Jul. 2021, doi: 10.1021/acsenergylett.1c00618.

[67] A. T. Besha, M. T. Tsehaye, D. Aili, W. Zhang, and R. A. Tufa, "Design of Monovalent Ion Selective Membranes for Reducing the Impacts of Multivalent Ions in Reverse Electrodialysis," Membranes (Basel), vol. 10, no. 1, p. 7, Dec. 2019, doi: 10.3390/membranes10010007.

[68] L. Ge, B. Wu, D. Yu, A. Mondal, L. Hou, N.Afsar, Q.Li, T. Xu, J. Miao, T.Xu "Monovalent cation perm-selective membranes (MCPMs): New developments and perspectives," Chin J Chem Eng, vol. 25, no. 11, pp. 1606–1615, Nov. 2017, doi: 10.1016/j.cjche.2017.06.002.

[69] A. H. Galama, N. A. Hoog, and D. R. Yntema, “Method for determining ion exchange membrane resistance for electrodialysis systems,” Desalination, vol. 380, pp. 1–11, Feb. 2016, doi: 10.1016/j.desal.2015.11.018.

[70] R. Pärnamäe et al., “Bipolar membranes: A review on principles, latest developments, and applications,” J Memb Sci, vol. 617, p. 118538, Jan. 2021, doi: 10.1016/j.memsci.2020.118538.

[71] “https://patents.google.com/patent/US20060173084A1/en.”

[72] R. Pärnamäe, S. Mareev, V. Nikonenko, S. Melnikov, N. Sheldeshov, V. Zabolotskii, H.V.M. Hamelers, M. Tedesco “Bipolar membranes: A review on principles, latest developments, and applications,” J Memb Sci, 2020, doi: 10.1016/j.memsci.2020.118538.

[73] “Ionics * Ion Exchange Membranes,” Ionics: Ion Exchange Membranes. Accessed: Sep. 12, 2022. [Online]. Available: www.Suezwatertechnologies.com

[74] V. Zabolotskii, N. Sheldeshov, and S. Melnikov, “Heterogeneous bipolar membranes and their application in electrodialysis,” Desalination, vol. 342, pp. 183–203, 2014, doi: 10.1016/j.desal.2013.11.043.

[75] A. Culcasi, L. Gurreri, A. Cipollina, A. Tamburini, and G. Micale, “A comprehensive multi-scale model for bipolar membrane electrodialysis (BMED),” Chemical Engineering Journal, vol. 437, no. P1, p. 135317, 2022, doi: 10.1016/j.cej.2022.135317.

[76] M. Reig, S. Casas, C. Valderrama, O. Gibert, and J. L. Cortina, “Integration of monopolar and bipolar electrodialysis for valorization of seawater reverse osmosis desalination brines: Production of strong acid and base,” Desalination, vol. 398, pp. 87–97, 2016, doi: 10.1016/j.desal.2016.07.024.

[77] C. Bertinetto, J. Engel, and J. Jansen, “ANOVA simultaneous component analysis: A tutorial review,” Anal Chim Acta X, vol. 6, p. 100061, 2020, doi: 10.1016/j.acax.2020.100061.

[78] K. Venugopal and S. Dharmalingam, “Desalination efficiency of a novel bipolar membrane based on functionalized polysulfone,” Desalination, vol. 296, pp. 37–45, 2012, doi: 10.1016/j.desal.2012.04.006.

[79] R. Ibáñez, A. Pérez-González, P. Gómez, A. M. Urtiaga, and I. Ortiz, “Acid and base recovery from softened reverse osmosis (RO) brines. Experimental assessment using model concentrates,” Desalination, vol. 309, pp. 165–170, 2013, doi: 10.1016/j.desal.2012.10.006.

[80] H. Strathmann, J. J. Krol, H. J. Rapp, and G. Eigenberger, “Limiting current density and water dissociation in bipolar membranes,” J Memb Sci, vol. 125, no. 1, pp. 123–142, 1997, doi: 10.1016/S0376-7388(96)00185-8.

[81] Y. Yang, X. Gao, A. Fan, L. Fu, and C. Gao, “An innovative beneficial reuse of seawater concentrate using bipolar membrane electrodialysis,” J Memb Sci, vol. 449, pp. 119–126, 2014, doi: 10.1016/j.memsci.2013.07.066.

[82] M. Herrero-Gonzalez, P. Diaz-Guridi, A. Dominguez-Ramos, A. Irabien, and R. Ibañez, “Highly concentrated HCl and NaOH from brines using electrodialysis with bipolar membranes,” Sep Purif Technol, vol. 242, Jul. 2020, doi: 10.1016/j.seppur.2020.116785.

[83] J. R. Davis, Y. Chen, J. C. Baygents, and J. Farrell, “Production of Acids and Bases for Ion Exchange Regeneration from Dilute Salt Solutions Using Bipolar Membrane Electrodialysis,” ACS Sustain Chem Eng, vol. 3, no. 9, pp. 2337–2342, Sep. 2015, doi: 10.1021/acssuschemeng.5b00654.

[84] T. León, J. López, R. Torres, J. Grau, L. Jofre, and J.-L. Cortina, “Describing ion transport and water splitting in an electrodialysis stack with bipolar membranes by a 2-D model: Experimental validation,” J Memb Sci, vol. 660, p. 120835, Oct. 2022, doi: 10.1016/j.memsci.2022.120835.

[85] J. Liu, F. Xu, J. Yuan, Z. Ji, Y. Zhao, F.Li, X. Guo “High-value conversion of Na2SO4 wastewater by a continuous electrodialytic metathesis process: Effects of coexisting ions,” J Memb Sci, vol. 615, p. 118584, Dec. 2020, doi: 10.1016/j.memsci.2020.118584.

[86] Y. Fernández-Nava, E. Marañón, J. Soons, and L. Castrillón, “Denitrification of wastewater containing high nitrate and calcium concentrations,” Bioresour Technol, vol. 99, no. 17, pp. 7976–7981, Nov. 2008, doi: 10.1016/j.biortech.2008.03.048.

[87] M. Yaqub and W. Lee, “Zero-liquid discharge (ZLD) technology for resource recovery from wastewater: A review,” Science of The Total Environment, vol. 681, pp. 551–563, Sep. 2019, doi: 10.1016/j.scitotenv.2019.05.062.

[88] T. Tong and M. Elimelech, “The Global Rise of Zero Liquid Discharge for Wastewater Management: Drivers, Technologies, and Future Directions,” Environ Sci Technol, vol. 50, no. 13, pp. 6846–6855, Jul. 2016, doi: 10.1021/acs.est.6b01000.

[89] Y. Zhang, K. Ghyselbrecht, R. Vanherpe, B. Meesschaert, L. Pinoy, and B. Van der Bruggen, “RO concentrate minimization by electrodialysis: Techno-economic analysis and environmental concerns,” J Environ Manage, vol. 107, pp. 28–36, Sep. 2012, doi: 10.1016/j.jenvman.2012.04.020.

[90] F. Macedonio, E. Drioli, A. A. Gusev, A. Bardow, R. Semiat, and M. Kurihara, “Efficient technologies for worldwide clean water supply,” Chemical Engineering and Processing: Process Intensification, vol. 51, pp. 2–17, Jan. 2012, doi: 10.1016/j.cep.2011.09.011.

[91] L. Jiang, L. Chen, and L. Zhu, “Fouling process of membrane distillation for seawater desalination: An especial focus on the thermal-effect and concentrating-effect during biofouling,” Desalination, vol. 485, p. 114457, Jul. 2020, doi: 10.1016/j.desal.2020.114457.

[92] H. Guo, P. Yuan, V. Pavlovic, J. Barber, and Y. Kim, “Ammonium sulfate production from wastewater and low-grade sulfuric acid using bipolar- and cation-exchange membranes,” J Clean Prod, vol. 285, p. 124888, Feb. 2021, doi: 10.1016/j.jclepro.2020.124888.

[93] A. Culcasi, L. Gurreri, A. Cipollina, A. Tamburini, and G. Micale, “A comprehensive multi-scale model for bipolar membrane electrodialysis (BMED),” Chemical Engineering Journal, vol. 437, p. 135317, Jun. 2022, doi: 10.1016/j.cej.2022.135317.

[94] M. Reig, C. Valderrama, O. Gibert, and J. L. Cortina, “Selectrodialysis and bipolar membrane electrodialysis combination for industrial process brines treatment: Monovalent-divalent ions separation and acid and base production,” Desalination, vol. 399, pp. 88–95, Dec. 2016, doi: 10.1016/j.desal.2016.08.010.

[95] Y. Liu, Y. Sun, and Z. Peng, “Evaluation of bipolar membrane electrodialysis for desalination of simulated salicylic acid wastewater,” Desalination, vol. 537, p. 115866, Sep. 2022, doi: 10.1016/j.desal.2022.115866.

[96] F. Vassallo, D. La Corte, N. Cancilla, A. Tamburini, M. Bevacqua, A. Cipollina, and G. Micale “A pilot-plant for the selective recovery of magnesium and calcium from waste brines,” Desalination, vol. 517, p. 115231, Dec. 2021, doi: 10.1016/j.desal.2021.115231.

[97] T. Rottiers, K. Ghyselbrecht, B. Meesschaert, B. Van der Bruggen, and L. Pinoy, “Influence of the type of anion membrane on solvent flux and back diffusion in electrodialysis of concentrated NaCl solutions,” Chem Eng Sci, vol. 113, pp. 95–100, Jul. 2014, doi: 10.1016/j.ces.2014.04.008.

[98] L. Fu, X. Gao, Y. Yang, F. Aiyong, H. Hao, and C. Gao, “Preparation of succinic acid using bipolar membrane electrodialysis,” Sep Purif Technol, vol. 127, pp. 212–218, Apr. 2014, doi: 10.1016/j.seppur.2014.02.028.

[99] K. Elsaid, E. T. Sayed, M. A. Abdelkareem, A. Baroutaji, and A. G. Olabi, “Environmental impact of desalination processes: Mitigation and control strategies,” Science of The Total Environment, vol. 740, p. 140125, Oct. 2020, doi: 10.1016/j.scitotenv.2020.140125.

[100] S. Miller, H. Shemer, and R. Semiat, “Energy and environmental issues in desalination,” Desalination, vol. 366, pp. 2–8, Jun. 2015, doi: 10.1016/j.desal.2014.11.034.

[101] M. Tedesco et al., “Reverse electrodialysis with saline waters and concentrated brines: A laboratory investigation towards technology scale-up,” J Memb Sci, vol. 492, pp. 9–20, Oct. 2015, doi: 10.1016/j.memsci.2015.05.020.

[102] S. Xu, Y. Liu, Y. Wang, M. Zhang, Q. Xiao, and Y. Duan, “Influential analysis of concentration polarization on water flux and power density in PRO process: Modeling and experiments,” Desalination, vol. 412, pp. 39–48, Jun. 2017, doi: 10.1016/j.desal.2017.02.020.

[103] J. W. Post et al., “Salinity-gradient power: Evaluation of pressure-retarded osmosis and reverse electrodialysis,” J Memb Sci, vol. 288, no. 1–2, pp. 218–230, Feb. 2007, doi: 10.1016/j.memsci.2006.11.018.

[104] S. Pawlowski, R. M. Huertas, C. F. Galinha, J. G. Crespo, and S. Velizarov, “On operation of reverse electrodialysis (RED) and membrane capacitive deionisation (MCDI) with natural saline streams: A critical review,” Desalination, vol. 476, p. 114183, Feb. 2020, doi: 10.1016/j.desal.2019.114183.

[105] S. Abdullah Shah, Z. Haider, M. Shahbabaei, and D. Kim, “Development of an Efficient System for Blue Energy Production Based on Reverse Electrodialysis (RED) by

Optimizing Electrolyte Composition: Experimental and Theoretical Simulations," Energy & Fuels, Jun. 2022, doi: 10.1021/acs.energyfuels.2c00763.

[106] S. A. Shah, S. Y. Choi, S. Cho, M. Shahbabaei, R. Singh, and D. Kim, "Modified single-wall carbon nanotube for reducing fouling in perfluorinated membrane-based reverse electrodialysis," Int J Hydrogen Energy, vol. 45, no. 55, pp. 30703–30719, Nov. 2020, doi: 10.1016/J.IJHYDENE.2020.08.111.

[107] S.-Y. Choi, P. P. Sharma, A. Shah, R. Singh, D. Kim, and K.-S. Jin, "Controlling Fuel Crossover in Open Electrochemical Cells by Tuning the Water Nanochannel for Power Generation," 2020, doi: 10.1021/acssuschemeng.0c01013.

[108] J. Strategically Altered Fluorinated et al., "Citation: membranes Strategically Altered Fluorinated Polymer at Nanoscale for Enhancing Proton Conduction and Power Generation from Salinity Gradient," Membranes 2022, vol. 12, p. 395, 2022, doi: 10.3390/membranes12040395.

[109] M. Turek and B. Bandura, "Renewable energy by reverse electrodialysis," Desalination, vol. 205, no. 1–3, pp. 67–74, Feb. 2007, doi: 10.1016/j.desal.2006.04.041.

[110] G. Doornbusch, M. van der Wal, M. Tedesco, J. Post, K. Nijmeijer, and Z. Borneman, "Multistage electrodialysis for desalination of natural seawater," Desalination, vol. 505, p. 114973, Jun. 2021, doi: 10.1016/j.desal.2021.114973.

[111] A. H. Avci, R. A. Tufa, E. Fontananova, G. Di Profio, and E. Curcio, "Reverse Electrodialysis for energy production from natural river water and seawater," Energy, vol. 165, pp. 512–521, Dec. 2018, doi: 10.1016/j.energy.2018.09.111.

[112] A. Cosenza et al., "Power Production from Produced Waters via Reverse Electrodialysis: A Preliminary Assessment," Energies (Basel), vol. 15, no. 11, p. 4177, Jun. 2022, doi: 10.3390/en15114177.

[113] A. Tamburini et al., “Reverse electrodialysis heat engine for sustainable power production,” Appl Energy, vol. 206, pp. 1334–1353, Nov. 2017, doi: 10.1016/j.apenergy.2017.10.008.

[114] B. Ortega-Delgado et al., “Reverse electrodialysis heat engine with multi-effect distillation: Exergy analysis and perspectives,” Energy Convers Manag, vol. 194, pp. 140–159, Aug. 2019, doi: 10.1016/j.enconman.2019.04.056.

[115] M. Micari, M. Bevacqua, A. Cipollina, A. Tamburini, W. Van Baak, T. Putts, G. Micale “Effect of different aqueous solutions of pure salts and salt mixtures in reverse electrodialysis systems for closed-loop applications,” J Memb Sci, vol. 551, pp. 315–325, Apr. 2018, doi: 10.1016/J.MEMSCI.2018.01.036.

[116] S. Kang, J. Li, Z. Wang, C. Zhang, and X. Kong, “Salinity gradient energy capture for power production by reverse electrodialysis experiment in thermal desalination plants,” J Power Sources, vol. 519, p. 230806, 2022, doi: 10.1016/j.jpowsour.2021.230806.

[117] A. Daniilidis, D. A. Vermaas, R. Herber, and K. Nijmeijer, “Experimentally obtainable energy from mixing river water, seawater or brines with reverse electrodialysis,” Renew Energy, vol. 64, pp. 123–131, Apr. 2014, doi: 10.1016/j.renene.2013.11.001.

[118] E. Brauns, “Towards a worldwide sustainable and simultaneous large-scale production of renewable energy and potable water through salinity gradient power by combining reversed electrodialysis and solar power?,” Desalination, vol. 219, no. 1–3, pp. 312–323, Jan. 2008, doi: 10.1016/j.desal.2007.04.056.

[119] M. Tedesco, C. Scalici, D. Vaccari, A. Cipollina, A. Tamburini, and G. Micale, “Performance of the first reverse electrodialysis pilot plant for power production from saline waters and concentrated brines,” J Memb Sci, vol. 500, pp. 33–45, Feb. 2016, doi: 10.1016/j.memsci.2015.10.057.

[120] “Consortium - SEArcular Mine.” Accessed: Mar. 03, 2022. [Online]. Available: ” https://searcularmine.eu/about/consortium/ (accessed Sep. 21, 2021).

[121] “https://www.Fujifilm.com/us/en/business/industrial-materials/ion-exchange-membranes/overview. .”

[122] “https://www.fumatech.com/en/products/membranes-water-treatment-processes/. .”

[123] “https://www.watertechnologies.com/products/ionics-ion-exchange-membranes.”

[124] M. Tedesco, E. Brauns, A. Cipollina, G. Micale, P. Modica, G. Russo, J. Helsen “Reverse electrodialysis with saline waters and concentrated brines: A laboratory investigation towards technology scale-up,” J Memb Sci, vol. 492, pp. 9–20, Oct. 2015, doi: 10.1016/j.memsci.2015.05.020.

[125] R. A. Tufa, S. Pawlowski, J. Veerman, K. Bouzek, E. Fontananova, G.D. Profio, S. Velizarov, J.G. Crespo, K. Nijmeijer, E. Curcio “Progress and prospects in reverse electrodialysis for salinity gradient energy conversion and storage,” *Applied Energy*, vol. 225. 2018. doi: 10.1016/j.apenergy.2018.04.111.

[126] S. Kang, J. Li, Z. Wang, C. Zhang, and X. Kong, “Salinity gradient energy capture for power production by reverse electrodialysis experiment in thermal desalination plants,” *J Power Sources*, vol. 519, p. 230806, 2022, doi: 10.1016/j.jpowsour.2021.230806.

[127] Z. Wang, J. Li, C. Zhang, H. Wang, and X. Kong, “Power production from seawater and discharge brine of thermal desalination units by reverse electrodialysis,” *Appl Energy*, vol. 314, p. 118977, May 2022, doi: 10.1016/j.apenergy.2022.118977.

[128] R. A. Tufa, E. Curcio, E. Brauns, W. van Baak, E. Fontananova, and G. Di Profio, “Membrane Distillation and Reverse Electrodialysis for Near-Zero Liquid Discharge and low energy seawater desalination,” *J Memb Sci*, vol. 496, 2015, doi: 10.1016/j.memsci.2015.09.008.

[129] Y. Mei and C. Y. Tang, “Co-locating reverse electrodialysis with reverse osmosis desalination: Synergies and implications,” *J Memb Sci*, vol. 539, pp. 305–312, Oct. 2017, doi: 10.1016/j.memsci.2017.06.014.

[130] J. N. Weinstein and F. B. Leitz, “Electric Power from Differences in Salinity: The Dialytic Battery,” *Science (1979)*, vol. 191, no. 4227, pp. 557–559, Feb. 1976, doi: 10.1126/science.191.4227.557.

[131] E. Fontananova, W. Zhang, I. Nicotera, C. Simari, W. V.Baak, G.D. Profio, E. Curcio, and E. Drioli “Probing membrane and interface properties in concentrated electrolyte solutions,” *J Memb Sci*, vol. 459, pp. 177–189, Jun. 2014, doi: 10.1016/J.MEMSCI.2014.01.057.

[132] A. M. Benneker, T. Rijnaarts, R. G. H. Lammertink, and J. A. Wood, “Effect of temperature gradients in (reverse) electrodialysis in the Ohmic regime,” *J Memb Sci*, vol. 548, pp. 421–428, Feb. 2018, doi: 10.1016/j.memsci.2017.11.029.

[133] W. Z. Cui *et al.*, “Response of salinity gradient power generation to inflow mode and temperature difference by reverse electrodialysis,” *J Environ Manage*, vol. 303, p. 114124, Feb. 2022, doi: 10.1016/J.JENVMAN.2021.114124.

[134] “International energy outlook 2013. 2013.” Accessed: Oct. 17, 2022. [Online]. Available: https://www.eia.gov/outlooks/ieo/pdf/0484(2013).pdf

[135] R. E. PATTLE, “Production of Electric Power by mixing Fresh and Salt Water in the Hydroelectric Pile,” *Nature*, vol. 174, no. 4431, pp. 660–660, Oct. 1954, doi: 10.1038/174660a0.

[136] J. Hu *et al.*, “Experimental investigation on the performance of series control multi-stage reverse electrodialysis,” *Energy Convers Manag*, vol. 204, p. 112284, Jan. 2020, doi: 10.1016/j.enconman.2019.112284.

[137] D. A. Vermaas, M. Saakes, and K. Nijmeijer, “Doubled power density from salinity gradients at reduced intermembrane distance,” *Environ Sci Technol*, vol. 45, no. 16, 2011, doi: 10.1021/es2012758.

[138] P. P. Sharma *et al.*, “Strategically Altered Fluorinated Polymer at Nanoscale for Enhancing Proton Conduction and Power Generation from Salinity Gradient,” *Membranes (Basel)*, vol. 12, no. 4, p. 395, Apr. 2022, doi: 10.3390/membranes12040395.

[139] M. Turek, B. Bandura, and P. Dydo, “Power production from coal-mine brine utilizing reversed electrodialysis,” *Desalination*, vol. 221, no. 1–3, pp. 462–466, Mar. 2008, doi: 10.1016/j.desal.2007.01.106.

[140] M. Tedesco, C. Scalici, D. Vaccari, A. Cipollina, A. Tamburini, and G. Micale, “Performance of the first reverse electrodialysis pilot plant for power production from saline waters and concentrated brines,” *J Memb Sci*, vol. 500, pp. 33–45, Feb. 2016, doi: 10.1016/j.memsci.2015.10.057.

[141] R. A. Tufa, E. Curcio, E. Brauns, W. van Baak, E. Fontananova, and G. di Profio, “Membrane Distillation and Reverse Electrodialysis for Near-Zero Liquid Discharge and low energy seawater desalination,” *J Memb Sci*, vol. 496, pp. 325–333, Dec. 2015, doi: 10.1016/j.memsci.2015.09.008.

[142] R. A. Tufa *et al.*, “Salinity gradient power-reverse electrodialysis and alkaline polymer electrolyte water electrolysis for hydrogen production,” *J Memb Sci*, vol. 514, pp. 155–164, Sep. 2016, doi: 10.1016/j.memsci.2016.04.067.

[143] A. Emdadi, P. Gikas, M. Farazaki, and Y. Emami, “Salinity gradient energy potential at the hyper saline Urmia Lake – ZarrinehRud River system in Iran,” *Renew Energy*, vol. 86, pp. 154–162, Feb. 2016, doi: 10.1016/j.renene.2015.08.015.

[144] S. Loeb and R. S. Norman, “Osmotic Power Plants,” *Science (1979)*, vol. 189, no. 4203, pp. 654–655, Aug. 1975, doi: 10.1126/science.189.4203.654.

[145] R. A. Tufa, E. Curcio, E. Fontananova, and G. di Profio, “3.8 Membrane-Based Processes for Sustainable Power Generation Using Water: Pressure-Retarded Osmosis (PRO), Reverse Electrodialysis (RED), and Capacitive Mixing (CAPMIX),” in *Comprehensive Membrane Science and Engineering*, Elsevier, 2017, pp. 206–248. doi: 10.1016/B978-0-12-409547-2.12278-4.

[146] B. B. Sales, M. Saakes, J. W. Post, C. J. N. Buisman, P. M. Biesheuvel, and H. V. M. Hamelers, “Direct Power Production from a Water Salinity Difference in a Membrane-Modified Supercapacitor Flow Cell,” *Environ Sci Technol*, vol. 44, no. 14, pp. 5661–5665, Jul. 2010, doi: 10.1021/es100852a.

[147] M. Olsson, G. L. Wick, and J. D. Isaacs, “Salinity Gradient Power: Utilizing Vapor Pressure Differences,” *Science (1979)*, vol. 206, no. 4417, pp. 452–454, Oct. 1979, doi: 10.1126/science.206.4417.452.

[148] F. Vassallo *et al.*, “A pilot-plant for the selective recovery of magnesium and calcium from waste brines,” *Desalination*, vol. 517, p. 115231, Dec. 2021, doi: 10.1016/j.desal.2021.115231.

[149] J. Veerman, M. Saakes, S. J. Metz, and G. J. Harmsen, “Reverse electrodialysis: Performance of a stack with 50 cells on the mixing of sea and river water,” *J Memb Sci*, vol. 327, no. 1–2, 2009, doi: 10.1016/j.memsci.2008.11.015.

[150] H.-K. Kim, M.-S. Lee, S.-Y. Lee, Y.-W. Choi, N.-J. Jeong, and C.-S. Kim, “High power density of reverse electrodialysis with pore-filling ion exchange membranes and a high-open-area spacer,” *J Mater Chem A Mater*, vol. 3, no. 31, pp. 16302–16306, 2015, doi: 10.1039/C5TA03571F.

[151] Z.-Y. Guo *et al.*, “Effect of ions (K+, Mg2+, Ca2+ and SO42−) and temperature on energy generation performance of reverse electrodialysis stack,” *Electrochim Acta*, vol. 290, pp. 282–290, Nov. 2018, doi: 10.1016/j.electacta.2018.09.015.

[152] C. Simões, B. Vital, T. Sleutels, M. Saakes, and W. Brilman, “Scaled-up multistage reverse electrodialysis pilot study with natural waters,” *Chemical Engineering Journal*, vol. 450, p. 138412, Dec. 2022, doi: 10.1016/j.cej.2022.138412.

[153] S. Abdullah Shah, R. Cucchiara, F. Vicari, A. Cipollina, A. Tamburini, and G. Micale, “Energetic Valorisation of Saltworks Bitterns via Reverse Electrodialysis: A Laboratory Experimental Campaign,” *Membranes (Basel)*, vol. 13, no. 3, p. 293, Feb. 2023, doi: 10.3390/membranes13030293.

[154] J. Veerman, M. Saakes, S. J. Metz, and G. J. Harmsen, “Reverse electrodialysis: A validated process model for design and optimization,” *Chemical Engineering Journal*, vol. 166, no. 1, pp. 256–268, Jan. 2011, doi: 10.1016/j.cej.2010.10.071.

[155] J. Kamcev *et al.*, “Partitioning of mobile ions between ion exchange polymers and aqueous salt solutions: importance of counter-ion condensation,” *Physical Chemistry Chemical Physics*, vol. 18, no. 8, pp. 6021–6031, 2016, doi: 10.1039/C5CP06747B.

[156] M. Galizia, F. M. Benedetti, D. R. Paul, and B. D. Freeman, “Monovalent and divalent ion sorption in a cation exchange membrane based on cross-linked poly (p-styrene sulfonate-co-divinylbenzene),” *J Memb Sci*, vol. 535, pp. 132–142, Aug. 2017, doi: 10.1016/j.memsci.2017.04.007.

[157] G. M. Geise, D. R. Paul, and B. D. Freeman, “Fundamental water and salt transport properties of polymeric materials,” *Prog Polym Sci*, vol. 39, no. 1, pp. 1–42, Jan. 2014, doi: 10.1016/j.progpolymsci.2013.07.001.

[158] A. R. Khare and N. A. Peppas, “Swelling/deswelling of anionic copolymer gels,” *Biomaterials*, vol. 16, no. 7, pp. 559–567, May 1995, doi: 10.1016/0142-9612(95)91130-Q.

[159] J. Bastide, S. Candau, and L. Leibler, “Osmotic deswelling of gels by polymer solutions,” *Macromolecules*, vol. 14, no. 3, pp. 719–726, May 1981, doi: 10.1021/ma50004a050.

[160] F. G. Donnan, “The Theory of Membrane Equilibria.,” *Chem Rev*, vol. 1, no. 1, pp. 73–90, Apr. 1924, doi: 10.1021/cr60001a003.

[161] M. Galizia, G. S. Manning, D. R. Paul, and B. D. Freeman, “Ion partitioning between brines and ion exchange polymers,” *Polymer (Guildf)*, vol. 165, pp. 91–100, Feb. 2019, doi: 10.1016/j.polymer.2019.01.026.

[162] A. Zlotorowicz, R. V. Strand, O. S. Burheim, Ø. Wilhelmsen, and S. Kjelstrup, “The permselectivity and water transference number of ion exchange membranes in reverse electrodialysis,” *J Memb Sci*, vol. 523, pp. 402–408, Feb. 2017, doi: 10.1016/j.memsci.2016.10.003.

[163] J. N. Weinstein and F. B. Leitz, “Electric Power from Differences in Salinity: The Dialytic Battery,” *Science (1979)*, vol. 191, no. 4227, pp. 557–559, Feb. 1976, doi: 10.1126/science.191.4227.557.

[164] J. G. Hong *et al.*, “Nanocomposite and nanostructured ion-exchange membrane in salinity gradient power generation using reverse electrodialysis,” in *Advanced Nanomaterials for Membrane Synthesis and its Applications*, Elsevier, 2019, pp. 295–316. doi: 10.1016/B978-0-12-814503-6.00013-6.

[165] D. A. Vermaas, J. Veerman, M. Saakes, and K. Nijmeijer, “Influence of multivalent ions on renewable energy generation in reverse electrodialysis,” in *Energy and Environmental Science*, 2014. doi: 10.1039/c3ee43501f.

[166] G. Q. Chen, K. Wei, A. Hassanvand, B. D. Freeman, and S. E. Kentish, “Single and binary ion sorption equilibria of monovalent and divalent ions in commercial ion exchange membranes,” *Water Res*, vol. 175, p. 115681, May 2020, doi: 10.1016/j.watres.2020.115681.

[167] M. Galizia, F. M. Benedetti, D. R. Paul, and B. D. Freeman, “Monovalent and divalent ion sorption in a cation exchange membrane based on cross-linked poly (p-styrene sulfonate-co-divinylbenzene),” *J Memb Sci*, vol. 535, pp. 132–142, Aug. 2017, doi: 10.1016/j.memsci.2017.04.007.

[168] H. Fan and N. Y. Yip, “Elucidating conductivity-permselectivity tradeoffs in electrodialysis and reverse electrodialysis by structure-property analysis of ion-exchange membranes,” *J Memb Sci*, vol. 573, pp. 668–681, Mar. 2019, doi: 10.1016/j.memsci.2018.11.045.

[169] L. Gurreri, A. Tamburini, A. Cipollina, G. Micale, and M. Ciofalo, “CFD prediction of concentration polarization phenomena in spacer-filled channels for reverse electrodialysis,” *J Memb Sci*, vol. 468, pp. 133–148, Oct. 2014, doi: 10.1016/j.memsci.2014.05.058.

[170] D. A. Vermaas, E. Guler, M. Saakes, and K. Nijmeijer, “Theoretical power density from salinity gradients using reverse electrodialysis,” *Energy Procedia*, vol. 20, pp. 170–184, 2012, doi: 10.1016/j.egypro.2012.03.018.